The Paton WELDING JOURNAL

February 2000 # 2

English translation of the monthly «Avtomaticheskaya Svarka» journal published in Russian since 1948

«The Paton Welding Journal» monthly is published by the E.O. Paton Electric Welding Institute of the National Academy of Sciences of Ukraine with the support rendered by the International Association «Welding».

Promotion group:
V.N.Lipodaev, V.I.Lokteva
A.T.Zelnichenko (Exec. director)

Editorial and advertising offices are located at PWI, Dept. 51, 11, Bozhenko str., 252650, Kyiv, Ukraine.
Tel.: (38044) 227 67 57
Fax: (38044) 268 04 86
E-mail: paton@i.kiev.ua; paton@iptelecom.net.ua

Subscriptions:
$460, 12 issues

«The Paton Welding Journal» Website: http://www.nas.gov.ua/pwj

CONTENTS

SCIENTIFIC AND TECHNICAL

INDUSTRIAL

ROLE OF TEMPERATURE IN HYDROGEN-INDUCED CRACKING OF STRUCTURAL STEELS AND WELDED JOINTS

I.K. POKHODNYA, S.N. STEPANYUK and V.I. SHVACHKO
The E.O. Paton Electric Welding Institute, NASU, Kyiv, Ukraine

ABSTRACT

A procedure is proposed for experimental study of the influence of hydrogen on mechanical properties of the metal in a broad range of temperatures. Temperature dependencies of the degree of hydrogen- induced embrittlement for St.20 and 17KhGNDSM steels in the temperature range of –196 – +400 °C are determined. It is shown that, alongside the structural state, content and distribution of hydrogen, stress level and straining rate, temperature is the main initial factor determining the process of hydrogen embrittlement.

Key words: *welding heating, physical modelling, structural steels, cold cracks, hydrogen embrittlement, temperature influence, microcleavage resistance, dislocation transfer of hydrogen.*

Hydrogen-induced cracking in structural steel welding is manifested in the form of cold cracks (CC). Their formation is an important technology problem in fabrication of welded items.

Proceeding from the results of numerous experimental studies [1 – 3] and experience accumulated by industry, a number of measures have been currently elaborated for prevention of cold cracking, namely performance of welding in the optimal modes; lowering of hydrogen content in the weld metal, limitation of hydrogen content in steel.

The impact of these measures, however, is ambiguous [2] and often ineffective, especially in welding of high-strength steels. In such cases preheating, concurrent or post-weld heating is used, which allows production of the welded joint without CC.

As the application of this method requires considerable additional power consumption, and leads to a marked deterioration of the welders' labour conditions, special attention is given to determination of the optimal preheating level, as well as development of the processes of welding without its application.

Many research centers are working on development of welding consumables not requiring preheating to ensure the cracking resistance of the weld metal. However, as noted in [4], the absence of an adequate concept of what actually occurs in hydrogen cracking (HC) does not allow effective methods of its elimination to be developed.

The heating modes are currently determined by generalising the empirical data or using the carbon equivalent C_{eq} of steel. The higher C_{eq} values, the higher the temperature at which heating must be performed. There exist a great number of different equations for calculation of C_{eq} [5]. This parameter, however, yields a rather conditional estimate of the steel susceptibility to CC [3, 6]. Introduction of the so-called sensitivity index [7] in which C_{eq} is complemented by hydrogen content does not allow an unambiguous determination of the optimal heating level, either, which, as follows from [8], depends on the joint thickness, width of the gap between the edges being welded, area (relative to the weld) on which heating should be performed.

During investigations to determine the ways of CC prevention, A.M.Makara [1] found that with temperature increase above 120 °C and in the case of its drop below –70 °C, the cracking process is completely inhibited during the entire time of the sample staying at these temperatures. However, in heating after freezing, CC initiate more intensively than prior to freezing. Despite the importance of these results, their interpretation based only on the temperature change of the conditions of plastic and quasi-viscous flow along the grain boundaries without hydrogen involvement [1], does not seem convincing.

Further on the influence of temperature on HC process was investigated in a number of other studies [3, 9, 10]. Yet the results given in them are sometimes contradictory, and reliable data for structural steels are insufficient. Thus, this most important issue is still unresolved, and requires further studies [11].

The aim of this work was to clarify the mechanism of temperature influence on CC process.

Equipment, procedure, materials

Investigation of CC mechanism is complicated by that under the conditions of the actual welding process all the factors causing HC are inter-related and continuously changing. Therefore, this work uses physical modelling allowing performance of not only qualitative but also quantitative studies of temperature influence on HC, while controlling all the other main parameters, namely structure, hydrogen presence, stress level and straining rate.

Investigations were performed on samples made of structural steels, namely St.20 and 17KhGNDSM. Their

Composition of the studied metals

Steel grade	Weight fraction of elements, %									
	C	*Si*	*Mn*	*Cr*	*Mo*	*S*	*P*	*Cu*	*Ni*	*As*
St.20	0.17	0.070	0.25	0.25	–	0.04	0.035	0.25	0.25	0.08
17KhGNDSM	0.17	0.237	0.58	0.43	0.44	0.03	0.032	0.16	0.13	0.02

compositions determined by spectral analysis, are shown in the Table.

For normalising the grain structure, the blanks of these steels were first heat-treated at a temperature of 900 °C for 1 h with subsequent cooling in air. After heat-treatment St.20 had a uniform ferritic-pearlitic structure and 17KhGNDSM a granular beinitic structure.

Blanks of both steels were used to make standard cylindrical samples for uniaxial tension of MI-12 type. Mechanical tests for uniaxial tension were performed in a versatile rupture testing machine «Instron 1251» with 5 mm/min straining rate in the temperature range of –196 up to 400 °C (temperature was controlled by a thermocouple). During these experiments samples of both steels in the non-hydrogenated and hydrogenated states were tested under the same conditions. The yield point and actual rupture stress S_k were determined for each sample from the test results.

One of the problems arising in testing under the conditions of an elevated temperature, is the need to provide some hydrogen in the samples. Three main methods of hydrogenation are currently known [11]:

in gaseous hydrogen atmosphere with application of high pressure or high temperature; the maximal effect is achieved with simultaneous increase of these parameters, this, however, involving considerable experimental difficulties;

by dissociation of molecular hydrogen and its ionisation in the gas-discharge plasma without pressure increase;

by cathode polarisation in electrolytes (electrolytical hydrogenation).

In this work electrolytical method of hydrogenation was used for testing at low temperatures. The electrolyte was 5 % sulphuric acid solution with addition of not more than 0.05 % of sodium thiosulphate. The current density was set to be not more than 10 mA/cm^2, thus allowing elimination of irreversible defects during hydrogenation. The diffusible hydrogen content was controlled by chromatographic analysis.

As intensive dehydrogenation of the sample during mechanical testing under the conditions of elevated temperatures (above the normal temperature) cannot be completely avoided with any of these methods, a new method based on the use of titanium hydride, was applied. The powder of this substance was poured into a cylindrical groove drilled in the sample along the axis for the entire gauge length. Then, the groove was welded up at the end face of the grip part, and titanium hydride powder was in a sealed volume. The prepared sample were preheated at the temperature of titanium hydride dissociation up to the moment of the start of hydrogen evolution outside.

A number of additional experiments were conducted for verification of this hydrogenation method. The first consisted in derivation of the curve of hydrogen evolution in heating of titanium hydride. The powder of this substance was heated in Knudsen cell in a linear fashion up to the temperature of 600 °C at a rate of 18 °C/min. Hydrogen evolution was recorded by mass-spectrometry method using an all-purpose gas analysis system based on MKh-7304A mass-analyser («Electron», Ukraine).

The experimental results are given in Figure 1, from which one can see that in heating above 350 °C, intensive evolution of gaseous hydrogen starts. Production of the required amount of hydrogen was achieved by varying the initial amount of powder.

The second experiment consisted in determination of the kinetic dependence of hydrogen evolution through the wall of the cavity in the sample after thermal decomposition of titanium hydride. The sample filled with titanium

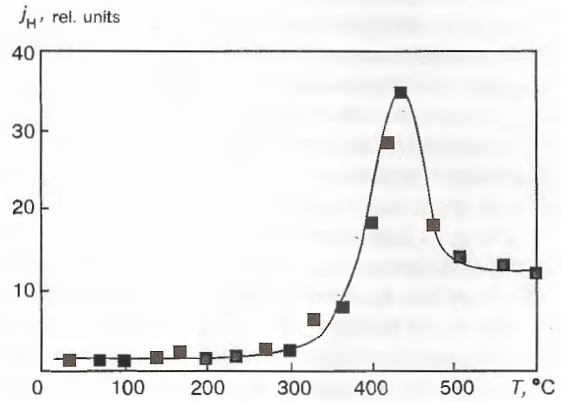

Figure 1. Hydrogen evolution in heating of titanium hydride: j_H — intensity of hydrogen evolution.

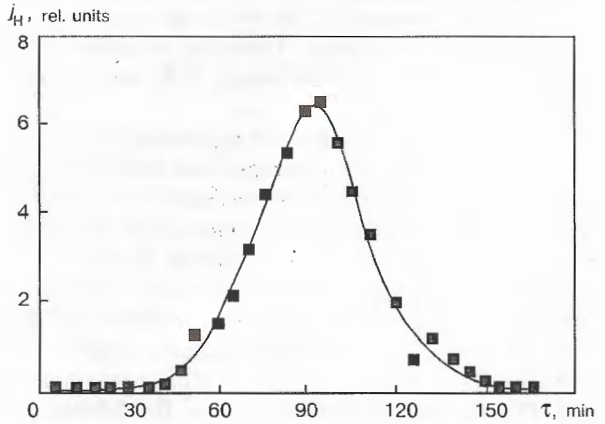

Figure 2. Hydrogen evolution from the sample with titanium hydride (T = 400 °C).

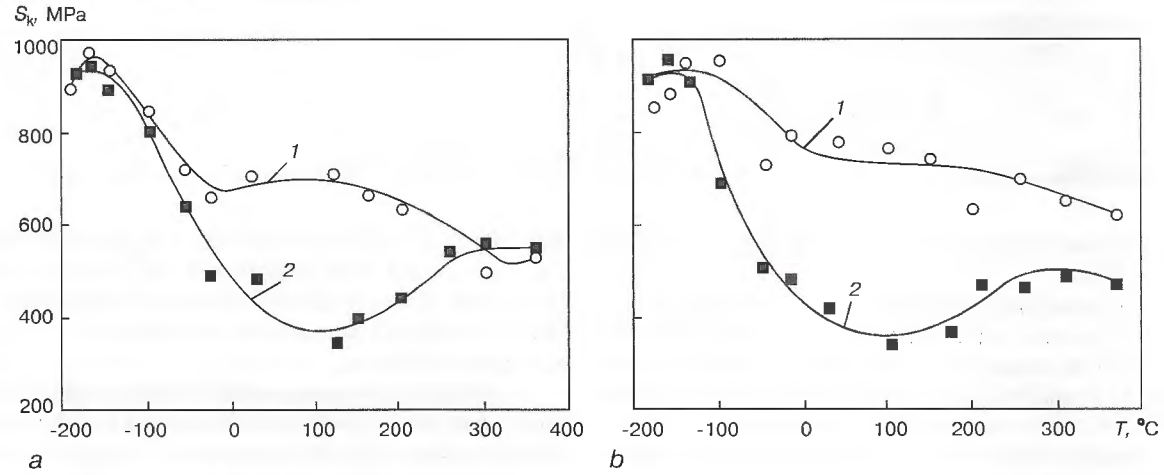

Figure 3. Temperature dependence of actual breaking stress for non-hydrogenated (*1*) and hydrogenated (*2*) samples of St.20 (*a*) and 17KhGNDSM (*b*) steels.

hydride, was soaked at the temperature of 400 °C for 180 min, recording hydrogen evolution from it. The derived curve (Figure 2) shows that hydrogen evolution began 45 min after the start of heating and went on for more than 1.5 h, this being much longer than the duration of tensile testing.

Thus, the conducted experiments confirmed that the proposed method of high-temperature hydrogenation of samples in mechanical tests, based on the use of titanium hydride as the hydrogen source, guarantees the sample staying in the hydrogenated state at high temperatures for a sufficiently long time much longer than the duration of mechanical testing. Application of this method eliminates many an inconvenience related to the use of gaseous hydrogen.

Thermal desorption spectra of hydrogen evolution from samples hydrogenated electrolytically, were also studied. In this case, linear heating up to 600 °C at a rate of 18 °C/min and mass-spectral recording of hydrogen were used.

Experimental results

It is rational to study the influence of temperature on embrittling action of hydrogen by temperature dependencies of S_k which is known [12] to be the average breaking stress in rupture in the neck. Therefore, variation of this value is an indication of the change of the strength properties of the material.

For this reason, the results of mechanical testing for uniaxial tension of non-hydrogenated and hydrogenated samples are presented in the form of temperature dependencies of S_k, average rupture stress for steels St.20 (Figure 3, *a*) and 17KhGNDSM (Figure 3, *b*). From the Figure one can see that when –100 °C is reached, S_k values of hydrogenated samples decrease relative to those of non- hydrogenated samples and reach a minimum at the temperature of approximately 100 °C, and starting from 150 °C they are restored, i.e. the influence of hydrogen decreases. Such a situation was found for both steels.

The temperature dependencies of yield point $\sigma_{0.2}$ of non-hydrogenated and hydrogenated samples of St.20 are shown in Figure 4, *a*, and of those of steel 17KhGNDSM is Figure 4, *b*. No change in $\sigma_{0.2}$ values after hydrogenation is characteristic for both steels in the studied range of HC manifestation.

Figure 5 shows a thermal desorption spectrum of hydrogen from electrolytically hydrogenated sample of St.20. The curve of thermal desorption has one peak at the temperature of 210 °C.

Discussion

A positive influence of welding heating is well known and has been effectively used for many years now. Different researchers provide different explanations for its cause [1, 3, 7, 8]. However, all of their statements are reduced, mainly, to that the application of heating leads to lowering of the cooling rate, without causing an excess coarsening of the grain in this case, and this, in its turn, promotes the formation of a more ductile metal structure; ordering of atomic structure on the grain boundaries; faster evolution of hydrogen from the weld metal; relaxation of internal stresses; smaller shrinkage; achievement of temperature values higher than the ultimate brittle fracture limit (for some steels).

Thus, it is assumed that the influence of temperature is only manifested through impact on other factors which are regarded as determinant in CC initiation [7], namely hydrogen content in the weld metal; formation of a sensitive structure (martensite); level of internal stresses whose main components are taken to be the stresses of austenitic-martensitic phase transformation [12].

Such an explanation, however, does not well agree with the situation arising in cooling to the temperatures much lower than the normal temperature, in our case below –100 °C. At this temperature HC is absent, although it does not make any favourable effect either on the structure, or on hydrogen content, or on the stress level. Moreover, such a cooling leads to deterioration of the above parameters.

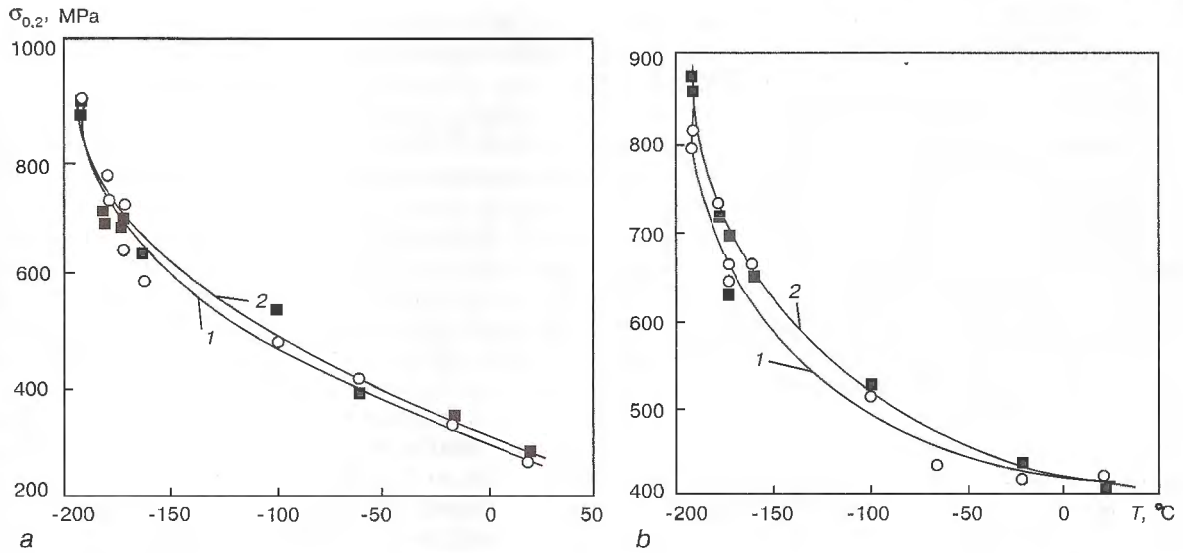

Figure 4. Temperature dependence for the yield point of non-hydrogenated (*1*) and hydrogenated (*2*) samples of St.20 (*a*) and 17KhGNDSM (*b*) steels.

It should be added that such an interpretation of the influence of temperature does not reveal the cause for the absence of the welded joint cracking at the moment of completion of the austenitic-martensitic transformation at still quite high temperatures (above 200 °C). Although the HC sensitive structure has already formed at this moment, no cracking occurs even with higher hydrogen content until the joint has cooled down to the temperature below 200 °C [1, 9].

Replies to the questions raised can only be provided by revealing the physical nature of HC and determining the role of temperature in this process.

In keeping with the concepts of CC nature set forth in [13], the mechanism of hydrogen embrittlement looks as follows. In the metal bulk, part of the dissolved hydrogen is entrapped by dislocations and during plastic deformation is transported by them to the site of the fracture crack initiation. The nucleus submicrocrack forms by one of the dislocation mechanisms. Thus, the transported hydrogen is freed to become chemically adsorbed on its juvenile surfaces. This leads to reduction of surface energy, which may result in the crack loosing elastic equilibrium at the moment of initiation and autocatalytically propagating in the field of external stresses. Now the temperature influences the effectiveness of proceeding of the main stages of the described HC mechanism.

The possibility of transfer of hydrogen atoms by dislocations at the set straining rate is unambiguously determined by the temperature level. In the region of low temperatures the mobility of the hydrogen atoms in the metal is so small, that the dislocations do not entrain the hydrogen atmospheres, but burst out of them. At these temperatures hydrogen does not come to the fracture sites in the required amount. Therefore, HC mechanism is not yet active.

With the increase of temperature, the mobility of hydrogen atoms rises and at its certain value (–50 °C) becomes comparable with the dislocations movement rate. A sufficient (for an essential lowering of surface energy) amount of hydrogen starts coming to the microcracks. This temperature value marks the beginning of the hydrogenated material strength lowering, namely transition of the submicrocrack into an unstable state of autocatalytic propagation becomes possible at a lower level of normal external stress. In a certain temperature range (from 0 up to 100 °C) HC process reaches its maximum.

With further increase of temperature (above 100 °C) hydrogen mobility rises to such a level when the hydrogen-dislocation bond energy becomes insufficient for its further containment and transportation to the initiating submicrocrack.

Moreover, the temperature directly influences the effectiveness of hydrogen impact in the fracture sites. With its rise the equilibrium concentration of hydrogen on the surface of the submicrocrack, decreases as a result of thermal desorption. This reduces the influence of adsorbed hydrogen on the surface energy of the crack. Thus, its embrittling action becomes weaker.

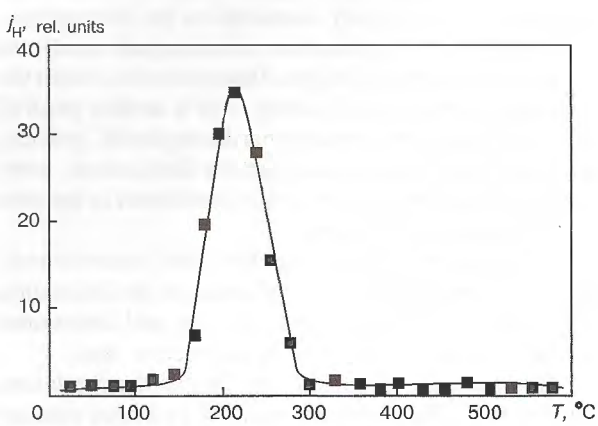

Figure 5. Hydrogen thermal desorption spectrum for St.20.

Attempts at a detailed description of the mechanism of temperature influence on HC process are found in the studies [9, 10]. All of them, however, are reduced only to recording the change of hydrogen interaction with dislocations. In our opinion, this is a one-sided and simplified approach to the issue being discussed, as the transportation by dislocations (although it is the most effective in this process) is only one of the six possible ways of hydrogen transfer in the solid phases [11], each of which essentially influences the nature of its localisation in the metal. Therefore, consideration of just the dynamic factor (hydrogen transfer) without giving due attention to the process of facilitated crack propagation, does not allow completely revealing the nature of the occurring phenomena, and, therefore, outlining the ways to prevent CC.

Moreover, such a consideration of HC process leads many supporters of the dislocation hypothesis to the conclusion that the dislocation movement is slowed down by hydrogen clouds, and this lowers the plastic properties of the metal [10].

The results of our investigations shown in Figure 4, indicate that hydrogen does not influence the yield point (in the temperature range of HC manifestation). It is known [14] that $\sigma_{0.2}$ determines the moment when a certain stage of micro yield (0.2 %) is achieved in the most unfavourably oriented metal grains. Therefore, hydrogen does not have any braking impact on the dislocation movement.

References [15, 16] give experimental data which confirm that in small concentrations (up to 10 ml/100 g) hydrogen does not slow down the dislocation movement like carbon or nitrogen.

The proposed in this work mechanism of temperature influence on HC process is confirmed by the results given in Figure 5. The peak of the thermal desorption curve is connected with hydrogen which was in certain traps. The temperature at which its evolution occurs, corresponds to the energy of the bond of these traps with hydrogen. In this case, the peak is formed at the temperature of 210 °C, this corresponding to hydrogen evolved from the dislocations [17]. Restoration of the strength properties of St.20 proceeds at the same temperature. Therefore, this is the hydrogen which participates in the embrittlement process, and it is mainly contained on the dislocations. The action of HC mechanism is interrupted exactly as result of violation of hydrogen-dislocation bond under the influence of temperature heating. This is another proof of the correctness of the concept that during the HC process, hydrogen actively interacts with the dislocations, however its embrittling impact is only manifested in the sites of submicrocrack initiation.

Thus, temperature is one of the main factors responsible for metal HC. It has an influence on the dislocation mechanism of hydrogen transportation and determines the effectiveness of its action in the fracture sites.

It is currently assumed [18 – 20] that the conditions leading to CC formation are a critical hydrogen concentration, residual and applied stresses exceeding a certain level, as well as a sensitive microstructure. Such a representation, however, is not quite adequate and limits the selection of the procedures to prevent HC.

As follows from the results of our investigations and a number of published data [9, 10, 13], the straining rate and temperature should be taken into account. Thus, cracks resulting from hydrogen embrittlement will initiate only in the presence simultaneously of a metal structure susceptible to HC, a critical local concentration of hydrogen, total stress of a certain level, low enough straining rate, metal temperature in the range of HC manifestation. Prevention of at least one of these conditions, reduces or completely eliminates the risk of CC occurrence.

This is the basis for the positive impact of welding heating. Detailed analysis, however, shows that heating (depending on the metal structure), can also have an adverse influence on the welded joint resistance to CC. On the one hand, long-term heating at a high temperature can lead to undesirable change of the structure, and uniform heating of dissimilar materials being welded or non-uniform heating of similar materials being welded can promote an increase in the internal stresses [7]. On the other hand, at a rather high-temperature heating hydrogen starts evolving from the traps with the bond energy corresponding to the heating temperatures. If it is brief, the content of the potentially dangerous hydrogen will not decrease, but will increase. This is another proof of the complex nature of the influence of welding heating and the need for its further detailed investigation.

CONCLUSIONS

1. A temperature dependence was established of hydrogen influence on the mechanical properties of structural steels (St.20 and 17KhGNDSM). The maximal embrittlement occurs at the temperature from –50 up to 150 °C.

2. The temperature, structural condition, content and distribution of hydrogen, stress level and straining rate are the main initial conditions which determine the HC process.

3. Selection of the welding heating modes should allow for the temperature interval of manifestation of hydrogen embrittlement of the welded joint metal.

REFERENCES

1. Makara, A.M. (1960) Investigation of the nature of cold near-weld cracks in welding of quenching steels. *Avtomaticheskaya Svarka*, **2**, 9 – 33.
2. Makara, A.M., Mosendz, N.A. (1971) *Welding of high-strength steels*. Kiev: Tekhnika.
3. Kozlov, R.A. (1969) *Hydrogen in welding of hull steels*. Leningrad: Sudostroeniye.
4. Backman, A. (1995) Development within materials technology — consumables in the XXI century. *Svetsaren*, **1**, 4 – 14.
5. Hrivnyak, I. (1998) Weldability of currently used high-strength steels. In: *Welding and allied technologies — into the XXI century*, 41 – 55. Kyiv: ESSE.
6. Mnushkin, O.S., Petrov, V.P. (1976) Influence of hydrogen on the properties of the heat-affected zone of low- and medium-alloyed steels. *Svarochnoye Proizvodstvo*, **12**, 6 –7.
7. Irving, B. (1992) Preheat: the main defense against hydrogen cracking. *Welding J.*, vol. 71, 7, 25 – 31.

8. Baker, J., Watkinson, F. (1970) Initiation and propagation of hydrogen-induced cracks. In: *Scientific problems of welding and special electrometallurgy*. Proc. of Intern. Symp. devoted to 100th anniversary of E.O. Paton, 7 – 21. Kiev: IES.
9. Craville, B.A., Baker, M.A., Watkinson, F. (1967) Effect of temperature and strain rate on hydrogen embrittlement of steel. *British Welding J.*, **6**, 337 – 342.
10. Kolachev, B.A. (1985) *Hydrogen brittleness of metals*. Moscow: Metallurgia.
11. Shapovalov, V.I. (1982) *Influence of hydrogen on structure and properties of iron-carbon alloys*. Moscow: Metallurgia.
12. Di-Jing, X., Hong, Q., Jianming, J. (1994) Investigation on susceptibility to hydrogen-assisted cracking in HSLA steel weldments. *Welding Research Supplement*, **12**, 285 – 290.
13. Pokhodnya, I.K., Shvachko, V.I. (1997) Physical nature of hydrogen-induced cold cracks in welded joints of structural steels. *Avtomaticheskaya Svarka*, **5**, 3 – 12.
14. Meshkov, Yu.Ya., Pakharenko, G.A. (1985) *Structure of metal and brittleness of steel joints*. Kiev: Nauk. Dumka.
15. Rogers, H.C. (1956) The influence of hydrogen on the yield point in iron. *Acta Metallurgica*, **2**, 114 – 117.
16. Rogers, H.C. (1957) The temperature-dependence of the hydrogen yield-point in steel. Ibid., **2**, 112 – 113.
17. Choo, W.Y., Lee, J.Y. (1982) Thermal analysis of trapped hydrogen in pure iron. *Met. Trans.*, **13A**, 135.
18. Davidson, J.L. (1998) Advances in hydrogen measurement: the science based design of low hydrogen consumables for the future. *Australasian Welding J.*, **43**, 33 – 39.
19. Lobanov, L.M., Mikhodui, L.I., Gordonnyi, V.G. (1998) The status and prospects for application in welded structures of high-strength steels with an improved weldability. *Avtomaticheskaya Svarka*, **12**, 29 – 34.
20. Tsaryuk, A.K., Brednev, V.I. (1996) Problem of cold crack prevention. Ibid., **1**, 36 – 40.

DETERMINATION OF RESIDUAL LIFE OF WELDED STRUCTURES WITH CREVICE-TYPE DEFECTS

O.E. ANDREYKIV and **M.V. LISHCHINSKA**
G.V. Karpenko Phys.-Mech. Institute, NASU, Lviv, Ukraine

ABSTRACT

The calculation model is suggested for investigation of the kinetics of propagation of fatigue cracks in plates whose material is heterogeneous in mechanical characteristics and resistance to fatigue fracture. The model is based on an energy criterion of fatigue fracture of materials. The system of differential equations has been derived to study the kinetics of growth of fatigue cracks in heterogeneous plates. Two problems in the determination of a period of sub-critical growth of a fatigue crack are considered: for a butt-welded plate and a cruciform welded joint. It is shown that the calculated service life values are in good agreement with the experimental data.

Key words: *welded structures, fatigue cracks, kinetic equations, residual stresses.*

The stage of fatigue crack propagation in the welded structures can be equal to 10 to 90 % of the total fatigue life of a welded element [1]. Therefore, theoretical determination of the subcritical crack growth acquires a great practical importance. In diagnostics of welded joints it is possible to determine the level of the initial cracklike defects in the item by the methods of non-destructive testing, and then calculate the residual fatigue life of the structure N_d by the known relationship [2]

$$N_d = \int_{l_0}^{l_*} v^{-1} dl, \qquad (1)$$

where v is the rate of the fatigue crack propagation; l_0 and l_* are the initial and critical crack length, respectively. In order to apply equation (1), it is necessary to know the cyclic fracture diagram (CFD) and kinetics of crack growth, which is determined from the kinetic equations of fatigue crack propagation. However, as is known from [3 – 6] the weld metal (WM), heat-affected zone (HAZ) and base metal (BM) are distinguished in the zone of the welded joint. More over, the strength properties and CFD of the material of these zones differ from each other (Figure 1) [7], and there is no doubt about the presence of residual welding stresses (Figure 2) [5, 6]. Comparison of the kinetic diagrams of fatigue fracture of materials from different zones of the welded joint [6, 8], also indicates that the rate of fatigue crack propagation in them is different. Therefore, in construction of the equations of the kinetics of fatigue crack growth, it is necessary to take into account the non-uniformity of the mechanical and fatigue fracture resistance properties of the material in the region of the welded joint, as well as the presence of residual stresses. The known [9] models of fatigue fracture are mostly valid for cases of similar materials. This paper proposes exactly the kinetic equations of fatigue crack propagation in the materials with non-uniform mechanical and fatigue properties. The proposed equations were derived on the basis of the energy criterion of fatigue fracture of materials which is based on such a hypothesis. Dissipation of energy of plastic deformations resulting

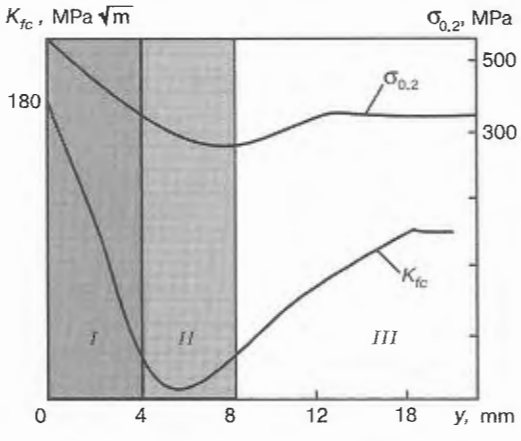

Figure 1. Distribution of mechanical $\sigma_{0.2}$ and fatigue K_{fc} properties in the zone of the welded joint on 10KhSND steel: *I* — WM; *II* — HAZ; *III* — BM.

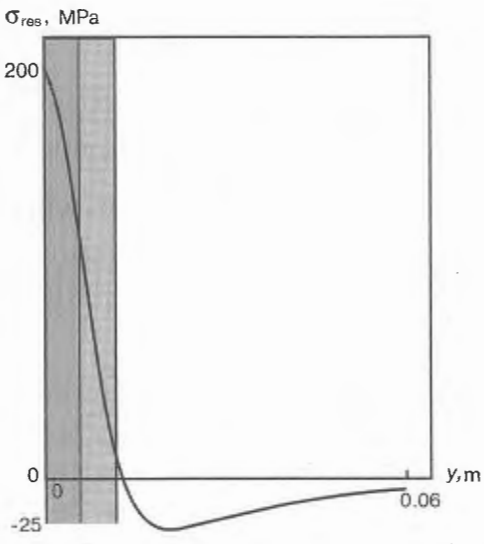

Figure 2. Distribution of residual stresses in the welded plate of St.3 steel.

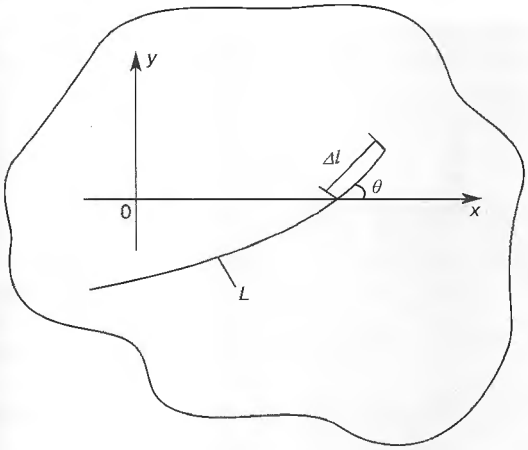

Figure 3. Schematic of a cracked plate.

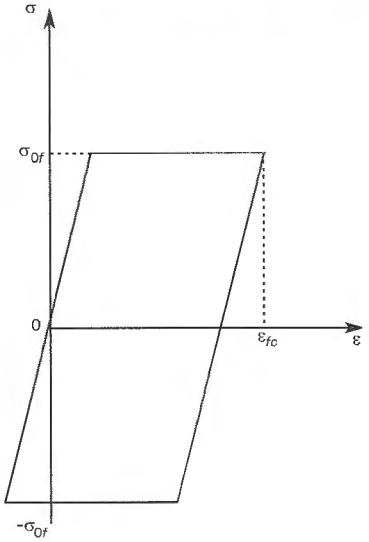

Figure 4. Model of the diagram of cyclic tension-compression.

from the fatigue crack propagation, per a unit of area of the newly formed surface, is a constant of the material at the specified external conditions and temperature [10 – 12].

Let us consider a plate of an elastic-plastic material weakened by a crack which is cyclically stretched. Let a crack of length L grow by Δl during ΔN cycles of loading (Figure 3). In this case a cyclic plastic zone of length l_{pf} ($\Delta l > l_{pf}$) has formed at its tip. It is known [13] that l_{pf} is smaller than the length of a static plastic zone l_p and depends on the cycle asymmetry R: $l_{pf} = 0.25(1 - R)^2 l_p$. In order to construct the equations of the kinetics of crack growth, let us use the energy criterion of fracture which envisages the existence for each material of a critical value of energy W_p required for one elementary act of fracture (energy of material fracture). In keeping with this criterion, for the fatigue crack to propagate for a length Δl during ΔN cycles of loading, the full energy of dissipation of plastic deformations in the material W should reach the value of the energy of material fracture W_p

$$W = W_p$$

or

$$W_s + \Delta N W_c = W_p\,, \qquad (2)$$

where W_s is the energy at static loading up to cycle maxim and W_c is the energy of dissipation of plastic deformations per one loading cycle. As in one act of fracture a maximal opening of the crack tip δ_{max} occurs in each point of Δl section, energy W_s can be determined as

$$W_s = \delta_{max}\,\sigma_{0f}\Delta l\,, \qquad (3)$$

where σ_{0f} is an averaged value of stresses in the pre-fracture zone in accordance with σ_k model [14], allowing for cyclic strengthening-softening of the material [15]. The value of σ_{0f} varies through the material bulk as a function of co-ordinates. Let us model the diagram of cyclic tension by a diagram for an ideally elastic-plastic material (Figure 4).

It is assumed that $\sigma_{0f} \approx (\sigma_{0.2} + \sigma_t)/2$ where $\sigma_{0.2}$ is the yield point, and σ_t is the ultimate strength of the material. As the plastic zone moves with the crack propagation, the elementary area near the crack tip goes through all the values (states) of plastic deformation which are found in a plastic zone of length l_{pf} ($l_{pl} < \Delta l$). Taking it into account and using the results of [10] for calculation of the energy of cyclic deformations W_c, we will have the following relationship:

$$W_c = \int_0^{l_{pf}} \sigma_{0f}\left[\delta^f_{max}(s) - \delta_0\right] ds\,, \qquad (4)$$

where $\delta^f_{max}(s)$ is the crack tip opening displacement along a cyclic plastic zone ($0 \le s \le l_{pf}$) which is connected with crack opening under static loading $\delta_{max}(s)$ through the following relationship: $\delta^f_{max}(s) = 0.5(1 - R)\delta_{max}(s)$ [13]. Here δ_0 is defined as follows:

$$\delta_0 = \max(\delta_{min}, \delta_{op}, \delta_{th})\,, \qquad (5)$$

where δ_{min} is the minimal opening in the cycle; δ_{op} is the residual opening of the crack and δ_{th} is the threshold value of opening δ, below which the crack does not grow. The energy of fracture of material W_p, necessary for formation of a crack section of length Δl, is defined as $W_p = \beta\gamma\Delta l$, where γ is the specific energy required for formation of a unity of the crack length; β is the Morrow correction coefficient [16], which represents the difference between the cyclic and static fracture energies. The specific energy can be given as $\gamma = \sigma_{0f}\,\delta_{fc}$ where δ_{fc} is the critical crack opening displacement of a fatigue crack. Hence, the fracture energy

$$W_p = \beta\sigma_{0f}\,\delta_{fc}\,\Delta l\,. \qquad (6)$$

Substituting expressions (3), (4) and (6) into equation (2), we will have the following relationship:

$$\Delta l\sigma_{0f}\,\delta_{max} + \Delta N\int_0^{l_{pf}} \sigma_{0f}\left[\delta^f_{max}(s) - \delta_0\right] ds = \Delta l\beta\sigma_{0f}\,\delta_{fc}\,.$$

From here through elementary transformations it is easy to determine

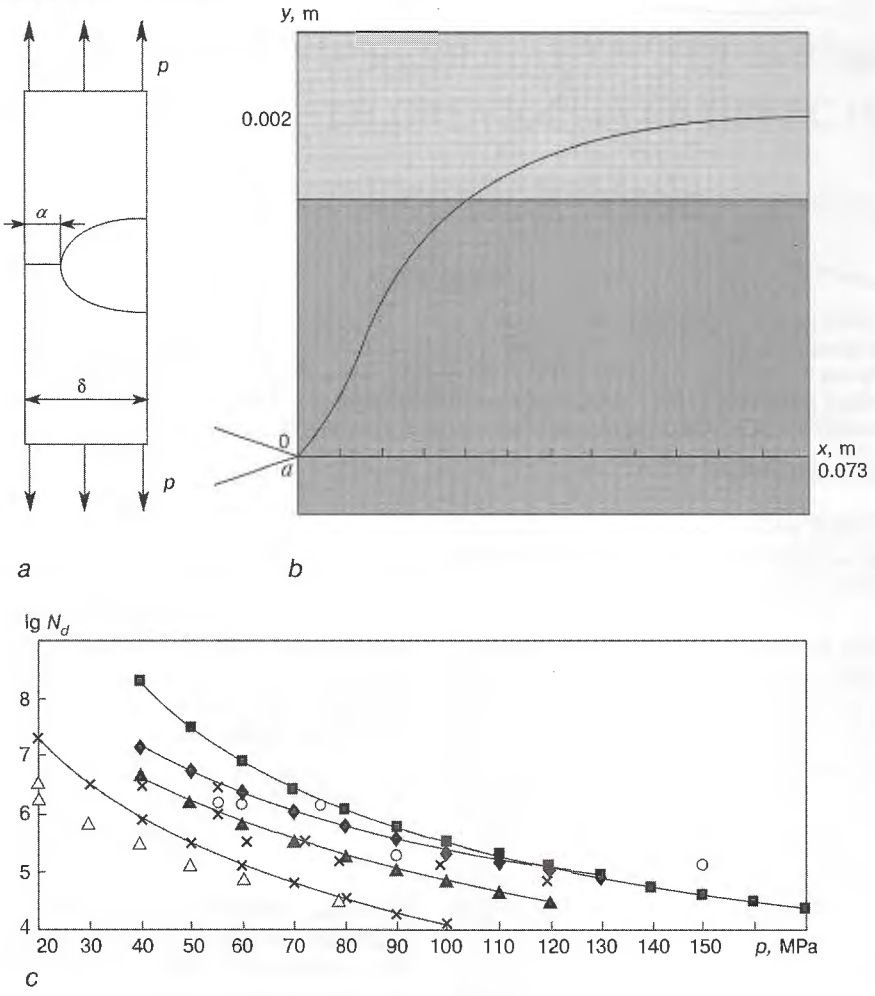

Figure 5. Butt welded joint with incomplete penetration (*a*), kinetics of the fatigue crack trajectory (*b*), comparison of theoretical (◆ — 0.1; ■ — 0.2; ▲ — 0.3; × — 0.4) and experimental (○ — 0.17 – 0.20; ❒ — 0.26 – 0.31; Δ — 0.44 – 0.49) evaluations of residual fatigue life (*c*).

$$\frac{\Delta l}{\Delta N} = \frac{\int_0^{l_{pf}} \sigma_{0f}\left[\delta^f_{\max}(s) - \delta_0\right] ds}{\beta\sigma_{0f}\delta_{fc} - \sigma_{0f}\delta_{\max}}.$$

Going to the limit at $\Delta N \to 0$, we will have a kinetic equation for determination of the crack propagation rate:

$$\frac{dl}{dN} = \frac{\int_0^{l_{pf}} \sigma_{0f}\left[\delta^f_{\max}(s) - \delta_0\right] ds}{\beta\sigma_{0f}\delta_{fc} - \sigma_{0f}\delta_{\max}}. \qquad (7)$$

Let θ be the angle of the direction of crack propagation relative to the axis of abscissas of the selected system of co-ordinates (Figure 3). As the crack propagates in the direction of the maximal possible rate, by differentiating the right-hand part of equation (7) by angle θ it is possible to derive the second kinetic equation for determination of the direction of the crack propagation:

$$\frac{\partial}{\partial\theta}\left(\frac{\int_0^{l_{pf}} \sigma_{0f}\left[\delta^f_{\max}(s) - \delta_0\right] ds}{\beta\sigma_{0f}\delta_{fc} - \sigma_{0f}\delta_{\max}}\right) = 0. \qquad (8)$$

Here $\delta^f_{\max}$, $\delta_{\max}$ and δ_0 are functions of θ.

The initial and terminal conditions should also be added to the derived equations (7) and (8):

$$N = 0, \quad l = l_0; \quad N = N_d, \quad l = l_*, \qquad (9)$$

where l_* is the critical crack length during N_d cycles of loading, which is determined from the criterion of the critical crack opening displacement [9]

$$\delta_{\max}(l_*) = \delta_{fc}. \qquad (10)$$

Thus, kinetic equations (7), (8), conditions (9), (10), together with the equation of elastic equilibrium of a body [17], make up a mathematical model for determination of the kinetics of propagation of fatigue cracks in non-uniform plates. Let us verify the model on two particular problems.

Case 1. A butt joint of St.3 with incomplete penetration of length a was performed by submerged-arc welding by Sv-08A wire using OSTs-5 flux (Figures 5, *a*; 6, *a*). Distribution of residual stresses and mechanical and fatigue properties in the region of welded joint is given in Figure 2 and Table 1, respectively [18]. A structure with the joint is subjected to cyclic tension with maximal stress p. The coefficient of the external loading cycle asymmetry $R = 0.1$. It is necessary to determine the kinetics of the fatigue crack trajectory and evaluate the residual fatigue life of the welded joint at different values of stress p and ratio $\alpha = a / \delta$.

In keeping with [19] the critical crack tip opening displacement can be determined from the following ratio:

$$\delta_{fc} = C_0 \frac{K_{fc}^2}{\sigma_0 E}. \qquad (11)$$

Here

$$C_0 = 0.6\,(1-\mu^2)\left(\frac{2(1+\mu)(1+\eta)\sigma_0}{\sqrt{3\eta E}}\right)^{\eta},$$

where μ is the Poisson's ratio; E is the modulus of elasticity and η is coefficient of strain hardening of the material. Other components $\delta_{\min}$, δ_{th}, d_{op}, $\delta_{\min}$ of equations (7), (8) are determined similar to equation (11).

Incorporating the results of [14, 15], the opening in the plastic zone $\delta_{\max}(l)$ was defined as

$$\delta_{\max}(l) = \frac{1}{\pi E}\left(K_{I\max}\sqrt{2\pi l} + 1600\ln\frac{|\sqrt{l_{pf}}-\sqrt{l}|}{|\sqrt{l_{pf}}+\sqrt{l}|}(l_{pf}-l)\right) +$$
$$+\frac{1}{\pi E}\left(3200\sqrt{l_{pf}}\sqrt{l} - \frac{250}{l_{pf}}\ln\frac{|\sqrt{l_{pf}}-\sqrt{l}|}{|\sqrt{l_{pf}}+\sqrt{l}|}(l_{pf}^2 - l^2)\right) + \qquad (12)$$
$$+ 500\frac{\sqrt{l}}{\sqrt{l_{pf}}}\left(\frac{l_{pf}}{3} - l\right).$$

After substitution of relationships (11), (12) and performance of certain mathematical transformations, we will reduce equations (7), (8) to the following form:

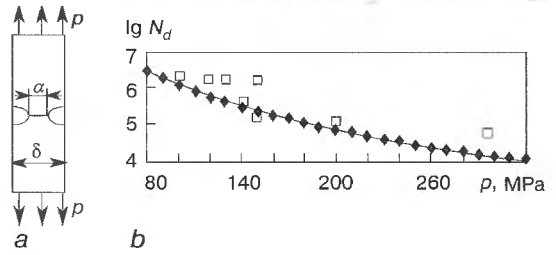

Figure 6. Butt welded joint with a lack-of-penetration (*a*) and comparison of theoretical (◆) and experimental (❒) evaluations of the residual fatigue life (*b*): $\alpha = 0.2$.

$$\frac{dl}{dN} = \frac{0.196}{\sigma_{0f}^2}\frac{\left(K_{I\max}^4\left(1+\frac{0.663bC_0}{\sigma_{0f}^3}K_{I\max}\sin\theta\right)\right)}{\beta K_{fc}^2 - K_{I\max}^2} -$$
$$-\frac{\left(K_0^4\left(1+\frac{0.663bC_0}{\sigma_{0f}^3}K_0^2\sin\theta\right)\right)}{\beta K_{fc}^2 - K_{I\max}^2}, \qquad (13)$$
$$\frac{\partial}{\partial\theta}\left(\frac{0.196}{\sigma_{0f}^2}\frac{\left(K_{I\max}^4\left(1+\frac{0.663bC_0}{\sigma_{0f}^3}K_{I\max}^2\sin\theta\right)\right)}{\beta K_{fc}^2 - K_{I\max}^2}\right) -$$
$$-\left(\frac{\left(K_0^4\left(1+\frac{0.663bC_0}{\sigma_{0f}^3}K_0^2\sin\theta\right)\right)}{\beta K_{fc}^2 - K_{I\max}^2}\right) = 0,$$

where $b = \partial\sigma_{0f}/\partial y$, in keeping with relationship (6) $K_0 = \max(K_{I\min}, K_{op}, K_{th})$. In keeping with [20], $K_{op} = (0.45 + 0.2R + 0.26R^2 + 0.1R^3)K_{\max}$, where R is the coefficient of cycle asymmetry. As in this case the crack will propagate along a curvilinear trajectory symmetrical relative to axis $0y$, $K_{I\max}$ can be calculated by the method proposed in [21], i.e.

$$K_{I\max} = \frac{(p+\sigma_{res})}{4}\sqrt{\pi a}\left(\cos\frac{\theta}{2}\frac{(3+\cos^2\theta)}{(3-\cos\theta)} + 2\cos\frac{3\theta}{2}\right). \qquad (14)$$

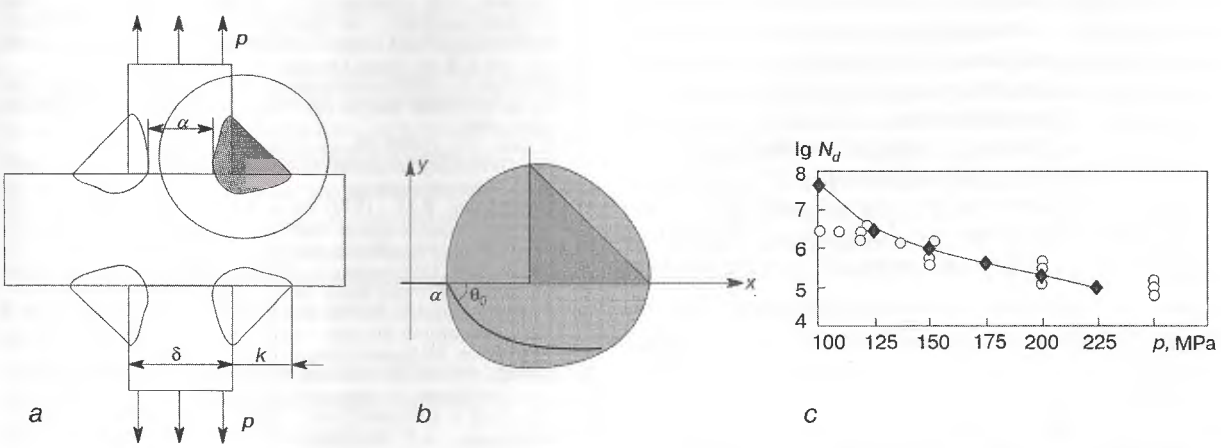

Figure 7. Cruciform welded joint with a lack of penetration (*a*), kinetics of the fatigue crack trajectory (*b*), comparison of theoretical (◆) and experimental (○) evaluations of the residual fatigue life (*c*).

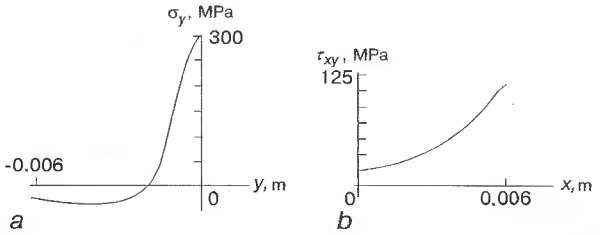

Figure 8. Distribution of residual normal (*a*) and tangential (*b*) stresses in the zone of a tee welded joint.

This problem was solved for the case when the plate material is not strengthened ($\eta = 0$). Equations (13), (14) were solved by the analytical method in combination with Runge method. In this case the kinetics of the crack trajectory was calculated by the method of limit interpolation [9] and shown in Figure 5, *b*. The residual fatigue life of the structure was calculated by equation (1), where the rate of fatigue crack propagation is determined by equation (7). Figures 5, *c*; 6, *b* give the results of calculation of the residual fatigue life compared to the experimental data, set forth in [22] for the joints shown in Figures 5, *a*; 6, *a*, respectively, at different values of α.

Case 2. A cruciform welded joint with incomplete penetration of length a is considered (Figure 7, *a*). The joint made of steel E355, the mechanical and fatigue properties of the material, its different zones, are given in Table 2. The structure with the appropriate joint is tested by cyclic tension with maximal stress p, coefficient of external loading cycle asymmetry $R = 0.1$, $\delta = 12$ mm, $a = 3$ mm, $k = 5$ mm. It is necessary to determine the kinetics of fatigue crack trajectory and plot the curve of the dependence of residual life on p values.

In order to solve this problem, first of all the distribution of residual stresses in the area of the welded joint was determined (Figure 8). Later on after calculation of the coefficients of stress intensity K_I and K_{II} using the relationships known from [22], the criterion of maximal tensile stresses (σ_θ-criterion) [9] was used to determine the initial direction of crack propagation $\theta_0 = -45°$. The kinetics of the fatigue crack trajectory was calculated using the method of limit interpolation [9] and is shown in Figure 7, *b*. The residual fatigue life of the structure was calculated by equation (1), where the rate of the fatigue crack growth is determined from equation (7). Comparison of experimental data [23] and theoretical estimates of the residual fatigue life is demonstrated in Figure 7, *c*.

Analysis of the data given in Figures 5, *c*; 6, *b*; 7, *c* shows that the calculated values of residual fatigue life agree well with the experimental results. This is evidence of the validity of applying the proposed calculation model for solving the problems which require investigation of the kinetics of fatigue crack propagation in the materials non-uniform as to their mechanical and fatigue fracture resistance properties.

Table 1. Mechanical and fatigue properties of different zones of a welded joint St.3

Welded joint zone	$\sigma_{0.2}$, *MPa*	σ_t, *MPa*	K_{fc}, *MPa*$\sqrt{m}$
WM	250	490	35
HAZ	167	388	23
BM	194	446	24

Table 2. Mechanical and fatigue properties of different zones of a welded joint on steel E355

Welded joint zone	$\sigma_{0.2}$, *MPa*	σ_t, *MPa*	K_{fc}, *MPa*$\sqrt{m}$
WM	579	680	62
HAZ	395	540	41
BM	449	620	48

REFERENCES

1. Pokhodnya, I.K. (1998) Problems of welding high-strength low-alloyed steels. In: *Modern material science of the XXI century*, 31 – 69. Kiev: Nauk. Dumka
2. Andreykiv, A.E., Darchuk, A.I. (1992) *Fatigue fracture and fatigue life of structures*. Kiev: Nauk. Dumka.
3. Makhnenko, V.I. (1998) Computer simulation of welding processes. In: *Modern material science of the XXI century*, 108 – 126. Kiev: Nauk. Dumka.
4. (1993) *Welded structures for construction. Fundamentals of structure design*, vol. 1. Edited by L.M. Lobanov. Kiev: Nauk. Dumka.
5. Karzov, G.P., Leonov, V.P., Timofeev, B.T. (1982) *Welded pressure vessels. Strength and fatigue life*. Leningrad: Mashinostrojenie.
6. Trufyakov, V.I. (1990) *Strength of welded joints at alternating loads*. Kiev: Nauk. Dumka.
7. Lepikhin, A.M., Moskvichev, V.V. (1991) Characteristics of crack resistance of welded joints: evaluation, calculation and statistical analysis. *Zavodskaya Laboratoria*, **12**, 48 – 51.
8. Ostash, O.P., Kunovskii, A.V., Laz'ko, V.E. *et al.* (1990) Cyclic crack resistance of welded joints of high-strength steels. *Avtomaticheskaya Svarka*, **7**, 8 – 12.
9. Panasyuk, V.V., Andreykiv, O.E., Parton, V.Z. (1988) Fracture mechanics and strength of materials. In: *Reference book. Fundamentals of fracture mechanics*, vol. 1. Kiev: Nauk. Dumka.
10. Li, Y. C., Huang, N.C. (1991) Fatigue crack speed of material with linear hardening. *Intern. J. Solids and Struct.*, vol. 27, **7**, 865 – 883.
11. Panasyuk, V.V., Andreykiv, O.E., Darchuk, O.I. (1995) Calculation model of fatigue crack growth in elastic-plastic materials under mixed mode loading. In: *Abstr. 7th Intern. Conf. on mechanical behaviour of materials*, 1995, May 28 – June 2, Hague, Netherlands, 119 – 120.
12. Panasyuk, V.V., Andreykiv, O.E., Kovchik, S.E. (1997) *Methods of evaluation of crack resistance of structural materials*. Kiev: Nauk. Dumka.
13. Panasyuk, V.V., Andreykiv, O.E., Darchuk, O.L. *et al.* (1994) Analysis of short and long fatigue cracks growth kinetics under non-regular loading. In: *Structural integrity: experiments, models, applications*. Proc. 10th Europ. Conf. on fracture, EMAS, 1271 – 1276.
14. Panasyuk, V.V. (1968) *Limit equilibrium of brittle bodies with cracks*. Kiev: Nauk. Dumka.
15. Romaniv, O.N., Yarema, S.Ya., Nikiforchin, G.N. *et al.* (1990) Fracture mechanics and strength of materials. In: *Reference book. Fatigue and cyclic crack resistance of structural materials*, vol. 4. Kiev: Nauk. Dumka.
16. Morrow, J. (1950) Investigation of plastic strain energy as a criterion for finite fatigue life. *The Garret Corporation Report*, 105 – 108.
17. Lourier, A.I. (1970) *Theory of elasticity*. Moscow: Nauka.
18. (1979) *Welding in mechanical engineering*. In 4 volumes. Moscow: Mashinostrojeinie.
19. McMeeking, R.M. (1977) Finite deformation analysis of crack opening in elastic-plastic materials and implication for fracture. *J. Mech. and Phys. Solids*, vol. 25, **5**, 357 – 381.
20. Finney, J.M., Deirmenjian, G. (1992) Delta-K-effective: which formulai, *Fatigue Fract. Engin. Mater. Struct.*, vol. 15, **2**, 151 – 158.
21. Lishchinska, M.V. (1988) Determination of the coefficients of stress intensity in the plates near the convex curvilinear cracks. *Phyz.-chim. Mekhanika Materialov*, **1**, 113 – 114.
22. Savruk, M.P. (1988) Fracture mechanics and strength of materials. Coefficients of stress intensity in cracked bodies. In: *Reference book* in 4 volumes, vol. 2. Kiev: Nauk Dumka.
23. Makhnenko, V.I., Pochinok, V.E. (1984) Resistance to cyclic loads of welded joints having welds with incomplete penetration. *Avtomaticheskaya Svarka*, **10**, 33 – 40.

APPLICATION OF EXPLOSION ENERGY FOR IMPROVING RELIABILITY OF WELDED STRUCTURES

V.G. PETUSHKOV
The E.O. Paton Electric Welding Institute, NASU, Kyiv, Ukraine

ABSTRACT

The essence, peculiarities and application fields of a new technology of explosion treatment of welded joints used to improve reliability and extend life of metal structures are outlined. Physical mechanism of the process and methods used for calculation of parameters of explosion loading of different-geometry weldments are described. Explosion treatment is shown to have a favourable effect on performance of welded structures and characterized by high productivity and cost effectiveness.

Key words: *welded joint, explosion treatment, explosive, reliability, corrosion resistance, fatigue, embrittlement, ecology of explosion.*

The radically new line in the field of explosion treatment of metals, i.e. explosion treatment (ET) of welded joints, put forward by PWI as early as the end of the 1960s [1], received further development and wide recognition in the fabrication and construction of various-application large-sized welded structures. Such treatment provides a drastic decrease in welding residual stresses (RS), exerts a positive effect on other physical and mechanical properties of joints and, thus, allows a marked improvement in a large number of service properties of welded structures, especially those which operate under extreme conditions. Usually, the ET is performed by using cheap and readily available explosives, it can be applied both under field and factory conditions, or in erection sites for construction of large-sized structures. It requires no specialized equipment or highly skilled personnel, gives a high consistency of good results of its impact on a workpiece and has high cost effectiveness and productivity.

By means of the relatively small superposed charges of explosives the explosion energy is locally introduced into the most critical places of welded joints, i.e. weld and/or HAZ, where defects, geometrical stress raisers and high RS are concentrated and where metal properties can greatly vary as a result of the thermal-deformation welding cycle. The effective factors of the ET are a drastic decrease or favourable redistribution of RS, formation of a new system of RS and strengthening of metal to a considerable depth accompanied by its saturation with thermodynamically stable faults of a crystalline structure. These factors taken together open up wide possibilities for improvement of service properties of welded joints and metal structures as a whole. As proved by the practice, the ET provides a considerable increase in resistance of welded joints to fatigue, brittle and corrosion-mechanical fractures, in static strength, hardness, dimensional stability, etc.

Information on the effect of the ET on service properties of welded metal structures and examples of its practical application in industry are given in [2 – 4]. It should be emphasized that the ET advantageously complements the available technologies for postweld treatment of welded joints and is often superior to them in a combination of its effects, productivity, cost effectiveness and a possibility of the large-scale commercial application. It will suffice to say that the ET of the process tank facilities and pipings used in 1976 – 77 for construction of a large alumina factory «Birach» in Zvornik, Yugoslavia, made it possible to save over $US 4 mln. All this makes the ET of welded joints very attractive for a wide range of specialists involved in design, construction and/or service of industrial buildings and structures, as well as in application of welding in machine-building and the ET of metals. At present, the information on this new type of metal treatment in a generalized form and, thus, more accessible for specialists than numerous journal publications can be found in recently published papers [5 – 7].

Calculation of ET parameters. *Circumferential welds in axially symmetric metal structures.* When calculating parameters of explosive charges for the ET of the said joints, it is possible to ignore the shock-wave stage of metal loading and, instead, to limit ourselves only to analysis of the radial movement of the shell wall under the effect of an explosion pulse [5]. The problem is subdivided into two stages. Firstly, loads acting on the wall are determined, assuming that this wall is absolutely rigid, and, secondly, its movement under the effect of this load is calculated, and solved for a case of instantaneous detonation of the charge (axially symmetric loading). This approach is widely used, for example, for strength design of explosion chambers. If sizes of the shell or other circumstances prevent the location of explosive charges inside a shell structure, RS in circumferential welds can be relieved by means of two superposed charges located outside at some distance from a weld. The value of each of the charges can be approximately calculated from the known equations [2, 5, 6] (Figure 1). The diagram plotted is based on using explosion loading to induce circumferential plastic shrinkage strains in the heat-affected zones, where circumferential compressive RS are effective. A sufficiently large loading pulse can result in the formation in the explosion treated zone of larger residual deflections than the shrinkage strains in the weld zone, which causes a change in sign of RS in the weld. Wave processes in the

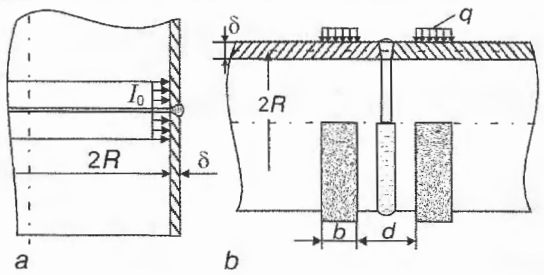

Figure 1. Schematics of ET of circumferential welds in thin-walled shells using internal (*a*) and external (*b*) explosive charges.

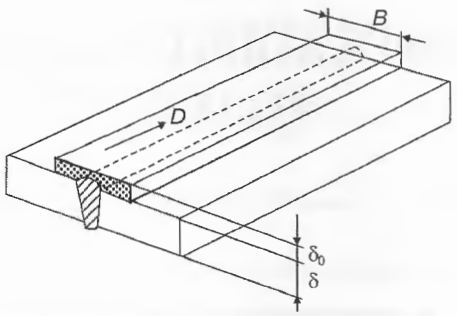

Figure 2. Typical location of an explosive charge in linear diagram of treatment of sheet structures: δ — sheet thickness, δ_0 — thickness of the explosive layer, *D* — explosive detonation rate.

pipe wall are ignored. A thin-walled cylindrical shell (δ — wall thickness; *R* — radius; I_0 — explosion pulse) with axially symmetric distribution of axial and circumferential RS is considered. The axially symmetric dynamic load during the ET is assigned by pressure *q* (Figure 1, *b*), distributed at the pipe regions of width *b* (d is the distance between them). The procedure used for numeric realization of the above deformation model is described in detail in [5]. Solution to the problem is found by successively tracing elastic-plastic strains, starting from a preset initial state. As a result, this makes it possible to predict the character of the effect of the force pulse parameters on the degree of a decrease in RS and to establish a criterion for simulation of the charge parameters to treat various dimensions of pipes or other types of the axially symmetric structures.

Calculation-experimental methods can be more efficient in this respect. One of them was developed to determine RS in circumferential zones of pipes subjected to a local ET using an external superposed charge [8]. For this, it is necessary to experimentally determine, using simple measurements, the distribution of residual elastic-plastic deflections in the generating line of a pipe within the short-range zone of the explosion using one circumferential explosive charge. The problem is solved analytically in a closed form using relationships of the theory of thin-walled shells also in its non-wave statement. It should be noted that using this geometry of explosion loading, it is possible to provide such a distribution of RS which is identical to that produced as a result of depositing a circumferential weld. This peculiarity of the ET is very important, if we take into account a substantial heterogeneity of the distribution in a direction of axes of the pipe and a poor reproducibility of the fields of RS induced by welding. The possibility of using the local ET of a pipe to simulate welding RS at a high degree of their reproducibility and uniformity of the distribution in the bulk of metal allows a scope of experimental studies intended for the development of means to prevent them to be fundamentally reduced. Also, it should be noted that such circumferential zones with RS formed by the ET is of independent interest, in particular in terms of avoiding extended fractures in pipelines. One of the versions of this purposeful treatment is considered in detail in [9].

Welded joints in sheet structures. In this case the effect of decreasing RS is caused mainly by changes in the physical and mechanical state of the explosion treated metal. In this connection, theoretical analysis of this version of the treatment, allowing for the necessity of investigating the shock-wave phenomena in metal, presents a more complicated problem. Chronologically, the initial approach was based on the theoretical-empirical phenomenology [10], which was developed as early as the beginning of the 1970s. This approach allows parameters of the explosive charges (B is the width of charge in the form of strip) for the ET of sheet weldments to be evaluated with sufficient accuracy by taking account of the peculiarities of their geometry (Figure 2). Later on, a physical mechanism of the phenomenon was suggested and experimentally proved in terms of an elastic-plastic model of the medium subjected to shock-wave loading in a unidimensional approximation [11]. This demonstrated the possibility that for a complete relief of RS it would be sufficient that pressure in the shock wave was 1.5 – 3 times in excess of the Hugonio elasticity limit, i.e. for low-carbon steels it was 1.6 – 3.3 GPa. The effect of a decrease in RS was explained on the basis of a stress trace formed in metal under shock-wave loading, induced by relaxation of tangential stresses.

Further investigations [12] made it possible to establish that a concept of the stress-strain trace (SST) interacting with the field of RS and strains in a long-range zone of the explosion and leading to their decrease in a weldment as a whole was more comprehensive. A more correct procedure for calculation of a residual stress-strain state of the metal subjected to local non-unidimensional explosion loading [13] is based on using the tough-elastic-plastic model of the medium with a constant toughness. Figure 3 shows the results of measuring the RS in a welded sheet of low-carbon steel (curve *1*: initial RS), allowing a comparison of the efficiency of relieving the RS by heat treatment (curve *2*: high tempering) and ET (curve *3*).

Analysis of interaction of residual stresses and strains induced by explosion loading and initially existing in metal, leading to the formation of a new stressed state of a welded joint as a whole, is done on the basis of a well-developed procedure [13] and normally causes no serious problems.

Measurement of RS. This operation is very important and, at the same time, very labour-consuming and complicated. There are several methods intended for

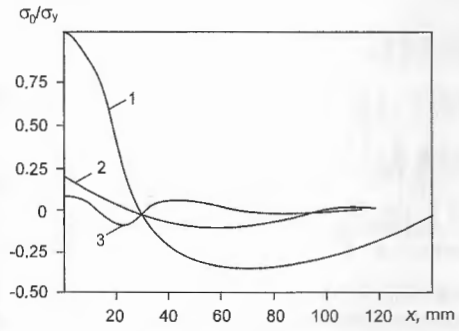

Figure 3. Diagrams of longitudinal RS (σ_0) in butt welded joint in low-carbon steel: x — distance from the weld axis.

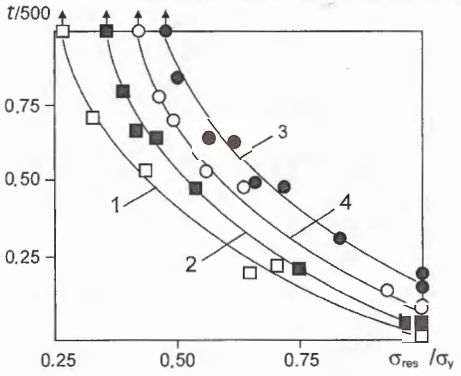

Figure 4. Life of explosion treated welded joints of steel St.3 (killed) in nitrate boiling solutions at different thickness δ: *1* — 6 – 8 mm; *2* — 10 – 14 mm; *3* — 16 – 22 mm; *4* — 24 – 30 mm (t — time to cracking, 500 h — test base).

measuring RS, including the so-called physical and mechanical (relaxation) methods [5].

Traditional mechanical methods which inevitably require partial or complete destruction of a workpiece are most reliable and accurate. But this presents problems in using them for measuring a stressed state of a metal structure under construction or in operation.

Non-destructive or physical methods used to measure RS are based on a dependency of certain physical characteristics of metal upon its stressed state and, as a rule, are associated with essential errors. Among them the typical one is a dependency of the measurement accuracy upon various external factors, such as the quality of surface preparation, structural state of a material investigated, presence of magnetic fields, temperature, etc. Whereas the effect of some of them can be eliminated by improving the measurement equipment and/or the measurement procedure, it is almost impossible to avoid the effect of the rest of the above external factors, while minimization of these effects is an independent and very complicated problem.

PWI developed two methods for non-destructive measurement of welding RS, requiring no destruction of a workpiece: modification of the magnetic-elastic method [14]; improved method for non-destructive mechanical strain measurement [15].

The suggested measurement methods and instruments designed for their application are characterized by simplicity, sufficient accuracy and good consistency of the results. They can be helpful for evaluation of the efficiency of some strain methods for reducing RS and development of the optimal conditions for loading structural elements for research and application purposes.

Some applied aspects of the technology. As far back as the late 1960s, it was proved by PWI that the use of the ET was an efficient means for improving the fatigue strength of welded joints. Later investigations concerning the successful utilization of the explosion energy to improve properties of welded structures confirmed that this method of treating welded joints had much wider capabilities. It was found, in particular, that the ET could relieve almost completely or redistribute the welding RS, and strengthen metal or alter its structure in a favourable manner during propagation of a shock wave through metal. Eventually, this appears in the formation of a peculiar SST in the metal adjoining the explosion treated zone. The SST is formed because of an intensive relaxation of tangential stresses and selective deformation of the metal behind the front of heterogeneous wave metal flows. The SST parameters were quantitatively estimated for a case of non-unidimensional loading of the elastic-plastic medium [11] and for the tough-elastic-plastic (relaxation) medium [12]. Peculiarities of interaction of the SST with the field of RS in a weldment as a whole were assessed in [13]. It can now be stated, with a sufficient level of confidence, that ET allows a marked improvement of the following service properties of welded joints and metal structures as a whole:

resistance to corrosion cracking in alkali (Figure 4) and hydrogen sulphide containing environments;

resistance to fatigue fracture (Figure 5);

probability and rate of development of plastic strains and fractures in welded joints at decreased temperatures and under static loading (Figure 6);

static strength of joints in light metal alloys;

resistance of welded joints to cracking during hydrogenation;

low-cycle fatigue life of large-sized coiled tanks as a result of removal of initial defects of a geometrical shape

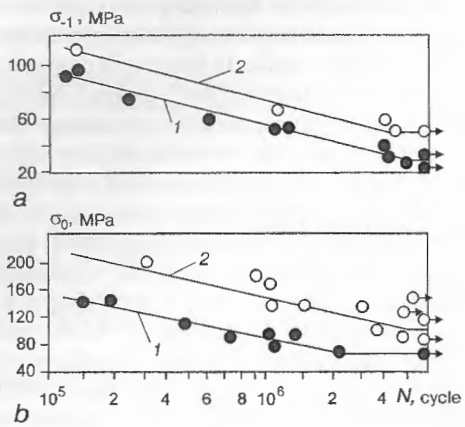

Figure 5. Results of fatigue tests of welded joints with a transverse stiffener before (*1*) and after (*2*) ET: *a* — steel 10G2S; $R_\sigma = -1$; *b* — steel M16S; $R_\sigma = 0$).

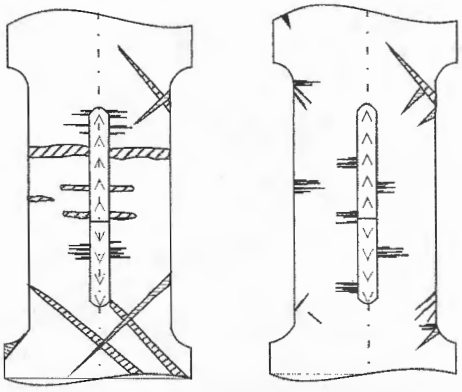

Figure 6. Yielding lines at a stress of 230 MPa in specimens of steel St.3 in the initial state (*a*) and after ET (*b*).

of the type of «angularity» of edges which close up the assembly joints.

Means for protection from side effects of the explosion. In metal working operations the explosion produces not only a beneficial effect (relieves RS, welds, strengthens, cuts, etc.), but also can have an adverse influence upon human and the environment, first of all through shock waves propagating from the explosion site. When the explosion occurs in open sites, there are shock waves. Therefore, to protect humans, buildings, structures, etc. from the shock waves, the blasting operations are performed either in special testing grounds away from cities and, thus, from metal working enterprises, or in the explosion chambers of various designs. However, both of these approaches are unsuitable when the ET is to be carried out on welded joints in large-sized structures in sites of their fabrication or erection.

Theoretical and experimental investigations conducted at PWI [16] have proved that the two-phase gas-containing media of a type of foam can be highly efficient and promising when used to suppress the air shock waves. In comparison with the single-phase media, the two-phase media allow a more effective absorption of the explosion energy by transforming it into thermal energy of a condensed phase (Figure 7).

Studies conducted in this area made it possible to develop a formal theory of the explosion gas dynamics in multiphase relaxing media. In terms of a physical model of the explosion phenomenon for a gaseous medium, this theory makes it possible to describe, on a single basis, the evolution of the explosion waves in media which are essentially differing in their structure and properties (gas, water, foam, sand, bubble media, snow, etc.) by using a minimum number of thermodynamic material constants. This theory allows a degree and speed of attenuation of the shock waves in various media, including gas-liquid foams, to be predicted with an accuracy which is sufficient for practical applications and, thus, allows selection of the media for creation of the efficient and cost-effective protective means to be substantiated from the scientific standpoint.

Now, such up-to-date methods for protection from the side effects of explosion often become an integral part of

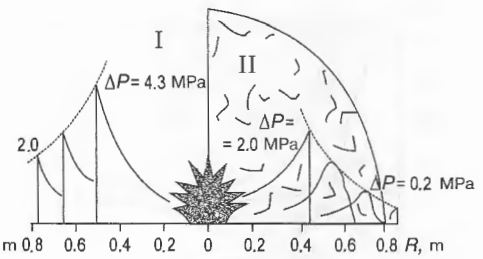

Figure 7. Evolution of the shock wave, initiated by explosion of 1 kg trinitrotoluene, at its propagation in air (*I*) and in mechanical water-foam (*II*): *R*— distance from charge centre.

the explosion metal working technologies. Making the explosion operations environmentally clean opens up new possibilities for employment of the explosion technologies, such as relief of RS, explosion cutting, etc., under special conditions (explosive atmosphere, closeness to other easily damaging structures, factory conditions, residential areas, etc.).

REFERENCES

1. Petushkov, V.G., Kudinov, V.B., Berezina, N.V. *et al. A method of welded joints workhardening.* USSR author's certificate **334880**, Int. Cl. C 22F 1/00. Publ. 10.01.72.
2. Petushkov, V.G., Kudinov, V.M. (1985) Explosion treatment of welded joints. *Avtomaticheskaya Svarka*, **7**, 1 – 7.
3. Petushkov, V.G. (1993) Residual stresses in explosion treated welded joints in steels up to 50 mm thick. Ibid., 7, 1 – 4.
4. Kudinov, V.M., Petushkov, V.G. (1973) The explosion treatment of welded joints, a new and effective method of improving the quality of structures. *Proc. of the Int. Symp. of Explosive Energy Used For Producing Metallic Materials With New Properties*, 333 – 337. Marianske Lazne.
5. Petushkov, V.G., Kudinov, V.M., Fadeenko, Yu.I. (1993) *Explosion treatment of welded joints in metal structures*. Moscow: Metallurgiya.
6. Petushkov, V.G. (1994) Explosion treatment of welded joints. *Weld. and Surfacing Reviews*. Edited by B.E. Paton. Harwood Academic Publishers.
7. Petushkov, V.G., Fadeenko, Yu.I. (1999) *Welding stress relief by explosion treatment*. Backbone Publishing.
8. Davydenko, A.V., Petushkov, V.G. (1983) Redistribution of an arbitrary system of stresses in a normal incident shock wave. *PMTF Journal*, **2**, 98 – 102.
9. Petushkov, V.G. (1992) Simulation of residual welding stresses in pipes by local explosion treatment. *Avtomaticheskaya Svarka*, **7 / 8**, 6 – 9.
10. Kudinov, V.M., Trufyakov, V.I., Petushkov, V.G. *et al.* (1976) Parameters of explosive charges for relieving residual stresses in butt welded joints. Ibid., **1**, 46 – 49, 61.
11. Petushkov, V.G. (1988) Methods for determination of parameters of explosion treatment of welded joints in metal structures. *FGV Journal*, **1**, 107 – 114.
12. Petushkov, V.G., Grishaenko, A.I. (1997) Calculation of the stressed state of a solid body subjected to local explosion treatment. Ibid., **6**, 92 – 101.
13. Petushkov, V.G. (1986) Formation of residual stresses in welded joints at explosion treatment. *Problemy Prochnosti*, **12**, 37 – 40.
14. Petushkov, V.G., Bryzgalin, A.G., Titov, V.A. (1992) Estimation of metal structures stressed state by magnetic-elastic method. *Avtomaticheskaya Svarka*, **5**, 15 – 18.
15. Petushkov, V.G. (1978) Nondestructive method for determining residual stresses (connection between observed decrease in strain and the magnitude of residual stress reduction). *Strength of Materials*, **10**, 1224 – 1228.
16. Petushkov, V.G., Palamarchuk, V.I., Malakhov, A.T. (1995) Shock waves and their suppression by foam at explosion treatment of welded joints. *Avtomaticheskaya Svarka*, **1**, 51 – 52.

EFFECT OF COMPOSITION OF SHIELDING GASES ON TECHNOLOGICAL CHARACTERISTICS OF ARC DURING NON-CONSUMABLE ELECTRODE WELDING OF ALUMINIUM ALLOYS

A.Ya. ISHCHENKO, V.P. BUDNIK, A.G. POKLYATSKY and **A.A. GRINYUK**
The E.O. Paton Electric Welding Institute, NASU, Kyiv, Ukraine

ABSTRACT

Experiments on using neon and its mixtures with argon as a shielding gas in non-consumable electrode welding are considered. Data are obtained on weld formation, penetration and also volt-ampere characteristics at direct and alternating currents. The feasibility of using neon separately or in mixtures of gases for protection of aluminium alloy welding zone is shown.

Key words: *arc welding, non-consumable electrode, shielding gases, aluminium alloys, volt-ampere characteristics, weld formation.*

When aluminium alloys are welded with the help of arc methods, the argon, helium or their mixtures are used as shielded gases. Argon is usually used in AC welding, while helium is used in DCSP welding. The latter is best for the oxide film destroying in the weld pool [1]. Other inert gases do not find at present application in aluminium alloy welding. At the same time, it is possible to produce helium together with neon, for example, from air, where at the first stage of its decomposition in the technological line the comparatively cheap helium-neon mixtures with 3 – 25 % of neon content are formed.

In some arc welding methods the use of pure helium is also justified technologically, in spite of its high cost. To make the welding process cheaper and to increase the quality of joints the helium-argon mixtures are sometimes used. Helium-neon mixture formed in gas production is cheaper than the pure helium. Therefore, its application instead of helium could make the welding processes cheaper, improve the quality of joints and increase the depth of metal penetration.

For this purpose, it is reasonable to investigate the operational properties of shielding media of mixtures made from conventional gases with neon and to evaluate the rationality of their use in welding processes.

As to its physical characteristics the neon occupies the intermediate position between argon and helium and, in comparison with argon, it has to increase the heat power of the arc [2] (Table).

The effect of composition of shielding gases on volt-ampere characteristics, formation and quality of weld metal surface during non-consumable welding at direct current of straight polarity and alternating current was investigated. Helium, argon, neon and their mixtures were used as shielding gases. In all cases beads were deposited without through penetration and filler wire using 10 m/h constant speed. The peculiarities of weld formation were examined by an appearance and measurement of sizes of penetration zone (H_p is the depth of penetration; B_w is the weld width) on macrosections using a toolmakers' microscope.

Welding at a straight polarity current

The 10 mm thick plates from alloy 1201 were deposited at 150 – 200 A current. In this case a depth of penetration was provided which is close to the thickness of the parent metal, thus allowing the effect of examined factors to be effectively revealed. A distance between the specimen and cathode (length of arc gap, L_a) was set equal to 0.3 and 1.2 mm. Helium, neon, mixture of He + 15 % Ne were used for shielding. As a rule, an argon is not used at the mentioned method of welding. However, it was taken for comparison. The effect of the shielding gas on the arc gap voltage can be evaluated from experimental data (Figure 1). It is seen that the relationships are strict. The change in welding current within the accepted range does not influence the voltage that is also confirmed by the reference data [3, 4]. The small growth in arc voltage can be explained by arc deepening into the parent metal with the welding current increase.

Maximum values of arc voltage are observed in helium welding. Voltage in mixture He + 15 % Ne is lower, while in neon it is much lower. As was to be expected, the arc voltage was minimum in argon welding. These facts can be explained by corresponding potentials of ioni-

Physical characteristics of inert gases [2]

Parameter	*He*	*Ne*	*Ar*
Density, kg/m^3	0.1785	0.8990	1.7840
Potential of ionization, eV	24.59	21.56	15.76
Coefficient of heat conductivity, W/(m × °C)	0.1430	0.0468	0.0167
Specific heat conductivity, J/(kg × °C)	5190	1030	520
Atomic mass	4.003	20.183	39.944
Radius of atom, nm	0.125	0.162	0.192
Boiling temperature, °C	–268.98	–246.03	–185.87
Content in air, vol. %	0.00052	0.00182	0.93400

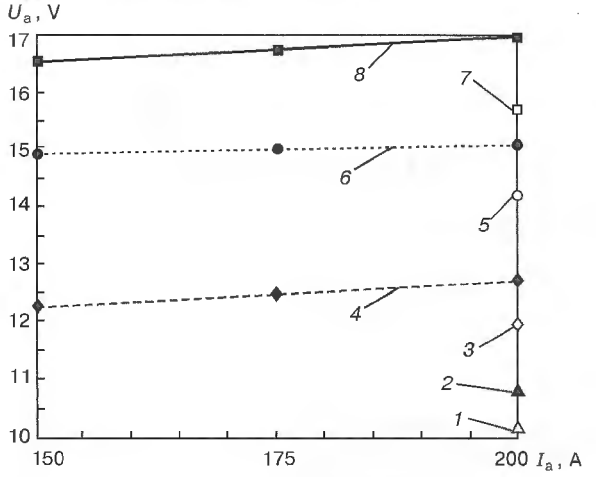

Figure 1. Value of voltage of DCSP arc at $L_a = 0.3$ (*1, 3, 5, 7*) and 1.2 mm (*2, 4, 6, 8*) in argon (*1, 2*), neon (*3, 4*), mixture He + 15 % Ne (*5, 6*), helium (*7, 8*).

zation of gases. High arc voltage in neon allows the arc power and heat input to the parent metal to be increased, thus approaching it to helium by this characteristic. The voltage increase at extension of the arc gap length is explained by an elongation of the arc column and corresponding voltage drop at it.

The weld surface quality was evaluated by an appearance. In argon welding the weld surface is dark due to a low-quality cleaning. Attempts to perform argon welding with a complete penetration of the parent metal do not provide the quality weld as a rule, because of unproper weld pool cleaning from the oxides [1]. The application of neon during weld deposition cleans satisfactory the weld surface. Welding in a mixture gives similar results. However, the best quality of the pool cleaning from the oxides and weld formation is attained by using helium.

In all versions the weld formation is typical for the process of welding at a straight polarity current. Geometric parameters of the weld depend mainly on the power input to the metal, which is determined by the arc voltage, providing all the rest parameters similar [5]. As the type of the gas influences the arc voltage, then this can explain

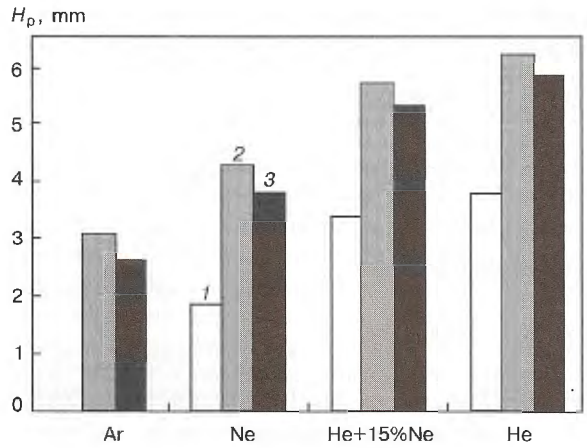

Figure 2. Effect shielding medium composition on penetration depth in welding at straight polarity current: *1* — $I_a = 150$ A, $L_a = 1.2$ mm; *2* — $I_a = 200$ A, $L_a = 1.2$ mm; *3* — $I_a = 200$ A, $L_a = 0.3$ mm.

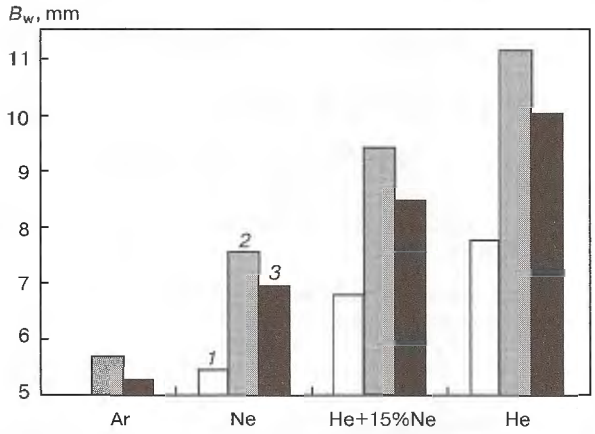

Figure 3. Effect of shielding medium composition on weld width in welding at straight polarity current (designation are given in Figure 2).

the results obtained (Figures 2 and 3). The largest depth of penetration is observed, respectively, in helium welding. In argon welding it is minimum and the neon gives the intermediate values. Addition of neon to helium. i.e. welding in mixtures of gases, increases the depth of penetration and makes it similar to welding in a pure helium.

Weld formation depends also on the arc gap. During its changing the opposite-directed processes proceed in the weld pool. The decrease in the arc gap leads to the arc deepening into the parent metal, increase in energy concentration in an anode spot and increase in a heat generation in the metal, thus contributing to the increase in penetration and reduction in weld width. At the same time, here, the decrease in voltage drop and in power share in the arc column is observed, thus decreasing the amount of heat transferred by it to the weld pool [5, 6]. Evidently, the action of the second process dominates in this case. Therefore, the decrease in the arc gap length from 1.2 to 0.3 mm leads to the reduction in the penetration gap.

Similar situation is observed during evaluation of the effect of welding parameters on the weld width. The change in welding parameters and type of the gas leads to the change in the arc power and weld width (Figure 3). The decrease in arc gap length leads to some arc deepening to the parent metal and reduction in power that decreases the thermal action of arc on the weld periphery.

The change in weld geometry depending on the type of the shielding gas is seen in macrosections (Figure 4). Minimum volume of the weld pool is typical of welding in argon, the maximum volume — in helium. The pool volume and geometric characteristics of weld in neon welding occupy the intermediate position.

Process of AC welding

During AC welding the 6 mm thick plates of alloy of Al–Cu–Li system were used. The set length of the arc gap was 2 and 4 mm. These sizes were selected to have a favourable weld formation. Power source MW-450 of «Fronius» company was used. To study the effect of gas on the weld formation the welding current was varied within 125 – 190 A and in construction of volt-ampere characteristics it was varied within the wider range 10 –

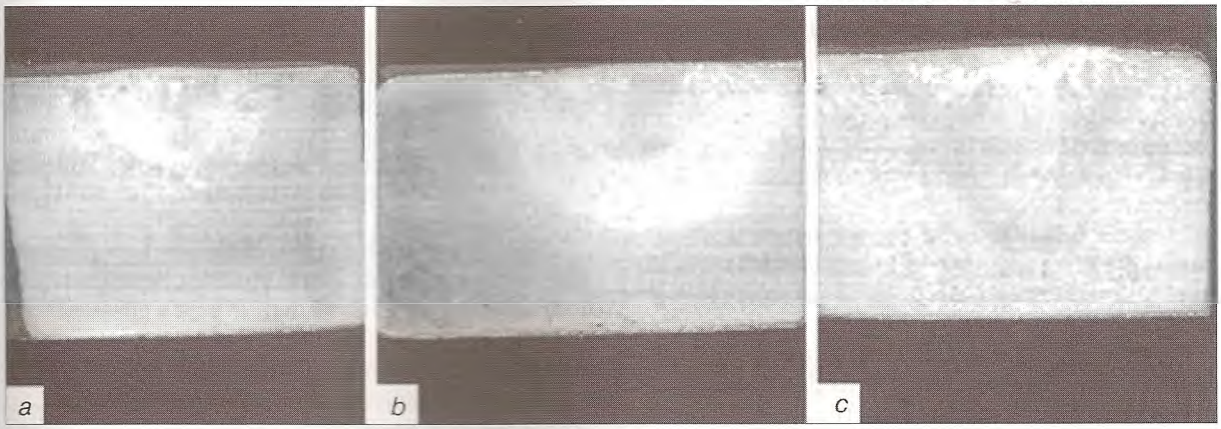

Figure 4. Effect of shielding medium composition on weld formation in welding at straight polarity current in argon (*a*), neon (*b*), helium (*c*) (×3.5) (reduced by 0.75).

190 A. The frequency of the alternating current was 250 Hz. Here, they proceeded from the fact that at widely-used frequency of 50 Hz the welding process is much more instable due to frequent breaks of the arc during current impulse transition through zero. Argon, neon and their mixtures were used as shielding gases.

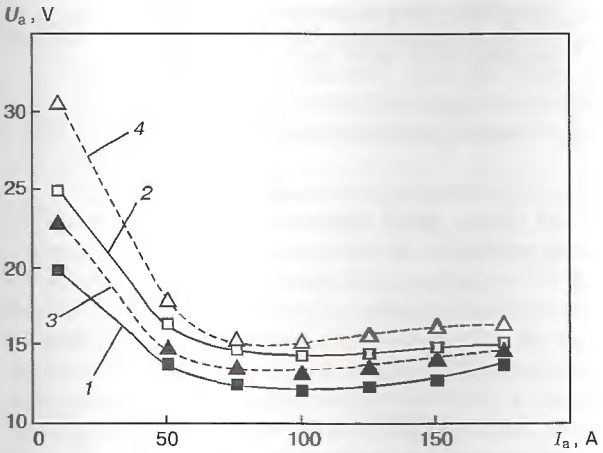

Figure 5. Volt-ampere characteristics of AC arc at L_a = 2 mm (*1*, *3*) and 4 mm (*2*, *4*) : 1, *2* — in argon; *3*, *4* — in neon.

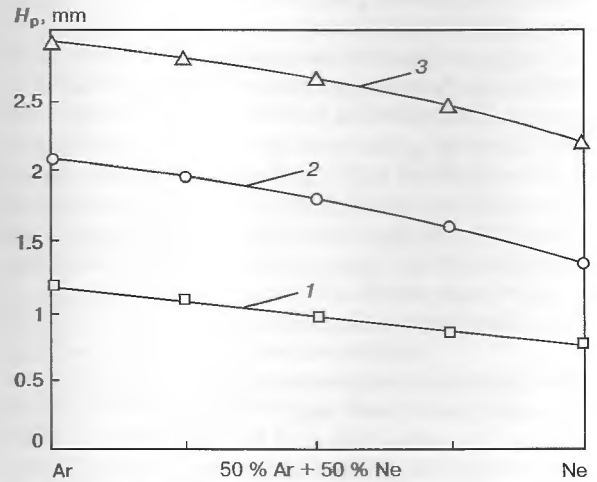

Figure 6. Effect of shielding gas medium on penetration depth in AC welding (L_a = 2 mm): *1* — I_a = 150 A; *2* — 175 A; *3* — 190 A.

Volt-ampere characteristics in AC welding are similar for all the gases examined (Figure 5). At current up to 60 A they are falling, but they are rigid at 60 – 120 A. At further increase in current the characteristics have a gently rising nature. The arc voltage in neon is higher than that in argon. During welding in mixtures the characteristics occupy the intermediate positions. The effect of neon causes the arc voltage increase. In this case the characteristics occupy the maximum position.

Taking into account that the energy characteristics of the arc in neon are higher than those in argon the life of tungsten electrodes was studied during AC welding. This was evaluated by the condition of the working surface during fusion. Increase in neon percentage in mixture in-

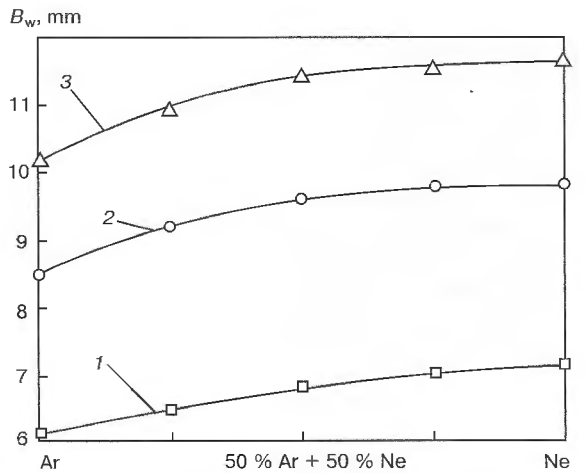

Figure 7. Effect of shielding medium composition on weld width in AC welding (designations are given in Figure 6).

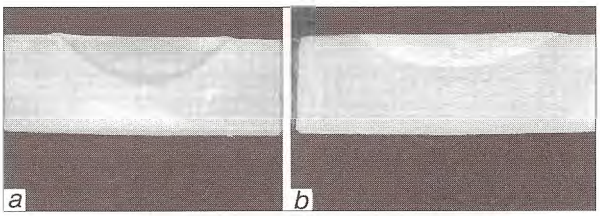

Figure 8. Effect of shielding medium composition on weld formation in AC welding in argon (*a*) and neon (*b*) at I_a = 190 A, L_a = 4 mm (×2) (reduced by 0.50).

creases the heat load on the electrode, thus increasing the extent of electrode fusion and decreasing its life.

The quality of weld surface, as to the appearance, is changed negligibly at neon addition to the shielding mixture up to 100 %. Both in pure argon welding and in neon application the weld surface is clean without any films or exogenous inclusions.

Figures 6 and 7 show relationships of weld geometric characteristics using various gases. The following features of the welding process using power source MW-450 (50 V open-circuit voltage) should be noted. The use of neon, having a higher potential of ionization, leads to instability of arc burning during transition of impulses to half-periods of a reverse polarity. The application of AC power sources, having higher open-circuit voltage, for example UDG-501 type, provides high stability of the welding process if the neon content in mixture with argon does not exceed 50 – 60 %. This can explain the decrease in the penetration depth at growing the neon percentage in its mixture with argon. At the same time the weld width is somewhat increased.

Macrosections of specimens (Figure 8) illustrate the formation of welds in AC welding. As compared with the current of a straight polarity an increase in weld width-depth ratio and comparative decrease in penetration are observed in this case [7].

CONCLUSIONS

1. Cost of helium-neon mixture with 3 – 25 % neon content, formed in decomposition of gases, is lower than that at their finer separation. The use of such mixture as a shielding gas is feasible in welding aluminium alloys with a non-consumable electrode both at AC and DCSP.

2. Energy characteristics of the arc in neon, and also in mixtures with argon or helium occupy the intermediate position as compared with the arc in pure argon or helium.

REFERENCES

1. Budnik, V.P. (1994) Effect of type of inert gas on pool temperature and oxide film destroying in aluminium welding. *Avtomaticheskaya Svarka*, **1**, 16 – 18.
2. (1985) *Properties of elements*. Edited by M.E. Drits. Moscow: Metallurgia.
3. (1974) *Technology of electric welding of metals and alloys by fusion*. Edited by B.E. Paton. Moscow: Mashinostroyeniye.
4. Rozarenov, Yu.M. (1987) *Equipment for electric fusion welding*. Moscow: Mashinostroyeniye.
5. Topchii, Yu.K., Kamenev, V.P. (1974) Equipment for determination of potential distribution in arc at non-consumable electrode. *Svarochnoye Proizvodstvo*, **1**, 51 – 52.
6. Ivanov, O.N., Fan Van Lan, Rabkin, D.M. (1977) Effect of composition of shielding gas medium on current density in anode spot of the welding arc. *Avtomaticheskaya Svarka*, **1**, 70.
7. Budnik, V.P., Steblovsky, B.A., Butsko, M.G. *et al.* (1982) Penetrability of AC and DC arc. Ibid., **8**, 68 – 70.

MATHEMATICAL MODELLING OF THERMAL STATE OF THE BONDING ZONE BETWEEN DISSIMILAR METALS IN GLOW-DISCHARGE DIFFUSION BONDING

G.P. BOLOTOV, D.I. KOTELNIKOV and A.F. ROGOVOJ
Chernigiv Technological Institute, Ukraine

ABSTRACT

The determinate mathematical model of the ion heating process has been developed on the basis of analysis of distribution of heat flows within the zone of contact between dissimilar materials. The model allows temperature of the bonding zone in bodies of the simplest shape (cylinder, parallelepiped) to be related to the process parameters and characteristics of the billets. The error in the calculation of temperature using this model is no more than 15 %.

Key words: *diffusion bonding, dissimilar metals, glow discharge, heating, modelling.*

Diffusion bonding in the glow-discharge plasma of medium pressures (4 – 15 kPa) in inert and active gases is used to manufacture comparatively small parts from similar and dissimilar metals and parts with sufficiently large mating surfaces, such as hard-alloy bonded dies and ultrasonic magnetostictive transducers [1]. The glow discharge used as a heat source is characterized by a slight dependence of the heating intensity upon the shape of billets joined, which provides a uniform and well-controlled heating of the joining zone in bonding pieces of various shapes.

Diffusion bonding is done at temperatures of 0.5 – 0.7 of the melting point of materials being joined, which makes it possible to produce parts with a minimum residual strain. As shown by numerous experiments [2], dependence of strength of the joint upon the bonding temperature is of an extreme character (Figure 1), as the maximum strength can be achieved within a sufficiently narrow range of heating temperatures. Therefore, a special consideration in diffusion bonding is given to the accuracy of maintaining the temperature conditions and methods used to control the temperature [3]. However, the high temperature and emission of the glow-discharge plasma hamper the control of a thermal state of the bonding zone using both contact (thermocouples) and contactless (optical and photoelectric pirometers) methods, which limits the capabilities of the efficient control at different stages of the process. At the same time, energy of the glow discharge consumed for haating of the billets joined is determined by parameters of the process: current and voltage of the discharge, and pressure and kind of the plasma gas, which allows an indirect control of the heating temperature by characteristics of the discharge and materials joined, i.e. on the basis of a mathematical model of occurrence of the thermal process in time.

The glow discharge is a heat source characterized by normal distribution of the heat flow in the cathode spot of the discharge located on a side surface of the billets joined. The wire-type anode which approximately copies contours of cross-sections of the billets is installed at a distance of $(5 - 20) \times 10^{-3}$ m from the surface near the zone of their contact (Figure 2). In this case the cathode spot of the discharge through which the energy is fed to the billets joined is a strip closed on the perimeter of the billets, whose width is determined by the concentration coefficient which under the bonding conditions is equal to $K = 0.2 - 0.5$ cm^{-2}, depending upon the discharge current and the gas pressure. This strip-type source may be replaced by a concentrated circular source [4] acting on the perimeter of the contact zone of the billets the heat of which has been fed by a time period t_0 earlier. Duration of $t_0 = 1 / 4aK$ for the above values of the concentration coefficient of different metals with thermal diffusivity from $a = 6 \times 10^{-2}$ cm^2 / s for titanium to 0.96 for copper is $t_0 \approx 1 - 20$ s.

As noted above, the glow discharge as a heat source is efficient for joining diverse sizes and shapes of pieces. Since capacities of the currently used industrial and laboratory units are as a rule not higher than 10 kW (which is attributable to a decrease in stability of the discharge at an increased power), sizes of the billets within the heating zone are limited to an actual or reduced (for bodies of an arbitrary shape) diameter of $2R < 0.1$ m. For such pieces the Biot criterion $Bi = \alpha R / \lambda$ (α is the convective surface heat exchange factor the value of which at mean heating temperature of $T = 873 - 973$ K is $\alpha = 60 - 80$ W/(m^2×K)

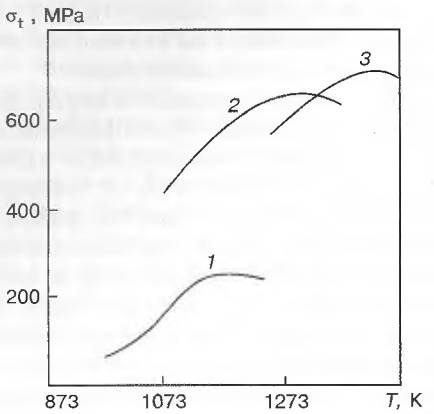

Figure 1. Dependence of strength of a bond upon the bonding temperature: *1* — copper M1; *2* — steel 45; *3* — alloy EI-602.

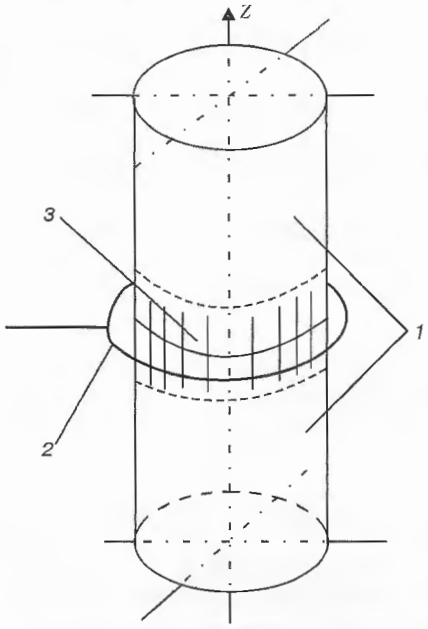

Figure 2. Diagram of heating in glow-discharge bonding: *1* — cathode (billets bonded); *2* — anode; *3* — cathode spot of the discharge (heating spot).

[4] and λ is the thermal diffusivity of the piece material at the same temperatures) that characterizes thermal resistance of the bodies in a direction of action of the outward heat flow is insignificant, Bi ≤ 0.25. This suggests that these pieces are «thin» from the heat engineering standpoint [5]. They are characterized by the dominant distribution of heat from the surface, where the source is effective, in a radial direction deep into the piece, and by a sufficiently uniform heating across its section. According to [4], the process of levelling of temperatures in a thin round disk, which is the contact zone of the billets, due to the effect of an instantaneous circular source arranged in the form of a circumference with radius R on the surface of the billets joined can be described by the following function:

$$\Phi(r, t_1) = \sum_{k=1}^{\infty} \frac{J_0\left(\mu_k \frac{r}{R}\right)}{J_0(\mu_k)} \exp\left(-\mu_k^2 \frac{a t_1}{R^2}\right), \qquad (1)$$

where μ_k are the roots of equation $J_1(\mu_k) = 0$; J_0 and J_1 are the Bessel's functions of the first kind and of the zero and first orders and r is the current radius.

As it follows from (1), duration of heating the section t_1 is determined by the radius of the billets joined and their thermal diffusivity and is characterized by a dimensionless time (Fourier criterion) $\tau = at_1 / R$. Heating the section close to being uniform, where the gradient of temperatures between surface and central regions of the billets is not higher than 5 %, occurs according to relationship $\Phi(r, t_1)$ from Figures 17, 21 in [6] at $\tau \geq 0.25$. The latter condition in real time allows estimation of the time of through heating of the joining zone, which is $t_1 = 0 - 40$ s for the above materials and sizes of the billets. Therefore, it can be suggested that a plane heat source will be formed in a time period of t_1 with regard to the moment of actual ignition of the glow discharge in a plane of contact of the billets ($Z = 0$).

Variations in temperature within the joining zone between the similar materials billets, caused by the effect of the instantaneous plane heat source located in this zone, in the case of symmetrical heat sinking, can be described by the following relationship:

$$dT = \frac{q dt}{2F\sqrt{\pi\lambda c\rho t}} \exp(-bt), \qquad (2)$$

where q is the discharge power; F is the cross section area of the billet; $c\rho$ is the volume heat capacity of the billet material and t is the heating time.

As the time of heating with the glow discharge for different conditions is $(3 - 12) \times 10^2$ s, it is necessary to take into account heat transfer to the environment at the surface of the billets joined, which is shown in expression (2) in terms of thermal diffusivity

$$b = \frac{\alpha P}{c\rho F} (c^{-1}),$$

where P is the perimeter of the cathode (billets joined).

For joining dissimilar metals, where the use of diffusion bonding proves most efficient, expression (2) should take into account the uniformity of distribution of the heat flows (from the zone where the assumed source is effective to the billets joined), which is determined by the difference of both thermal-physical properties of the materials heated, characterized by the heat accumulation coefficient $\sqrt{\lambda c\rho}$ [7], and their cross section area within the contact zone.

In the case of the instantaneous plane source with power q, acting at the interface of $Z = 0$, heat q_1 and q_2 will transfer to the billets joined, respectively, on condition that $q_1 + q_2 = q$.

It follows from this condition, as well as from the conditions of equality of temperatures of the mating ends of the billets that

$$q_1 = q \frac{F_1\sqrt{\lambda_1 c_1 \rho_1}}{F_1\sqrt{\lambda_1 c_1 \rho_1} + F_2\sqrt{\lambda_2 c_2 \rho_2}}. \qquad (3)$$

Expression for the flow of q_2 is of a similar type (except for indices in the numerator that change).

To determine increase in temperature within the zone of contact of dissimilar metals in the case of a continuous plane source, transform (2) allowing for (3) and integrate the resulting expression in an interval from 0 to t_h

$$T(t_h) = \frac{q}{\sqrt{\pi}\,[F_1\sqrt{\lambda_1 c_1 \rho_1} + F_2\sqrt{\lambda_2 c_2 \rho_2}]} \int_0^{t_h} \frac{\exp(-bt)}{\sqrt{t}}\, dt, \qquad (4)$$

where $t_h = t + t_0 - t_1$ and t is the current time.

To simplify it, assume b, t_0 and t_1 in expression (4) to be the arithmetic means of the corresponding values of the materials joined. This simplification appreas to add certain errors to the calculation dependence, but since the temperature transfer coefficients for different metals dif-

fer just slightly and the values of the given time constants constitute an insignificant part of the total heating time, it can be considered acceptable.

As it is impossible to take the integral in expression (4) in its explicit form, the solution can be found either by expansion into a Taylor series with a termwise integration [8], or by replacement of the integration limits in order to reduce it to the error function, the values of which are tabulated [7] or can be calculated by approximation using the rational functions [9]. In the second case the intergand has the following form:

$$\int_0^{\sqrt{bt_h}} \frac{\exp(-bt)}{\sqrt{t}}\,dt = \frac{2}{\sqrt{b}}\int_0 \exp(-x^2)\,dx = \sqrt{\frac{\pi}{b}}\,\mathrm{erf}(\sqrt{bt_h})\,. \qquad (5)$$

In the above expressions, the power of the discharge introduced into the billets joined, which has the following form:

$$q = \eta I_p U_p\,, \qquad (6)$$

in a general case is determined by the discharge current I_d and by the voltage drop at the electrode spacing, U_d, i.e. parameters which are controlled and can be readily regulated during the bonding process; η is the net efficiency of heating using the glow discharge (for argon $\eta = 0.75 - 0.80$).

Allowing for (5) and (6), expression (4) will have the following form:

$$T(t_h) = \frac{\eta I_d U_d}{\sqrt{b}\,[F_1\sqrt{\lambda_1 c_1 \rho_1} + F_2\sqrt{\lambda_2 c_2 \rho_2}]}\,\mathrm{erf}(bt_h)\,. \qquad (7)$$

Experimental validation of adequacy of the developed model was done by results of heating components of the cylindrical samples steel 12Kh18N10T — copper MB and steel 12Kh18N10T — titanium alloy VTZ-1, using the glow discharge in the argon atmosphere. The samples had a diameter of 0.028 m, and their length was 2.5 times larger than their diameter. This makes it possible to consider the distribution of heat to be uniform along the billets, and use expression (7) characterizing heating two semi-infinite mating bodies with the plane heat source to estimate temperature of the joining zone. The temperature of the contact zone was controlled using a chromel-alumel thermocouple installed at the centre of the sample (Figure 3). To decrease the measurement errors, the thermocouples were attached to each pair of metals in a sample with a lower thermal resistance (copper and steel, respectively). Heating was done following the diagram shown in Figure 2. The anode was a steel wire ring and the electrode spacing was 0.006 m. For the first pair of the samples heating was done at a discharge current of 6 A and the second — at 4 A. The pressure of gas in the chamber was 13.3 kPa. In the calculation dependencies the values of thermal-physical characteristics of the materials joined were assumed to be corresponding to those at a temperature of 873 K.

The value of the current temperatures of heating determined experimentally by the results of five experiments for each pair of the samples and those obtained by calculations are indicated in Figure 3, *b*. It follows from this Figure that the calculated values of the temperature are close to the actual values, being ahead of them by 40 – 90 K for copper-steel samples and 70 – 190 K for titanium-steel samples at different stages of heating.

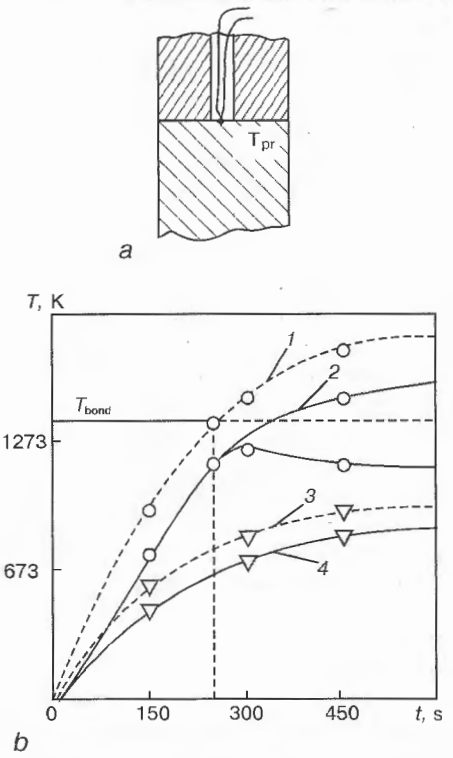

Figure 3. Diagram of control of temperatures (*a*) and character of their variations within the contact zone (*b*) in dissimilar rod-type samples (heating parameters are given in the text): T_c — point of connecting the thermocouple; *1*, *2* — steel 12Kh18N10T — alloy VTZ-1; *3*, *4* — steel 12Kh18N10T — copper MB; dotted curve — calculation; solid cirve — experiment.

While developing the model, no such task was posed as to use it to estimate the distribution of temperatures in the plane of the contact, since, as it was noted above, for the earlier indicated materials and standard sizes of billets the parts bonded are classed with the «thin» ones in terms of heat engineering, characterized by an insignificant temperature gradient across the section in surface heating. Levelling the temperatures is aided also by a comparatively low density of energy of the glow discharge and a substantial heating time.

Upon reaching the bonding temperature, to avoid overheating, the power of the glow discharge is decreased by decreasing the discharge current to a value required to ensure the preset thermal parameters of the parts at a stage of isothermal holding. The power of the discharge required for this stage can be determined by assigning in (7) the bonding temperature instead of $T(t_h)$ and by taking the heating temperature to be $t_h \to \infty$. In this case the error function $\mathrm{erf}(\sqrt{bt_h}) = 1$, which corresponds to the limiting thermal state of the heating zone.

For the titanium-steel samples used in the experiments, this state at a bonding temperature of $T_{bond} =$

= 1373 K can be achieved (according to the calculation results obtained using expression (7) at erf ($\sqrt{bt_h}$) = 1) by decreasing the discharge current to 2.8 A at a heating time of $t_h \approx 240$ s. The character of variation in temperatures within the joining zone after correction of the discharge power is also shown in Figure 3.

New designs are available now [10], which provide a substantial increase in the power of the glow discharge without any degradation in its stability. They allow joining of billets of considerable dimensions, having a marked thermal resistance within the heating zone. An increase in dimensions of the parts joined makes inefficient the use of the suggested diagram of heating with the glow discharge as a plane heat source, as it causes an increase in the temperature gradient between the surface affected by the actual heat source and the central regions, which requires the use of the calculation methods, allowing the temperature fields in the contact plane of the billets to be estimated during the heating process.

CONCLUSIONS

The process of heating in glow-discharge bonding of extended billets (cylinder, parallelepiped, etc.) from dissimilar metals, the transverse sizes of which allow nonuniformity of temperatures across their sections to be neglected, can be reduced to a diagram of heating semi-infinite bodies with a plane heat source acting within their contact zone, the power of the source corresponding to that released by the glow discharge at a side surface of the billets, allowing for the net efficiency of heating.

Error of the suggested diagram of heating at temperatures close to the bonding ones is 11 – 16 % and can be decreased by adding to the calculation dependence a correction factor equal approximately to 0.85 – 0.9. In this form, the developed model can be recommended for prediction and control of a thermal state of the joining zone between dissimilar metals in glow-discharge bonding.

REFERENCES

1. Kotelnikov, D.I. (1981) *Glow-discharge pressure bonding*. Moscow: Metallurgiya.
2. Kazakov, N.F. (1968) *Diffusion bonding in vacuum*. Moscow: Mashinostroyeniye.
3. Chistyakov, Yu.A., Gorysheva, E.V. (1982) Errors in measurement of temperature in diffusion bonding. *Svarochnoye Proizvodstvo*, 7, 11 – 12.
4. Rykalin, N.N. (1951) *Calculations of thermal processes in welding*. Moscow: Mashgiz.
5. Pekhovich, A.I., Zhydkikh, V.M. (1968) *Calculation of thermal parameters of solid bodies*. Leningrad: Energiya.
6. (1970) *Theoretical principles of welding*. Edided by V.V. Frolov. Moscow: Vysshaya Shkola.
7. Karslow, G., Eger, D. (1964) *Thermal conductivity of solids*. Moscow: Nauka.
8. Chernysh, V.P., Bolotov, G.P., Kotelnikov, D.I. *et al.* (1984) Calculation of heating temperature in glow-discharge diffusion bonding. *Avtomaticheskaya Svarka*, **9**, 54 – 56.
9. (1979) *Special functions handbook*. Edided by M. Abramovits, I. Stigan. Moscow: Nauka.
10. Bolotov, G.P., Satyukov, A.I. (1998) Increase in stability of high-current glow discharge under bonding conditions. *Avtomaticheskaya Svarka*, **1**, 18 – 21.

IMPROVEMENT OF HEAT AND WEAR RESISTANCE OF PARTS USING THE METHOD OF THERMAL SPRAYING OF COATINGS OF CHROMIUM-BASED ALLOYS

V.F. GORBAN
I.M. Frantsevich Institute for Materials Science Problems, NASU, Kyiv, Ukraine

ABSTRACT

Effect of initial state of chromium-based materials used for thermal spraying on the properties of coatings is investigated. Interrelation between physical-chemical properties of coatings and technology of spraying and their effect on service characteristics of chromium coatings are studied.

Key words: *thermal spraying, wear, coatings, chromium-based alloys.*

Chromium, due to its high heat and wear resistance, finds a wide application in different electrolytic coatings. Application of thermal coatings on the chromium base is limited until now because of a lack of industrial methods of producing quality materials for spraying.

The use of methods developed at the I.M. Frantsevich Institute for Materials Science Problems of NAS of Ukraine for the improvement of ductility of refractory metals [1 – 3] made it possible to develop the compositions of alloys and technologies and to produce materials in the form of rods, flexible cord [4] and powder [5].

The present work was aimed at the investigation of effect of thermal spraying methods on the formation processes and service characteristics of coatings made from chromium-based alloys.

The coatings were deposited by the methods of flame, plasma and detonation spraying on cast iron without using intermediate sublayers. The thickness of coatings was from 0.3 to 0.6 mm. The chromium alloy 4 mm diameter rod and granulated powder of 20 – 160 μm fractions were used as initial material. Structure of coatings was examined by scanning and transmission electron microscopy. Composition of coatings was controlled by a chemical analysis and Auger-spectroscopy. The phase analysis was made by X-ray examination in «Dron-4» installation using Cr-K_α radiation. To measure microhardness the instrument PMT-3 at 1 and 10 N loading was used. The adhesion strength was determined by an adhesion method on specimens of 25.4 × 25.4 mm diameter, that corresponds to standard ASTM C6 3-79. Total porosity was determined on coatings, separated from a substrate, in accordance with GOST 18898–89. The wear of chromium coatings was examined on high-strength cast iron of grade VCh-42-12 (HB 2.5 – 2.7 GPa) in the condition of a boundary lubrication using equipment of a face friction. The procedure of testing is described in [6]. The coating was deposited on specimen of 1 cm^2 area. Investigations were performed at 3 – 14 m/s sliding rate, 1 – 6 MPa pressure and 298 and 473 K temperatures.

To determine an effect of a size of initial particles on characteristics of coatings, they were deposited by spraying with powder of different fractions. Coatings were deposited by a supersonic air-gas plasma as the most efficient and economic method of spraying. [7].

Table 1 shows some characteristics of plasma coatings depending on a fraction composition of the powder.

The powder fraction greatly influences the characteristics of coatings. Microhardness, porosity and roughness of surfaces depend directly on the fraction. The finest fraction is characteristic of a maximum hardness and minimum surface roughness and also, porosity. At the same time the maximum adhesion strength is attained when 40 – 60 μm fractions are sprayed. The use of finer fractions leads to the fact that the adhesion strength of the coating is determined by cohesion characteristics which in this case are lower than the forces of coating adhesion with a substrate due to increase in the area of contact of oxidized surfaces.

The process of formation of structure of the thermal coatings is associated with a deformation of particles, gas saturation of the coating material with interstitial impurities, appearance of new chemical compounds or their decay, thus influencing the properties of the coatings.

For BCC metals the deformation, dispersion and solid-solution mechanisms are the main mechanisms of strengthening [2] whose action is also manifested in structure formation of thermal chromium-based coatings.

It is impossible to define precisely the size of a structural component (lamella) for the thermal coatings because of a high randomness in their distribution, large difference in longitudinal and transverse directions.

Table 1. Effect of a size of particles of the material being sprayed on the characteristics of coatings produced by an air-gas spraying

Powder fraction, μm	*Microhardness, GPa*	*Adhesion strength, MPa*	*Porosity, vol. %*	*Surface roughness, R_a, μm*
20 – 40	9.0 – 11.5	30 – 40	0.5 – 1.5	5 – 6
40 – 60	7.5 – 10.5	50 – 55	0.5 – 1.5	8 – 10
< 50	7.0 – 9.5	40 – 50	1.0 – 3.0	7 – 9
50 – 100	5.5 – 8.0	30 – 40	1.0 – 3.0	10 – 12
100 – 160	4.0 – 6.5	20 – 25	2.0 – 5.0	10 – 15

Table 2. Distribution of elements from lamella surface in chromium-based thermal coating

Element	Distribution of elements (wt. %) at the distance from lamella surface (μm)			
	1	4	7	10
Chromium	48.0	53.6	54.0	57.0
Iron	12.8	11.5	16.0	15.5
Nickel	5.9	6.4	8.1	10.5
Aluminium	6.3	7.5	10.0	10.0
Oxygen	27.0	21.0	7.9	6.0

If to take into attention that the initial hardness of powders is similar, and the contribution of mechanisms of deformation and solid-solution strengthening is identical for all the fractions at the same technology, then the difference in values of microhardness can be explained by a different saturation of lamellas with interstitial impurities. Results of Auger-spectroscopical examination of thermal coatings produced from the powder of 100 – 160 μm fraction and 4 mm diameter rod showed the great difference in saturation of large lamellas with oxygen across the section (Table 2).

The data obtained showed that the oxygen content decreases from 27.0 % at the surface to 7.9 % at the 7 μm depth. For coating particles, which preserve a spherical shape (that confirms the absence of deformation) the difference in microhardness across the section was observed. The larger duration of particles in the plasma stream the greater difference in microhardness: from 25 % for supersonic air-gas plasma up to 50 % for flame spraying.

The main forming characteristics of the structure of thermal coatings is the level of kinetic energy at particles collision with a substrate. The methods of thermal spraying can vary the flying rate of particles within the range from 25 to 600 m/s, that influences the properties of the coatings.

Table 3 gives the data about the effect of spraying technology on some characteristics of coatings on the chromium base.

As the flying rate of particles increases, the porosity decreases and adhesion strength, microhardness and tensile strength increase. Difference between the parameters of characteristics of flame and detonation coatings exceeds 2 – 3 times.

Electron-microscopic examinations of structure of thermal coatings from complexly-alloyed chromium alloys showed that the lamellas represent a polycrystal formation from equiaxial grains of size from 0.1 to 10 μm (most part of grains has sizes of 1 – 5 μm). From the data of diffraction of electrons, the phase composition corres-ponds to BCC-lattice with parameters which are close to chromium. This composition is typical both of large grains and also of fine grains. Sometimes, a characteristic growth of «colonies» of small elongated grains around the large grain is observed. The equiaxiality of grains inside the deformed lamella indicates the proceeding of polygonization processes that occur within the 900 – 1100 K temperature interval for chromium-based alloys [2].

The grain boundaries are rather smooth (similar to the grain boundaries in a recrystallized metal). However, the banded contrast on them is not usually observed, this being explained by a high level of an intragrain defectness and defect clustering at the boundaries and near them. Defects in a chromium coating are distributed non-uniformly. Their mean density does not exceed 1×10^{9} – 1×10^{10} cm^{2}. In the major part of grains a dislocation structure is revealed in the form of coils and interlocks and also clusters and spot defects, forming «fringing » near the dislocations. In some grains the clusters of dislocation loops of sizes of not less than 0.1 μm are observed. Loops are usually distributed within the grain volume non-uniformly , their density is decreased towards the grain centre, while near the boundary it is so high that separate loops are not distinguishable. In grains of small sizes the density of defects exceeds often 1×10^{11} cm^{2}. Here, it is impossible to distinguish separate defects and the relatively uniform contrast in the form of ripples is observed.

X-ray and electron microscopic examinations of surface layers of the chromium-based coatings showed that the main factors, which influence the phase composition formation, are an atmosphere of spraying and a cooling rate. The results of these examinations are given in Table 4.

In coatings produced in a dynamic vacuum (1×10^{-2} Pa) using inert gases of a commercial purity only a chromium matrix is observed. In the rest cases of a thermal spraying where the contact of a heated matrix material with oxygen and nitrogen is inevitable the different oxide and nitride phases are observed. Phases of chromium nitride in chromium-based coatings, sprayed in air, were nor earlier observed.

High values of heating temperature (more than 1300 K) and cooling rates (1×10^{3} – 1×10^{5} K/s) promote the formation of high-temperature, instable phases of chromium oxide Cr_3O_4 and CrO. The formation of tetragonal oxide of chromium in thermal coatings was revealed earlier [3], while the presence of oxide CrO is observed for the first time.

Table 3. Effect of technological characteristics on properties of chromium-based thermal coatings

Method of spraying	Size of material to be sprayed, μm	Total porosity, vol. %	Adhesion strength, MPa	Microhardness, MPa	Ultimate tensile strength, MPa
Flame	Rod, dia. 3000	6.0 – 8.0	16 – 25	~ 4500	75
Plasma	Powder, 40 – 80	3.0 – 6.0	21 – 32	~ 6500	100
Supersonic air-gas plasma	Powder, 40 – 60	1.0 – 3.0	40 – 50	~ 9000	180
Detonation	Powder, 20 – 40	0.5 – 1.5	45 – 60	~ 10000	185

Table 4. Phase composition of chromium-based coatings depending on technological parameters of spraying in initial state and after friction contact

Method of spraying	*Plasma-forming and transportation gas*	*Phase composition of coating*		
		Initial	*After annealing*	*After friction*
Flame	C_2H_2, O_2	Cr, Cr_2O_3, Cr_3O_4, Cr_2N	Cr, Cr_2O_3, Cr_2N	Cr, Cr_2O_3, Cr_2N
Plasma in dynamic vacuum	Ar, He	Cr	Cr	Cr, Cr_2N
Plasma	Ar, O_2	Cr, Cr_2O_3, Cr_3O_4, CrN	Cr, Cr_2O_3, CrN	Cr, Cr_2O_3, Cr_2N
Supersonic air-gas plasma	CN_4, O_2	Cr, Cr_2O_3, Cr_3O_4, CrO, CrN	Cr, Cr_2O_3, CrN	Cr, Cr_2O_3, CrN, Cr_2N,
[illegible]ion	CH_4, air	Cr, Cr_2O_3, Cr_3O_4, CrO, CrN	Cr, Cr_2O_3, CrN	Cr, Cr_2O_3, CrN, Cr_2N,

In [8] the presence of oxide CrO in subsurface layers of the oxidized chromium was revealed at heating temperatures up to 1474 K that was due to the chromium oxidizing in the conditions of a scarce oxygen.

We have observed the formation of oxide CrO only in the coatings produced in the streams of a high-speed plasma (detonation and supersonic air-gas spraying). A short-time stay in the plasma stream and formation of a vapour jacket of products of sublimation around a flying particle of chromium makes their heating above 1400 K difficult, and high rates of cooling contribute to the oxide CrO preservation in the coatings.

The presence of a low-temperature phase of chromium nitride CrN in the mentioned coatings testify the fact that the particles of chromium powder at high-speed thermal spraying are not heated above 1400 K. The presence of phase of chromium nitride Cr_2N in initial layers of coatings testify the metal overheating during spraying above 1400 K. Chromium nitride Cr_2N was revealed only during producing coatings from a rod (flame spraying) when the metal is heated to the melting temperature. In this case the oxide CrO is also absent.

Phase composition of thermal coatings on the chromium base undergoes changes both during heating and friction. The annealing of coatings, as is seen from Table 4, leads to the decay of high-temperature instable phases of chromium oxides CrO and Cr_3O_4. During friction, alongside with a decay of high-temperature instable phases of chromium oxides CrO and Cr_3O_4, the appearance of nitride Cr_2N in the surface layer of the coatings is revealed, while in initial state it was not observed. This is explained by a more probable formation of nitride Cr_2N in the conditions of friction at low temperatures and a lack of nitrogen. The removal of a surface layer for 2 – 5 μm depth leads to the recovery of initial phase composition of the chromium coating.

The high stability of structure and mechanical properties of alloys on the chromium base suggests their high serviceability at contact interaction under the conditions of high temperatures and pressures. The investigation of wear resistance of chromium coatings in a pair with a high-strength cast iron, which is a base metal in manufacture of sleeves of inner combustion engine cylinders, showed that at loads above 2 MPa and sliding rate of more than 2 m/s the advantage of thermal coatings as compared with wide-used galvanic chromium coatings becomes more evident (Table 5).

The above-given data indicate that the change in a sliding rate and load has no similar influence on the wear of the pairs examined. Increase in sliding rate by 9 times (from 1 to 9 m/s) leads to the wear of cast iron in a pair with a galvanic chromium from 0.4 to 2.5 μm. Increase in pressure by 3 times (from 1 to 3 MPa) intensifies its wear from 0.4 to 8.4 μm. The effect of parameters of test for wear of cast iron in a pair with a flame-sprayed chromium is less remarkable. In similar conditions the cast iron wear increases, respectively, from 0.5 to 2.5 and from 0.5 to 3.1 μm.

The change in test parameters has a lower effect on the wear of the coating itself. Increase in sliding rate from 1 to 9 m/s leads to the increase in wear of the galvanic and flame-sprayed coatings by 6.5 and 2.1 μm, respec-

Table 5. Wear of cast iron and chromium coating depending on the spraying technology and test conditions

Pressure, MPa	*Wear (μm) at deposition rate (m/s)*								
	Galvanic coating				*Flame coating*				
	1	*2*	*4*	*9*	*1*	*3*	*6*	*9*	*14*
1	0.4 / 2.5	0.7 / 2.9	1.5 / 5.0	2.5 / 9.0	0.5 / 2.0	1.0 / 2.5	1.2 / 3.0	2.5 / 4.6	2.7 / 6.2
2	3.0 / 5.0	5.3 / 7.8	7.6 / 9.5	–	0.6 / 2.1	1.2 / 2.1	1.5 / 2.7	3.2 / 4.7	4.5 / 7.0
3	8.4 / 7.0	14.0 / 10.0	16.4 / 12.0	32.0 / 16.0	3.1 / 4.0	4.2 / 7.0	5.6 / 8.5	7.2 / 8.6	7.9 / 9.0

Note. In numerator the wear of cast iron is given, in denominator — the wear of coating. Test duration is 10 h.

Table 6. Wear of piston ring and bushing (mm) for 1000 h operation of medium-speed diesel of 8000 kW capacity

Pair of friction	*Material and method of spraying*					
	Molybdenum, electric arc	*Steel, electric arc*	*Steel–molybdemun, electric arc*	*Chromium, galvanic*	*Chromium alloy VKh-2K, flame*	*Chromium-based alloy (20 % alloying), plasma*
Ring	0.020	0.024	0.013	0.015	0.011	0.019
Bushing	0.050	0.060	0.040	0.032	0.009	0.011

tively. Increase in wear at pressure increase from 1 to 3 MPa was 4.5 μm for the galvanic coating and 2.0 μm for the flame-sprayed coating.

The abrupt increase in wear of an abradant as compared with a coating leads in some cases (piston ring — cylinder sleeve pair) to more intensive wear of the part, whose sizes restoration will require great expenses as compared with a replacement of a piston ring.

The analysis of results obtained showed that increase in pressure for the chromium galvanic coatings leads to the growth of wear of the abradant as compared with the coating. At pressure of more than 2 MPa the ratio of an abradant wear to coating wear exceeds the unity, which is not observed in thermal coatings even at 6 MPa pressure.

The values of chromium flame coating wear intensity J_{ch} in a pair with a high-strength cast iron under the conditions of a boundary friction indicate the high wear resistance of the coatings. This is confirmed by the results of bench tests (Table 6).

It should be noted that for the above-mentioned pair J_{ch} in the conditions of bench tests on 2000 h base reaches 2×10^{12}, that is by one order lower than that at the boundary friction. The lubrication conditions greatly influence the wear intensity. Thus, J_{ch} is increased to 4×10^{-10} for the above pair under the conditions of a dry friction. Nevertheless, it should be noted that independently of the lubrication conditions the lower values of wear of an abradant as compared to the coating are characteristic of cast iron-flame chromium-based coating pair of friction.

For other pairs (high-strength cast-iron — coating) the increased wear of a bushing is typical. There is a tendency to increasing the wear of a bushing with a hardness increase in the coating, while the wear of the coating itself does not coincide with the values of hardness. Here, such parameters of the coating have an influence as porosity, cohesion strength, ductility margin of a lamella and its structural size. Thus, the wear of a chromium galvanic and flame coating is differed negligibly as compared with the bushing wear.

The problem of improving heat resistance of products, in power engineering in particular, is actual. The creation of coatings capable to increase the operating temperature of products is very important. The study of heat resistance characteristics of chromium thermal coatings showed that the porosity influences the level of heat resistance in the specimens only at the initial stage of oxidizing that is due to filling of voids. It is noted that the rates of oxidizing of both the coating itself and also the steel with deposited chromium coating are not differed essentially. The rates of cooling over the rest 30 h are close to each other, thus proving good protective characteristics of thermal coatings on the chromium base, mg / (cm × h): low-alloyed chromium — 0.0092; chromium alloy coating — 0.0101; steel St.3 with chromium coating — 0.0107.

CONCLUSIONS

1. Saturation of surface layers of slightly-deformed particles of the coatings with oxygen and nitrogen leads to a significant (up to 50 %) increase in microhardness as compared with a base metal.

2. Heating of powder particles during spraying under the conditions of temperature of more than 1400 K and high rates of cooling lead to the formation of a high-temperature phase of instable oxide CrO in the chromium coatings.

3. Contact interaction of chromium-based coatings during friction causes the appearance of nitride Cr_2N in surface layers which is inactive to iron.

4. Advantages of thermal chromium coatings as compared with galvanic coatings are visually manifested at friction using specific loads above 2 MPa.

5. Deposition of chromium thermal coatings can increase the operating temperature of the part surface up to 1300 K.

REFERENCES

1. Gridnev, V.N., Trefilov, V.I. (1968) Investigations on chromium problems. Physico-chemical investigations of heat-resistant alloys. *Transactions*, 154 – 162. Moscow: Nauka.
2. Trefilov, V.I., Milman, Yu.V., Firstov, S.A. (1975) *Physical fundamentals of strength of refractory metals.* Kiev: Naukova Dumka.
3. Turtsevich, E.V., Rakitsky, A.N., Gorban, V.F. *et al.* (1987) Structure and phase composition of thermal coatings from low-alloyed chromium alloys. *Poroshkovaya Metallurgia*, **11**, 51 – 55.
4. Gorban, V.F., Rakitsky, A.N.,Trefilov, V.I. *et al. Chromium alloy.* USSR author's certificate **963305**, Int. Cl. C22 C27/06/C23 C7/00. Publ. 01.07.82.
5. Tsypunov, A.G., Chernyak, V.I., Rakitsky, A.N. *et. al.* (1993) Granulated chromium powders for thermal spraying. *Materials of III All-Union Conf. on Granule Metallurgy*, 139 – 143. Moscow: VILS.
6. Rakitsky, A.N., Sychyov, V.V., Andreev, S.A. (1991) Procedure of tribotechnical tests of chromium coatings for piston rings of inner combustion engines. *Zavodskaya Laboratoria*, **5**, 47 – 50.
7. Borisov, Yu.S., Petrov, S.V. (1995) Application of supersonic jets in the technology of thermal spraying. *Avtomaticheskaya Svarka*, **1**, 41 – 44.
8. Tavadze, F.N., Mikadze, O.I., Kuteliya, E.R. *et al.* (1984) Mechanisms of high-temperature oxidizing of chromium. *Izv. AN USSR. Neorganich. Materialy*, 7, 1121 – 1125.

DEVELOPMENT OF THE TECHNOLOGY FOR THE MANUFACTURE OF ARTILLERY STEEL CARTRIDGES AND BOTTOMS BASED ON HIGH-TEMPERATURE INDUCTION BRAZING

L.I. BONDARENKO and **L.G. PUZRIN**
STC for Artillery and Rifle Arms, Ministry for Industrial Policy, Kyiv, Ukraine

ABSTRACT

Economical technology based on high-temperature induction brazing for the manufacture of cartridges and bottoms is suggested. Peculiarities of the technology are described and characteristics of the brazed joints are given.

Key words: *high-temperature induction brazing, capillary brazing, auto-vacuum effect, artillery steel cartridge, bottom.*

According to the known technology, 100 – 152 mm steel cartridges and bottoms are made by gradual drawing of a thin portion from a solid billet. This is a very labour-consuming operation which is carried out using an expensive equipment and comprises many runs, intermediate annealing and etching of billets and phosphatizing their surfaces. As a result, out of 45 operations used for the manufacture of cartridges, almost half involves forming and processing of the thin-walled portion.

In addition to a considerable cost of the basic equipment, a high labour consumption of the process of forming the thin-walled portion of a cartridge is also responsible for the high manufacture costs. Therefore, to arrange production of steel cartridges and bottoms in Ukraine, it is necessary to consider all alternative methods for their manufacture, which would be less labour-extensive, require no expensive equipment and, as a result, provide more competitive products.

One of such alternatives available for the manufacture of steel cartridges and bottoms is a method proposed by the STC for Artillery and Rifle Arms, based on a separate manufacture of a massive bottom and a thin-walled case, followed by their joining by high-temperature induction brazing. Using no special expensive equipment, this method allows the bottoms to be made from cast hot-formed billets or even billets cut out from a plate by machining, and the thin-walled cases to be made by drawing from the plate using automatic presses readily available at the relevant facilities of Ukraine and used to manufacture enamelled steel kitchen utensils.

This article describes the technological process developed for joining the thin-walled cases to the massive bottoms by high-temperature brazing by an example of the 125 mm steel tank bottom [1].

High-temperature brazing was selected as a basic joining method owing to its advantages, the main of which being that it provides full-strength joints with a high degree of reliability. For example, it is reported that in the modern rocket engines which are manufactured by making an extensive use of high-temperature brazing, the rate of failure of the brazed joints is ten times lower than in the welded engines. The brazed joints exhibit superior reliability under alternating pulsed loading.

According to the terminology standards in force, high-temperature brazing is brazing which requires heating to a temperature above 475 °C. This allows the use of more refractory and stronger filler metals. Therefore, the use of high-temperature brazing for joining parts of bottoms subjected to a high force effect in firing stems from the need to produce the strong joints.

To join the cylindrical portion having an ultimate strength of about 350 MPa to the massive portion of the bottom, the suitable filler metal is brass L63 (37 % zinc, balance — copper) which provides tensile strength of the brazed joints equal to more than 300 MPa in St.3 steel. This filler metal, which is extensively used for brazing steels of different grades, has a high power of penetrating into the brazing gap, that is why it is especially attractive for capillary brazing. The temperature of brazing using the L63 filler metal is 950 – 1000 °C [2].

Capillary brazing is the most commonly used type of brazing. With this method the filler metal is placed near the brazing gap, and after melting it spontaneously fills out the gap under the effect of the capillary force. This is the simplest method of brazing, requiring no extra manipulations during heating.

The filler metal penetrates into the gap under the effect of the capillary force only on condition that it wets the base metal. For this, surfaces of the base and filler metals should be cleaned from an oxide film which is inevitably formed in heating. This can be done by different methods. For example, brazing fluxes are widely used in this case to dissolve oxide films formed during heating. The PV 200 and PV 201 fluxes (GOST 23178–78) or borax are applied for brazing using the brass filler metals.

Flux brazing is successfully employed in the case of relatively shallow brazing gaps (to 10 mm). The filler metal penetrates into such a gap only after it is filled with a flux that removes the oxide film. This circumstance should be taken into account while designing a brazed joint, allowing for conditions of forcing out the flux with the molten filler metal. In brazing deep gaps extending to

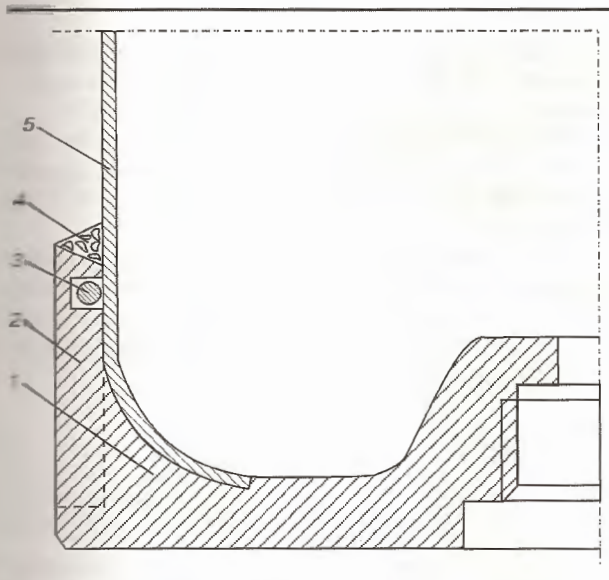

Figure 1. Billet for induction brazing of a bottom or cartridge: *1* — massive bottom; *2* — removable process allowance; *3* — filler metal; *4* — brazing flux; *5* — thin-walled case.

tens of millimeters, as is the case of brazing cartridges and bottoms, one can hardly expect their reliable filling with the flux and subsequent forcing out the flux with the filler metal, as the flux, causing dissolution of refractory oxides on the gap walls and partially the base metal, loses its fluidity. The flux penetrates into the narrow gaps to a small depth and hermetically seals the gap. This is sufficient for deep gaps to be reliably filled out with the filler metal, as steels are capable of dissolving the oxide film during heating with no access for air, which was found out by the E.O. Paton Electric Welding Institute as far back as 1963 [3]. This is so-called «auto-vacuum effect». Its point is that heating the steel parts to be joined is accompanied by dissolution of oxide films and atmospheric gases contained in the sealed gap. The filler metal easily flows into such a gap because of the absence of gases in it and reliably wets the walls, since they have no oxide films on them. In this case there are no limitations on depth to which the filler metal may flow.

This effect was used for the development of a design of the joint to be used in the bottom brazed. The gap in this case is sealed with the flux and the filler metal is preliminarily placed in the feed groove open to the gap at a certain depth, from which it flows to the gap to wet both parts joined under the effect of the capillary force and gravity.

Figure 3. Microstructure of the brazed joint near the feed groove (×50) (reduced by 0.50).

The suggested design of a sectional bottom (Figure 1) provides for a process allowance for the circular feed groove to be made at an external part of the massive bottom to accommodate the filler metal. In addition, this allowance provides fixation of the thin-walled case in brazing and serves as the location of induction heating. After brazing, during finish treatment the allowance with the feed groove is removed, except for its lower part, which is used then to form a flange to choke the bottom in shooting and to extract it after a shot.

The induction method provides a local heating of the joining zone, which makes it possible to avoid intensive oxidation of a larger part of the bottom. Therefore, the bottom can be made in the near-net shape for brazing, and after brazing machining might be done only from the out-

Figure 2. Induction brazing of a simulation sample.

Figure 4. Brazed bottoms.

side, i.e. within the allowance zone. Induction heating of the process allowance should be done under moderate conditions to provide a uniform heating of the bottom within the joining zone and heating of the thin-walled case from the bottom due to thermal conductivity. For a more uniform heating, the bottom is imparted a rotary motion in an induction coil. The temperature is monitored using a contactless thermocouple or optical pyrometer.

In our experiments the single-winding induction coil powered from the VPCh 100 – 8000 machine transformer (power 100 kW and current frequency 8000 Hz) was used for heating, although any other high-frequency current source can be tolerated.

The technological process was optimized on simulation samples of steel 20 at a set optimal electrical parameters. Brazing of the simulation sample is shown in Figure 2. Using the optimal diameter of the filler metal wire, it was established that sound joints over the entire surface could be provided with baked borax used as the flux (Figure 3).

The shear tests of the brazed joints showed that their strength was 265 – 285 MPa, which fits the values characteristic of this type of the joints (260 – 270 MPa).

Brazing of a batch of the bottoms intended for field tests was done under the optimized conditions. Appearance of the brazed bottoms for the field tests is shown in Figure 4.

The investigations conducted proved the possibility of producing the 100 – 152 mm steel bottoms and cartridges by making separately the bottom and the thin-walled case, followed by their joining to each other by high-temperature induction brazing.

REFERENCES

1. (1976) *Frames for location and designs of ground-artillery arms and ammunition.* Edited by N.N. Korolkov. Moscow: Voenizdat.
2. Khryapin, V.E. (1981) *Brazing and soldering operator's handbook.* Moscow: Mashinostroyeniye.
3. Paton, B.E., Medovar, B.I., Kirdo, I.V. *et al.* (1964) *Spontaneous cleaning of metal from oxide films.* Doklady AN SSSR, vol. 159, **1**, 72 – 73.

ARGON-ARC SURFACE QUENCHING — METHOD FOR HARDENING ARTILLERY BARRELS

L.I. BONDARENKO and **L.G. PUZRIN**
STC for Artillery and Rifle Arms, Ministry for Industrial Policy, Kyiv, Ukraine

ABSTRACT

Surface quenching using concentrated heat sources and travel speed of the source needed to heat a layer of the required thickness and hardness are considered. The method, equipment and operational parameters have been developed for argon-arc surface quenching of the inside surfaces of barrels. Quenching of the full-scale barrels for the service life tests has been conducted.

Key words: argon-arc quenching, surface, hardening, artillery barrel.

One of the causes of losses in viability of threaded barrels of automatic guns is their mechanical wear within the zone where a leading ring of the shell enters into the thread. It was suggested to try out hardening of this zone by subjecting it to surface quenching to check the possibility of increasing resistance of the barrels to the above type of wear. The barrel of the 30 mm automatic gun was used as an object for the investigations. It loses viability almost after 6000 shots with a maximum wear taking place in areas of the polygonal thread, extending to 0.35 per side.

In view that quenching leads to a decrease in metal ductility and a risk of brittle fracture, thickness of the quenched layer should be not much in excess of the tolerated value of wear, and for a 30 mm barrel it should be about 0.5 mm. The metal layer of such a small thickness should be heated to a temperature above the quenching point for a limited time to avoid heating of a thicker metal layer due to thermal conductivity. This can be achieved by using a movable concentrated heat source.

The most convenient source for surface quenching is laser [1], as it allows the energy density within the heating zone, size of this zone and speed of its movement to be varied within wide ranges. Available are the dependencies which make it possible to preliminarily evaluate the process parameters for hardening a workpiece to a desirable depth [1].

The use of the laser equipment, which is very expensive, for quenching is justifiable only under mass production conditions. In addition, the current economical situation makes it necessary to look for less expensive ways of solving this problem.

Since surface quenching requires a lower energy density, as compared with welding [1], plasmatrons which showed themselves to advantage in surface hardening of, e.g. wheelsets [2], can be used in this case as the concentrated heat sources. Detailed investigations into the quality of the quenched layer showed high mechanical properties of wheelsets achieved by plasma hardening through varying the heating process parameters [3].

With the plasmatrons used for quenching the gun barrels, we face an extra difficulty associated with a limited work space inside a 30 mm barrel. This generated the need to develop a technological process and equipment for hardening the surface of the barrel channel using a conventional tungsten arc burning in argon [4] as a heat source. For this, a special torch with a tungsten electrode 4 mm in diameter was developed. It maintains the electrode in a required position inside the barrel, serves as a reliable water-cooled current conductor and feeds argon to the arc burning zone (Figure 1). The outside diameter of the torch without the electrode is 14 mm, which makes it possible to accommodate it not only in a 30 mm barrel, but also in smaller caliber barrels.

The arc quenching process was investigated using the experimental-industrial unit designed for electric-spark hardening of barrels. The basic element of this unit is a lathe of the 1K62 grade with a frame extended to a sufficient length to locate on it the 30 mm barrels*.

During the quenching experiments the barrels or samples were mounted in a chuck of the lathe to make them rotate at a required speed, while heating their inside surfaces with the argon arc. The torch with the tungsten electrode was mounted in an insulator on the support. The current was supplied directly to the chuck and torch casing using a special sliding contact. The direct-polarity current (minus at the electrode) was fed to the arc from the VD301 welding rectifier through the RB300 ballast.

The barrels should be subjected to surface quenching in a finished form. Therefore, no surface melting is tolerated in this case. At the same time, the barrel wall should be heated to a sufficiently high temperature, so that metal can be heated to a required depth within a short period of time.

Quenching of steel involving an increase in hardness occurs after rapid cooling from a temperature ensuring partial or full dissolution of carbides. Sufficiently rapid cooling of the hot surface layer is done at a travel speed of the heat source varied over wide ranges, as it is determined by a high rate of removal of heat to the cold metal. Besides, the time required for at least partial dissolution of carbides is determined by the heating temperature, the type of carbides, i.e. steel alloying system, and by peculiarities of its structure in the initial state.

* The unit was developed by V.P. Melnik, STC for Artillery and Rifle Arms.

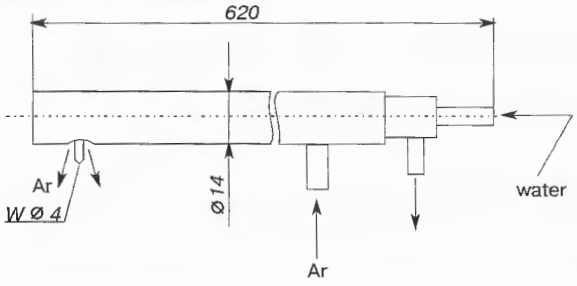

Figure 1. Torch for argon-arc quenching of inside surfaces of the barrels.

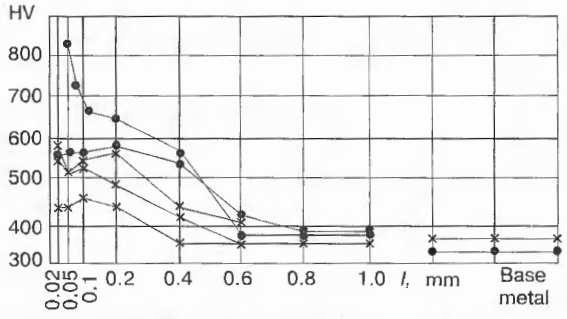

Figure 2. Microhardness of the channel surface of the 30 mm barrel after argon-arc quenching along a region 150 mm long.

In surface quenching of the finished barrels, it is possible to vary only the time of heating and the temperature of the surface heated, which depend upon the energy density in the heating spot, size of the spot and its travel speed.

Like laser and plasma, the arc heats up the spot which is close to a circle in shape. The time of heating the metal layer under the spot centre is equal to a ratio of diameter of the heating spot to its movement speed. This time and the energy density in the heating spot determine the maximum temperature and depth to which the metal is heated.

In carbon steels, carbides at a normal quenching temperature are fully dissolved for a time of over 1 min, whereas in alloyed steels this time is more than 2 min [5].

At the high rates of heating characteristic of surface quenching, the metal temperature is such that it provides dissolution of carbides for just a few seconds. In plasma quenching of wheelsets, the time of heating, according to our estimation based on the data of [3], is from 1.5 to 3.0 s. This suggests that dissolution of carbides and subsequent quenching can take place only within the layer of metal which is heated to a temperature much in excess of the normal quenching temperature. However, in this case the time is too short for grain to grow and ductility to drop, as is the case of furnace high-temperature heating.

In surface quenching, it is a short time that seems to be responsible for just a partial dissolution of carbides. The absence of a full dissolution of carbides shows up in a decrease in hardness with an increase in the heat source travel speed [6]. When this speed is increased from 20 to 40 m/h, hardness of the quenched surface for steel 45 decreases from 740 to 600 HV and that for steel 30KhGSA — from 630 to 460 HV. At a speed of 50 m/h hardness falls almost to 300 HV, i.e. here quenching hardly has any effect. In this case the depth of the quenched layer is reduced to 0.1 mm.

Analysis of the known data on surface quenching allowed formulation of requirements for this process as applied to the barrels. To produce the quenched layer with a thickness of about 0.5 mm, it is necessary to have a heat source with an energy density of about 30 W/mm^2, which when it moves ensures heating for approximately 3 s.

The energy density in the argon arc is extremely non-uniform. It is more than 200 W/mm^2 in the central column and dramatically decreases towards the peripheral regions. This gives rise to difficulties for using the argon arc as a heat source for surface quenching, which is the main reason for the plasma heaters, having a much more uniform energy density, being the sources of choice. Decreasing the intensity of heating by increasing the arc travel speed appears to have no potential as a result of a dramatic reduction of the time of heating and the absence of the hardness increase effect. Decreasing the travel speed with a simultaneous overall decrease in the current is also ineffective because of an unstable burning of the arc and an extremely low productivity of the process.

So, the way out was found and it consisted in the fact that during the arc quenching process the rotary motion at a speed of about 5 rps was imparted to the barrel, which ensured a uniform heating of the circumferential zone on the surface of the barrel channel, while the time of heating needed for carbides to dissolve was provided by selecting the proper speed of displacement of the circumferential zone of heating along the barrel.

Quenching carried out under optimal conditions provided the layer of an increased hardness and a required thickness (Figure 2). These conditions were used for surface quenching of experimental barrels to conduct the fatigue tests. The developed method for argon-arc quenching of the inside surfaces of the barrels is suitable for hardening the channels of arms of any caliber.

REFERENCES

1. (1998) Introduction to industrial laser mate rails processing. In: *ROFIN-SINAR Laser GmbH*.
2. Lashko, A.D., Petrov, S.V., Saakov, A.G. (1997) Plasma hardening of surfaces of wheelsets. *Zaliznychnyi Transport Ukrainy*, **23**, 22 – 25.
3. Petrov, S.V., Saakov, A.G., Grigorenko, G.M. *et al.* (1998) Microstructure peculiarities of surface layers of steel treated by plasma. *Problemy Spetselectrometallurgii*, **1**, 74 – 80.
4. Belfor, M.G., Paton, V.E. (1974) *Equipment for arc and slag welding and surfacing*. Moscow: Vysshaya Shkola.
5. Gulyaev, A.P. (1986) *Metals Science*. Moscow: Metallurgiya.
6. Leshchinsky, A.K., Samotugin, S.S., Pirch, I.I. *et al.* (1990) *Surface plasma hardening*. Kyiv: Tekhnika.

STRUCTURE AND PROPERTIES OF HYPEREUTECTOID GRAPHITIZED ROLL STEEL AFTER PLASMA HARDENING

S.S. SAMOTUGIN
Priazov State Technical University, Mariupol, Ukraine

ABSTRACT

Structure, hardness, impact toughness and character of fracture of hypereutectoid steel 150KhNM under dynamic loading after plasma hardening, as compared with volumetric quenching, are investigated. Hardness and impact toughness of steel after plasma hardening are higher than after volumetric quenching, which is caused by a highly dispersed martensite-carbide structure formed by plasma treatment. Fracture of metal of the hardened zone occurs by the mechanism of dispersed quasi-cleavage, while that of metal after surface micro- and macro-melting occurs by the mechanism of intercrystalline cleavage.

Key words: *surface plasma hardening, graphitized roll steel, structure, service properties, character of fracture.*

Surface treatment using a highly concentrated plasma jet is the efficient method for hardening metal-cutting tools [1, 2]. High thermal power density of the plasma jet (approximately 10^5 W/cm^2) provides a high-rate hardening of various-application steels and alloys, such as low-carbon alloyed deposited metal [1, 3], tool steels [2], cast iron [4] and sintered hard alloys [5].

Metallurgical production equipment and parts present one of the most promising fields for application of plasma hardening. The effect of plasma treatment on structure and properties of roll materials, such as hypoeutectoid and eutectoid steels (50KhN, 65KhZMF, 90KhF) [1], roll cast iron [4] and deposited metal of the Kh5MF type used for repair of rolls [1, 3], was investigated earlier. Hypereutectoid graphitized steels [6] are also among materials which hold promise for the manufacture of hot rolls.

The work described in this article was dedicated to investigation of peculiarities of phase and structural transformations, service properties and character of fracture of graphitized steel 150KhNM in plasma treatment, as compared with the as-received state (after normalizing) and volumetric quenching.

Plates measuring $60 \times 40 \times 160$ mm of steel 150KhNM (1.40 % C, 0.54 % Mn, 0.90 % Cr, 0.84 % Ni, 0.54 % Si, 0.12 % Mo) in the as-received (normalized) condition were subjected to plasma treatment and volumetric quenching in a furnace. The specific thermal power of the plasma jet (transferred-arc plasmatron with a sectional inter-electrode insert [1]) was 1.2×10^5 W/cm^2 and the treatment distance was 5±1 mm. The travel speed of the plasmatron varied from 15 to 30 m/h to achieve maximum hardness without surface melting, and with micro- and macro-melting, according to recommendations given in [7]. Volumetric quenching in a furnace was done under conditions commonly accepted for hypereutectoid steels: heating to 800 °C (50 – 70 °C higher than critical temperature) and oil quenching. Sections for microscopic studies using the «Neophot-21» microscope and unnotched specimens for impact toughness tests using procedure described in [1] were cut out from the plates in different conditions. After the tests, fractography was done to analyse fracture using the SEM-200 scanning electron microscope. Results are given in the Table below (mean values for 10 specimens of each series) and shown in Figures 1 and 2.

In the as-received condition, graphitized steel has a heterogeneous structure. The matrix consists of coarse-grained laminated pearlite (Figure 1, *a*). The hardening phase, i.e. redundant cementite, has the form of a continuous mesh extending along the primary austenite grain boundaries, as well as the form of eutectic clusters of the acicular-laminated shape with inclusions of spherical or flaky graphite particles inside it (Figure 1, *b*). In the case of volumetric quenching, acicular and plate cementites and graphite are partially dissolved to form a ternary structure: coarse-acicular martensite, cementite comprising the continuous mesh and the remaining acicular particles, and local light-colour regions of retained austenite, surrounding cementite (Figure 1, *c*).

Heating hypereutectoid steel to be hardened to a critical temperature or higher involves two processes that occur simultaneously. These are transformation of pearlite into austenite and dissolution of redundant cementite starting from the boundary with pearlitic ferrite. Completion of transformation of pearlite into austenite and levelling of the carbon concentration in the bulk of prior pearlite grain are followed by acceleration of the process of dissolution of redundant cementite.

Unlike volumetric quenching, in plasma treatment without surface melting the temperature of heating is much in excess of the critical point (it may reach T_{melt}) [1], which leads to almost complete dissolution of redun-

Properties of steel 150KhNM subjected to different hardening methods

Hardening method	*Vickers hardness*	*Impact toughness, J/cm²*
As-received condition	285 – 300	4.8
Volumetric quenching	695 – 715	2.1
Plasma hardening:		
without surface melting	865 – 880	4.3
with micro-melting	895 – 910	3.2
with macro-melting	865 – 880	3.0

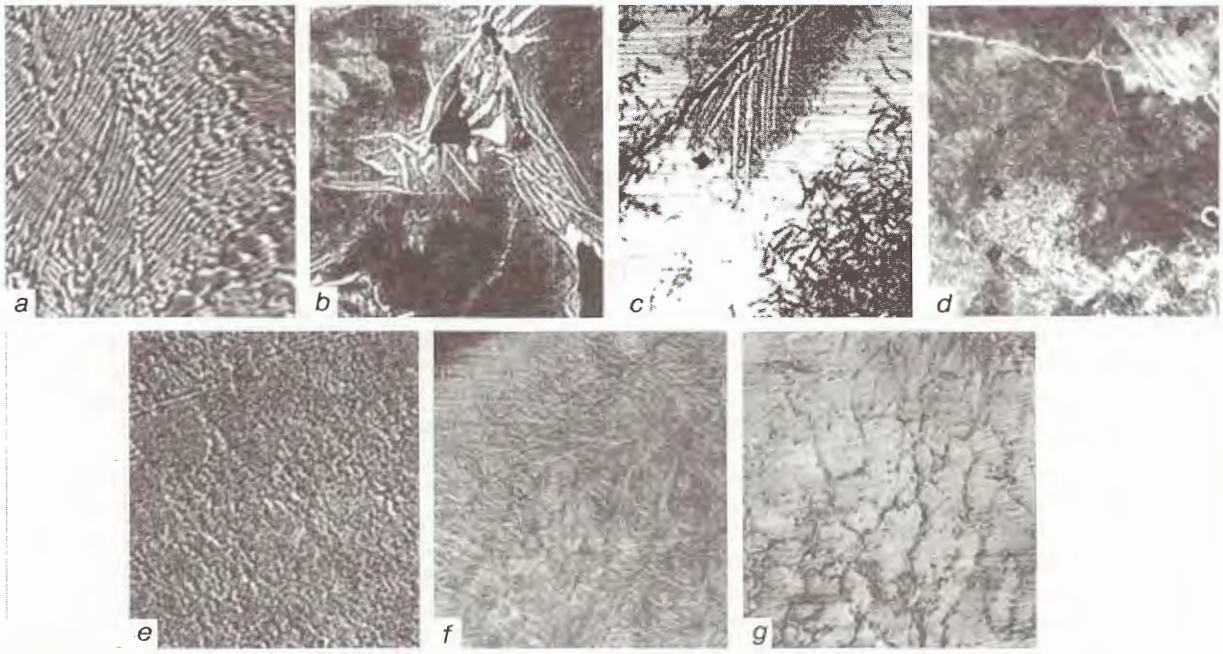

Figure 1. Microstructure of steel 150KhNM: *a, b* — as-received state; *c* — after volumetric quenching; *d* — transition zone; *e – g* — after plasma hardening without melting and with micro- and macro-melting, respectively (*a* — ×500; *b, d* — ×200, *c, f, g* — ×700, *e* — ×400) (reduced by 0.60).

dant cementite (individual fragments of undissolved particles of acicular cementite persist only in lower layers of the hardened zone, i.e. near the transition zone) (Figure 1, *d*). Solid solution is additionally saturated with carbon and alloying elements, and is characterized by a high concentration heterogeneity. This is attributable to very high heating and cooling rates and to an extremely short time of holding (approximately 0.1 – 0.01 s), which causes homogenization to slow down. No growth of austenite grain occurs under such temperature-time conditions. As a result, the structure of the plasma-hardened zone is characterized by a high degree of dispersion.

Extra hardening of the plasma-hardened zone metal is achieved owing to partial dissociation (self-tempering) of martensite and precipitation of the secondary carbide particles of a globular shape along the boundaries and in the bulk of grain [6]. Thermal-physical peculiarities of plasma hardening cause dispersion strengthening to be fixed at the initial stage [2]: the precipitating particles are of submicroscopic sizes, have no time to coagulate and are uniformly distributed in the highly dispersed martensitic matrix (Figure 1, *e*). Hardness of steel 150KhNM after plasma hardening is much higher than after volumetric quenching (see the Table).

Structural heterogeneity of graphitized steel in the as-received condition results in a heterogeneous structure of fractures formed under dynamic loading*, i.e. intercrystalline cleavage in the cementite mesh and eutectic cementite (Figure 2, *a*) and transcrystalline cleavage accompanied by the formation of a specific groove-shaped pattern on the pearlitic matrix (Figure 2, *b*). The similar structure of fracture in such steels was observed by the authors of [6]. Fracture after volumetric quenching is more uniform in character. Here intercrystalline cleavage is dominating in the cementite mesh and at the austenite grain boundaries (Figure 2, *c*). This leads to a more than two times decrease in impact toughness (see the Table).

In the zone affected by plasma hardening the structure of fracture changes in a qualitative manner. The highly dispersed martensitic structure and the submicroscopic carbide particles uniformly distributed in the martensitic matrix cause fracture to occur by the micro-mechanism of dispersed quasi-cleavage (Figure 2, *d*). It should be noted that this mechanism is characteristic of static and dynamic conditions of loading different compositions of materials hardened by the highly concentrated heat sources, the plasma jet in particular [1 – 5]. Impact toughness of steel 150KhNM after plasma hardening also decreases, although to a much lesser degree than after volumetric quenching (see the Table).

One of the methods of surface treatment is treatment involving melting of a surface layer, i.e. hardening from a liquid state. In some cases this method is considered more preferable than treatment without melting, especially in laser and electron beam hardening. Specific peculiarities of plasma melting, as compared with beam melting, are described in [7]. Because of a high gas-dynamic pressure of the plasma jet and melting to a substantial depth (to 1 mm or more — macro-melting), this method provides partial removal (splashing) of molten metal and results in a lower quality of the hardened surface. In melting to a depth of about 0.1 – 0.3 mm (micro-melting) the rate of solidification of metal is very high (10^5 °C/s), this making molten metal solidify almost immediately and preventing splashing, i.e. there is almost

* Participating in the investigations were A.V. Puiko and N.Kh. Solyanik.

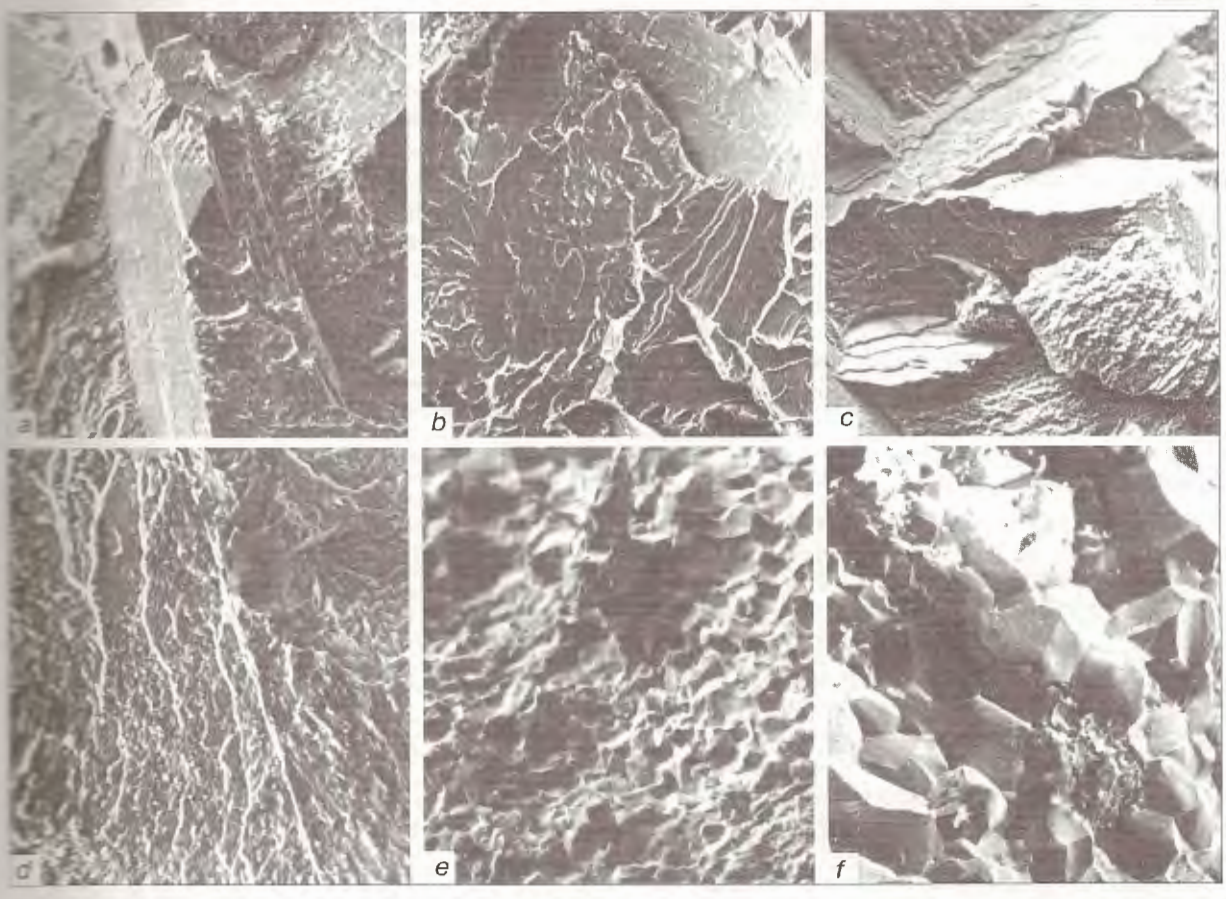

Figure 2. Electron microfractograms of fracture of steel 150KhNM samples: *a*, *b* — as-received state, cleavage in cementite and pearlite, respectively; *c* — after volumetric quenching; *d* – *f* — zone of plasma hardening in treatment without melting and with micro- and macro-melting, respectively (×400) (reduced by 0.60).

no deterioration in the hardened surface quality. Ensuring an increase in the total depth of the hardened zone, plasma treatment with micro-melting has high potential for hardening large-sized tools (rolls, dies, etc.). Practical application of either method of plasma treatment is based on adjustment of its parameters, i.e. the travel speed of the plasmatron being kept unchanged, the travel speed of the plasmatron is selected depending upon the application [7].

Plasma treatment of steel 150KhNM with micro-melting of the workpiece surface leads to a complete dissolution of the cementite and graphite phases and to an extra saturation of solid solution with carbon and alloying elements. Hardness of the zone affected by micro-melting is higher than that of the zone hardened without melting. The degree of dispersion of the structure during melting decreases, which is attributable to an increased heating temperature, longer holding time and decreased heat sink to the unaffected metal. At the same time, structure of the hardened zone treated by micro-melting is sufficiently homogeneous and consists of martensite with cells 2 – 8 μm in size (see Figure 1, *f*). Fracture of the hardened zone in the upper (melted) layer occurs by the micro-mechanism of dispersed intercrystalline cleavage which is gradually transformed into quasi-cleavage within the hardening zone in the solid state. A decrease in the degree of dispersion of the structure and the intergranular nature of crack propagation lead to a decrease in impact toughness, as compared with treatment without melting (see the Table).

Elevation of the heating temperature and an increase in the molten metal pool volume under conditions of high-rate solidification (in plasma macro-melting) results in the formation of a cast structure with the equiaxed crystalline grains, which are degenerated dendrites. Unlike treatment without melting and with micro-melting, in this case we have a clearly defined structural heterogeneity: there are regions of coarse-acicular martensite and light regions of retained austenite (see Figure 1, *g*), the content of which, according to the data of X-ray diffraction analysis, increases almost by 50 % [7].

An increase in the content of retained austenite is caused by oversaturation of solid solution with carbon and alloying elements and, as a consequence, by a decrease in temperature at which martensite transformation begins. Under conditions of high-rate solidification the processes of diffusion and homogenization of austenite have no time to be completed. The zones with a higher content of carbon and alloying elements, more resistant to decomposition during high-rate cooling, replace the former cementite and graphite phases. An increased content of retained

austenite causes a partial decrease in the effect of solid solution hardening [2]: hardness of steel 150KhNM after plasma treatment with macro-melting is at a level of that achieved by treatment without melting (see the Table). At the same time, an increase in size of actual austenite grain, structural and chemical heterogeneity of the melted layer lead to a decrease in impact toughness and extra embrittlement. Fracture of the macro-melted layer occurs by the intercrystalline mechanism to form coarse facets of cleavage at the intergranular boundaries (Figure 2, *f*). Therefore, plasma hardening of steel 150KhNM involving surface macro-melting causes no increase in hardness, deteriorates quality of the hardened surface and aggravates brittleness.

CONCLUSIONS

1. Plasma surface treatment is an efficient method for hardening tools made from hypereutectoid graphitized steels of the 150KhNM type. It provides an increase of HV 150 – 180 in hardness and doubles impact toughness, as compared with volumetric quenching, owing to the formation of the hardened zone with a highly dispersed martensite-carbide structure. Fracture of the hardened zone metal under dynamic loading occurs by the mechanism of dispersed quasi-cleavage.

2. Extra increase in hardness of the surface is achieved by plasma treatment with micro-melting. However, this method is characterized by a high probability of the intercrystalline fracture mechanism, which can lead to a decrease in resistance of hardened tools to in-service crack initiation and propagation.

3. Plasma hardening of steel 150KhNM with macro-melting does not lead to an extra increase in hardness, causes deterioration in quality of the hardened zone and increases brittleness.

REFERENCES

1. Leshchinsky, L.K., Samotugin, S.S., Pirch, I.I. *et al.* (1990) *Plasma surface hardening*. Kyiv: Tekhnika.
2. Samotugin, S.S. (1996) Plasma treatment of tool materials. *Avtomaticheskaya Svarka*, **8**, 48 – 51.
3. Leshchinsky, L.K., Samotugin, S.S., Goritsky, B.M. *et al.* (1996) Structure and crack resistance of deposited metal 18Kh6GMFS after plasma hardening. Ibid., **8**, 31 – 35.
4. Samotugin, S.S., Kovalchuk, A.V., Solyanik, N.Kh. *et al.* (1996) Structure of tough fracture of high-strength pearlite-cementite cast iron after plasma treatment. *Metallovedenie i Term. Obrabotka Metallov*, **4**, 2 – 6.
5. Samotugin, S.S. (1997) Fracture toughness of hard alloys hardened by plasma treatment. *Fizika i Khimiya Obrabotki Materialov*, **4**, 45 – 51.
6. Rudnyuk, S.I., Mikhailova, I.V., Tomenko, Yu.S. (1990) Effect of alloying and heat treatment on properties of hypereutectoid roll steels. *Metallovedenie i Term. Obrabotka Metallov*, **4**, 21 – 24.
7. Samotugin, S.S., Solyanik, N.Kh., Puiko, A.V. (1994) Properties of tools steels in plasma hardening with surface melting. *Svarochnoye Proizvodstvo*, **11**, 20 – 24.

ELECTRON BEAM REMELTING OF OPERATING SURFACE OF EXHAUST VALVES OF AIRCRAFT ENGINES

A.V. BONDAR[1], M.V. ERYOMIN[1], S.N. FYODOROV[1] and V.V. SHURUPOV[2]
[1]Mechanical Works, Voronezh, Russia
[2]State Technical University, Voronezh, Russia

ABSTRACT

Problems of repair of flaws of a discontinuity type, which are formed in a layer of the operating surface of aircraft engine exhaust valve, surfaced with a flame method, is considered. It is shown that, when using electron beam treatment with an ellipsoid scanning of beam, the flaws are eliminated in the deposited surfaces. During electron beam treatment the inner structure of the deposited layer is changed by refining and reorienting chromium carbides that increases the microhardness of the working surface.

Key words: *electron beam remelting, valve, surfacing zone, microstructure, chromium carbide.*

The aircraft engine exhaust valve is operating under complex conditions, such as: an increased temperature, erosion action of gas medium, dynamic loads. To ensure a service reliability an operating surface of the valve made from EI-69 heat-resistant steel is subjected to surfacing into a shaping groove using a cast 6.0 ± 0.5 mm diameter rod of VKhN-1 alloy. The surfacing is performed from two sides manually using an oxyacetylene flame. Often, the flaws in the form of pores, cavities, slag inclusions are formed in the deposited layer, which are difficult to repair completely by a flame method, and, due to a large zone of heating, the geometric sizes of the valve itself are deviated from the preset data, thus leading to the valve rejection. In addition, the iron content in the deposited layer is limited and should be within ranges of 10 %, that is not always provided when the repair technology is used.

The electron beam remelting of the valve operating surface is aimed at the elimination of flaws and improvement of physical and mechanical characteristics of the deposited layer.

Experiments were carried out in the ELU-9B type installation using an electron beam equipment of ELA-15 type. It was assumed that, due to a complicated configuration of the valve deposited zone, and also necessity in providing better conditions of degassing and uniform remelting in the whole depth of the deposited layer of the metal, the electron beam should be directed normal to the surface of treatment, and the geometry of the beam scanning should be selected in the form of ellipse with an arrangement of a large axis along the radius of the valve operating surface. This procedure can decrease the amount of pores and discontinuities in the deposited layer.

A batch of valves with flaws (pores, cavities, slag inclusions), which were revealed by X-ray technique, was examined.

Surface	*Current, mA*		*Focusing distance, mm*
	Emission	*Focusing*	
A	27	790	450
B	37	721	458

Note. Rate of treatment of both surfaces is 20 m/h, accelerating voltage is 60 kV.

Table shows optimum remelting conditions which were established experimentally. The angle of electron beam deflection from the gun axis is 7°, while an angle of valve axis deviation from the gun axis at the surface A is 30 ± 1°, at the surface B it is 48 ± 1°. Shape of the beam scanning is an ellipse with axes $X = 6$ mm and $Y = 2$ mm. Vacuum in chamber reaches 1.33×10^{-2} Pa, and in the cavity of the electron beam gun — $5 \times 1.33 \times 10^{-3}$ Pa.

The selected conditions could provide melting of the deposited layer without its dilution with the valve parent material (Figure 1).

Geometry of the surfacing and electron beam remelting zones is given in Figure 2.

The elimination of flaws was examined by X-ray method. Examination confirmed the complete absence of flaws after the electron beam remelting.

The spectral analysis before and after the electron beam remelting showed that the iron content was changed negligibly (within 1.5 %) after remelting and corresponded to the admissible standards.

Microanalysis of the material of zones deposited by the flame method and remelted by the electron beam showed the following. Structure of the deposited material

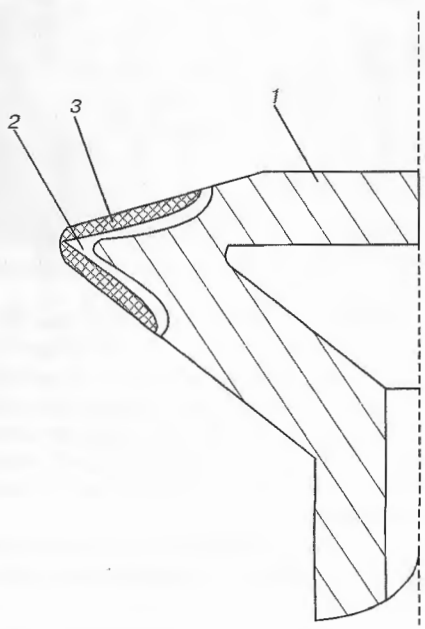

Figure 1. Zones of valve treatment: *1* — parent metal (steel EI-69); *2* — deposited zone (alloy VKhN-1); *3* — electron beam remelted zone.

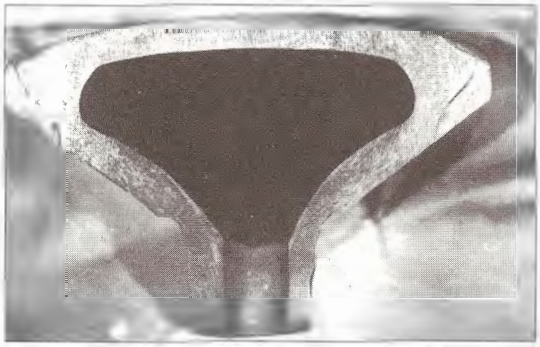

Figure 2. Metallography of geometry of as-deposited and as-electron beam remelted valve zones (×1.5) (reduced by 0.75).

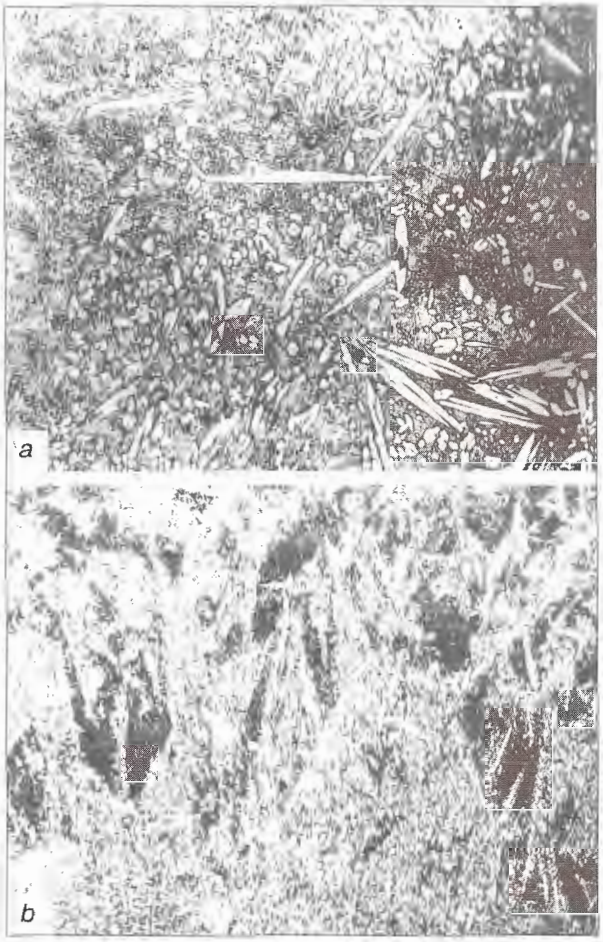

Figure 3. Microstructure of metal of deposited (*a*) and remelted (*b*) zones (×200) (reduced by 0.75).

is a solid solution on the base of nickel and chromium carbide. Microstructures of the material of deposited and remelted zones are differed by the way of arrangement, shape and sizes of the chromium carbides. Chromium carbides in the material of the deposited zone have a random arrangement. Inclusions of hexahedral and needle-like shape are greatly larger in their sizes than the inclusions in the remelted zone.

Near the parent metal+deposited metal boundary (Figure 3, *a*) the sizes of carbides are increased. Chro-

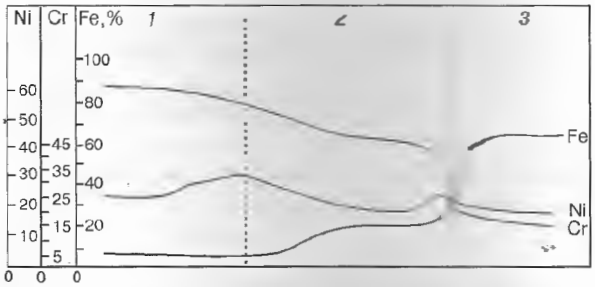

Figure 4. Distribution of iron, nickel and [illegible] valve material: *1* — electron beam remelted zone; *2* — flame [illegible] zone; *3* — parent metal.

mium carbides in the remelted zone [illegible]ial (Figure 3, *b*) have a more uniform distribution [illegible] directivity of growth, oriented normal to the val[illegible]perating surface, as compared with the zone of surfacing.

X-ray diffraction microanalysis was used to examine the distribution of alloying elements [illegible] the material of deposited and remelted zones, and also [illegible] estimate quantitatively the degree of a chemical inhomogeneity. Distribution of iron, chromium and nickel was determined in X-ray microanalyzer of MAR-2 type from the lines taken conditionally in the middle of deposited and remelted zones. From analysis of the distributions obtained (Figure 4) it can be noted that the distribution of iron and nickel after the electron beam remelting became more uniform in depth of the remelted zone. At the same time, the distribution of chromium near the boundary of the deposited and remelted zones is changed abruptly, and then (on approaching the surface of the remelted zone) becomes uniform. This is, evidently, caused by the formation of the chromium carbides and their further refining.

Microhardness was measured to confirm the effect of the uniformity of distribution of a refined structure of the chromium carbide on the stability of hardness values of the deposited metal in the whole depth of the remelted zone. It was established that the mean values of material hardness of the electron beam remelted zone are higher than those of the material of the zone deposited by the flame method, by 12 %, that corresponds to the upper limit of admissible values.

CONCLUSIONS

1. Electron beam remelting of operating surfaces of aircraft engine exhaust valves with experimentally selected optimum parameters allows the flaws in the form of discontinuities in the deposited zone to be eliminated without deterioration of required geometric sizes of the part.

2. The use of electron beam remelting contributes to the more uniform distribution of iron, chromium and nickel.

3. In electron beam remelting the structure of carbide inclusions is refined that promotes their more uniform distribution in the material of the surfacing zone and orientation of needle-like chromium carbides normal to the operating surface. This increases hardness of the valve deposited material to the maximum admissible limits and, being one of the important factors, improves the service life of the aircraft engine.

APPLICATION OF HEAT SINKS FOR REDUCTION OF WELDING STRAINS AND STRESSES (Review)

A.I. GEDROVICH and **A.B. ZHIDKOV**
East-Ukrainian University, Lugansk, Ukraine

ABSTRACT

The possibilities of controlling the strains and stresses in the joints with artificial heat sink are considered. Classification of welding processes with heat removal by the technological and physical features, is proposed. It is found that for up to 3 mm thick metal the most effective is the application of the heat-absorbing pastes and crystalline heat-absorbing rods, and for 3 – 8 mm thick metal it is water cooling. Welding with heat sink should be regarded as a resources-saving process.

Key words: *welding, stress, strain, heat removal, artificial, devices, methods.*

One of the principal possibilities to reduce the welding strains and stresses, is reduction of the plastic deformation of shrinkage or of the width of the zone of its propagation in heating, $2B$, by controlling the thermal impact in welding [1, 2]. This is the basic principle of the methods of controlling the welding strains and stresses, which envisage an impact on the thermal characteristics of the process [3], related to selection of the appropriate welding modes, allowing for reduction of the extent of plastic shrinkage, total or local preheating of the parts prior to welding and heat removal from the weld zone. In welding in the optimal modes, the thermal pattern cannot be regulated by changing their parameters. The preheating and concurrent heating require considerable power consumption (of gas in heating with gas torches, of power at high-frequency and resistance heating, etc.). Therefore, the heat sink proper during welding can be regarded as resources saving. It is rational to apply it in welding of low-carbon steels which form no quenching structures, of copper and aluminium alloys, austenitic steels prone to grain coarsening in overheating. Several dozens of methods and devices for heat removal in welding are known, but their classification or evaluation of their effectiveness in any form, are absent. This paper is exactly devoted to analysis of the methods and devices for cooling during welding.

Heat removal from the welded joint occurs naturally (convection, radiation) or artificially. The natural heat removal depends on the environmental temperature, air flow velocity, degree of welded joint blackness, its surface roughness, etc. The heat losses through natural heat removal being negligible, artificial heat removal is used.

Welding with heat removal is understood to be welding with a forced removal from the welding zone of the heat put into the welded joint by the heat source (Figure 1). Heat q introduced by the heat source, is distributed for melting of the base metal and the filler and propagates in the item in keeping with the laws of heat conduction q_i, and then goes from the workpiece surface through natural convective heat exchange q_n and artificial heat removal q_a into the process fixtures and heat sinks which are located on the face *1* or reverse *2* side of the workpiece.

Thus, any welding process in which the heat removal from the workpiece is intensified can be regarded as the welding process with artificial heat removal. In keeping with the theoretical calculations of N.N. Rykalin, the ratio of the heat required for complete penetration, to the heat put into the workpiece in butt welding of sheets, i.e. the thermal efficiency, cannot exceed 48.4 % [4], and the rest of the heat does not participate in the welded joint formation, but leads to development of welding stresses and strains (parasitic heat).

During welding the heat can be removed from the weld, the heat-affected zone (HAZ) or the weld and the HAZ simultaneously. The available heat removal methods can be classified by the following features:

aggregate state of the heat-absorber (HA) prior to welding (heat removal into the solid, liquid and gaseous HA);

combination of functions (only heat removal; weld root formation and heat removal; clamps and heat removal);

HA temperature (room temperature HA; low-temperature HA);

degree of the devices mobility (heat removal using both stationary and moving heat sinks);

physical effects (heat removal at the expense of the difference in heat capacity; heat removal using latent heat of phase transition (melting or boiling); combined heat removal (heat capacity and melting; heat capacity and boiling, heat capacity, melting and boiling)).

The simplest heat sinks are copper backings used for weld root formation in welding with complete penetration (for instance, C18 joints, GOST 8713–79) [5 – 7]. According to the above classification, these are devices in

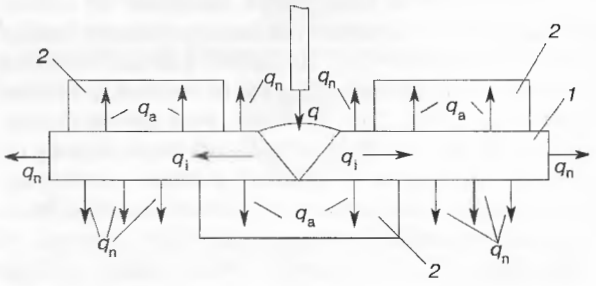

Figure 1. Schematic of welding with forced heat removal: *1* — parts being welded; *2* — fixtures.

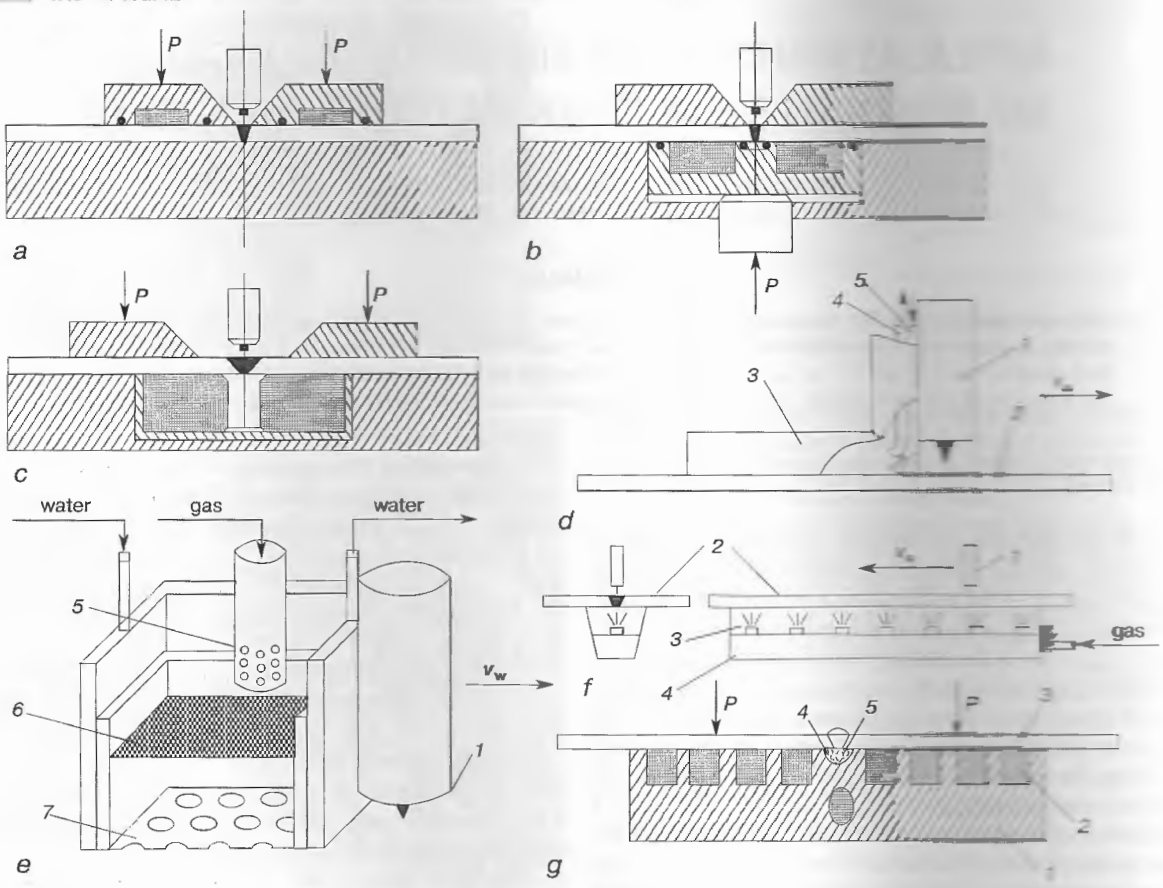

Figure 2. Devices washing the workpiece with water jets (*a – c*) and blowing it with gas (*e*, *f*): *a – c* — stationary devices in the form of clamps and backing [12]; *d* — mobile device [16]: *1* — welding head; *2* — parts being welded; *3* — device case; *4* — suction; *5* — feeding tube; *e*, *f* — stationary and mobile device, respectively: *1* — welding head; *2* — parts being welded; *3* — injector; *4* — channel-bar; *5* — feeding tube; *6* — gas dissector grid; *7* — plate with holes; *g* — copper-flux backing [18]: *1* — copper bar; *2* — channels; *3* — parts being welded; *4* — flux; *5* — forming groove.

which the heat removal is performed through a solid body, the device is used for weld root formation and heat removal with room temperature HA, the device is stationary and the heat removal is due to heat capacity. The effectiveness of the heat removal with backings, depends on their dimensions, difference between the temperatures of the backing and the welded joint, heat resistance of the zone of contact between the backing and the welded joint.

Cooling channels increase the effectiveness of the heat removal and stabilize the heat-removal properties of heat-removing backings [8]. With a forced heat removal, the cooling rates in the weld can exceed the critical ones. Therefore, in order to lower them, backings are used in the weld, which, alongside the cooling channels, also incorporate the heating elements located under the weld root [9]. To achieve a better formation of the weld root, the backings can be made of individual sections [10, 11]. This, however, does not essentially reduce the heat resistance of the workpiece-backing interface. The total area of direct contact is extremely small, because of roughness of the surface of the backing and the welded joint, as well as the presence of oxide films [12]. Heat transfer mainly occurs through the air gap whose thickness depends on the degree of surface finish. For instance, for quality grade 6 the heat resistance of the air gap (15 μm) is equal to heat resistance of 30 mm carbon steel, the heat resistance of the backing body being negligible in comparison [13]. This is the main reason for the low effectiveness of the heat-removing backings designed for lowering the welding stresses and strains. Nonetheless, backings fit well into the welding fixtures and permit both mechanized and manual welding by different processes (coated-electrode welding, gas-shielded and submerged-arc welding).

Besides the backings, also heat-removing clamps can be applied which simultaneously serve for workpiece fastening and heat removal. The heat is removed into the solid (HA is at room temperature, the heat removal being due to difference in heat capacity) [2].

The clamps and backings are often used simultaneously. As they are stationary devices and of a similar design, they have common advantages and drawbacks. A common disadvantage of the stationary devices is their length, which should be equal to the weld length. If shorter clamps are to be used, it is necessary to place them with a smaller spacing for a more uniform cooling of the welded joint along its length. Moreover, they are characterized by poor contact and high heat resistance of the air gap. In the case of elimination or an essential lowering of

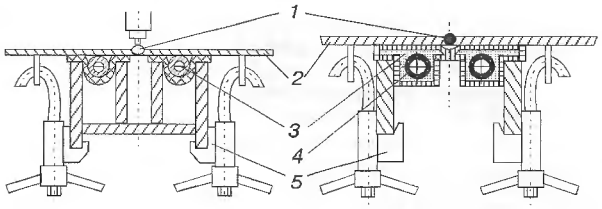

Figure 3. Example of porous materials application without [19] and with continuous [20] water circulation: *1* — weld; *2* — items being welded; *3* — porous materials; *4* — feed tube; *5* — fixtures.

the heat resistance of the air gap, the effectiveness of the backings and clamps is essentially increased.

The next kind of heat-sinks used in welding with cooling, are shoes (heat removal into a solid, weld root formation, room temperature HA, mobile device, heat removal at the expense of heat capacity). The shoes have a smaller material content as their length does not usually exceed 250 to 300 mm, but they are applicable only for the welding processes with a constant speed of the heat source displacement (automatic welding). They are mounted from the reverse side of the welded joint and are rigidly fastened to the welding head via the gap. Such a design limits the range of the performed welded joints (it is impossible to make joints with a zero gap), and it is also difficult to provide a sufficient force of clamping to the surface being cooled, this lowering the cooling efficiency.

Thus, for manual welding the best suited are stationary devices, not requiring welding at a constant speed, and for automatic welding the mobile devices with a low material content.

Another kind of welding with cooling, is welding with application of heat-sinks blowing the surface being cooled with gas or washing it by a water jet (Figure 2). The devices can be mobile, using gas (argon, helium, carbon dioxide or their mixtures or compressed air) [14] and water [15 – 17], and stationary. Some can combine the functions of the heat sink and formation of the back side of the weld [18], or can serve just for heat removal [12]. Their common merit is a close contact of the heat carrier with the surface being cooled.

Surface blowing with gas has a low effectiveness, as with the forced convection into the gas medium, the heat removal coefficient is by two to three orders of magnitude lower than with the forced convection into the water. Cooling by jets of running water is the most effective, but poorly adaptable to fabrication, as it is difficult to provide the sealing of the channels with the water and eliminate the influence of the air film forming around the workpiece being welded each time it is placed on top. During mounting, the water level should be below the device edge so that the water does not flow out. After sealing, the water level is increased up to the upper point of the outlet nozzle which invariably turns out to be below the surface of the item and, as a result, an air film forms under the item which is a thermal insulator.

A great number of devices have been proposed using porous materials and capillarity effects [19 – 21] (Figure 3). All of them have a common advantage, namely a close fitting to the surface of the workpiece being cooled

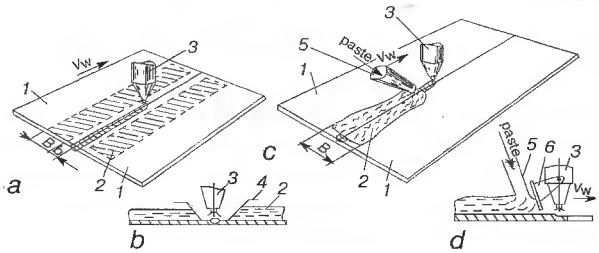

Figure 4. Process diagrams of application of heat-absorbing paste in welding [25]: *a*, *b* — prior application of the paste; *c*, *d* — paste feeding behind the torch concurrent with welding: *1* — plates being welded; *2* — applied paste; *3* — torch; *4* — protective stationary screen; *5* — outlet nozzle of the paste feeding device; *6* — mobile protective screen.

and good contact of HA (water) with the cooled surface. Moreover, in impregnation of porous materials with water, their heat conductivity can exceed the heat conductivity of the material and water taken together [13]. Their common disadvantage is that at a high heating energy, an intensive boiling of the water occurs in the porous material zone adjacent to the heated surface, with formation of a steam film which does not disintegrate because of the absence of stirring and is a thermal insulator.

Cooling methods based on allowing for the phase transition heat, are related to the application of heat-removing pastes [22, 23] (Figure 4) and crystalline heat absorbers [24]. The heat-removing pastes are a mixture of water or salt melts with technological additives increasing their viscosity and other properties. Heat absorption in application of the heat-removing pastes is due to heating and evaporation of the water contained in them. The pastes

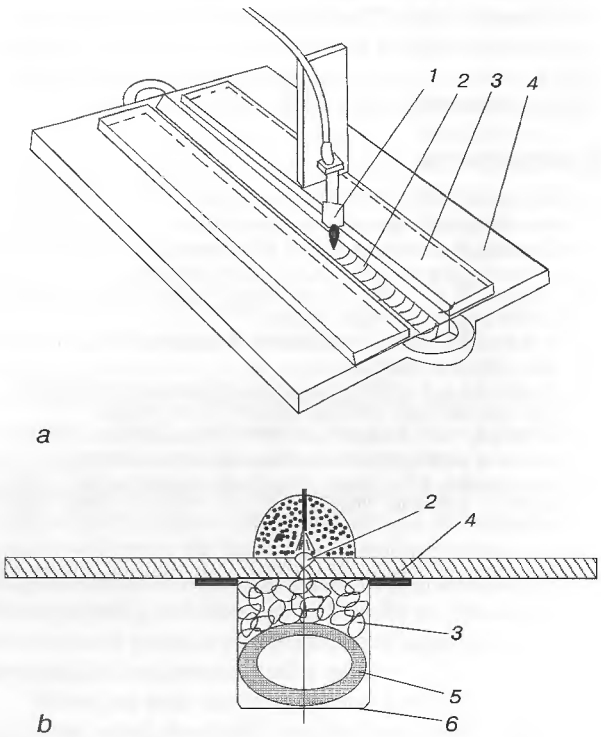

Figure 5. Example of application of dry ice [17, 27]: *a* — cooling of heat-affected zone; *b* — cooling of the weld and heat-affected zone: *1* — welding head; *2* — weld; *3* — dry ice; *4* — parts being welded; *5* — pneumatic hose; *6* — channel-bar.

are applied onto the surface of the workpiece being welded and cool it.

Crystalline heat absorbers are crystalline hydrates of salts. Heat removal is the result of crystallites melting with formation of water and its subsequent heating and evaporation. The advantages of the processes of heat removal using heat removing pastes and crystalline heat absorbers, are their simplicity, high adaptability to fabrication and versatility. The disadvantages consist in the pastes and crystalline heat absorbers being consumable materials capable of removing a limited amount of heat, therefore, they are only used for low-melting materials (aluminium and magnesium alloys) or thin metal (up to 3 mm) [25].

Methods using low-temperature media as heat absorbers, are described in publications. For instance, some authors recommend cooling the weld by a liquid nitrogen jet (–196 °C) [26] or dry ice (–78.5 °C)) [17, 27] (Figure 5). Such methods are quite effective in terms of heat removal, but poorly adaptable to fabrication, because of the complexity of using the low- temperature media, also being quite expensive.

CONCLUSIONS

1. Designs of cooling devices and methods of cooling are highly diverse. Selection of a concrete design and cooling method depends on the item being welded, material and welding process.

2. For extended welds made by automatic welding, preferable are the mobile devices, and stationary devices for manual welding. The most effective is the use of water and low-temperature HA. The best adaptable to fabrication are the methods using heat-removing backings and clamps, their effectiveness being low, however.

REFERENCES

1. Sagalevich, V.M. (1974) *Methods of elimination of welding strains and stresses*. Moscow: Mashinostrojenie.
2. Kasatkin, B.S., Prokhorenko, V.M., Chertov, I.M. (1987) *Stresses and strains in welding*. Kiev: Vyshcha Shkola.
3. Lobanov, L.M. (1983) *Technological means for reduction of strains and stresses*. Kiev: Znanie.
4. Rykalin, N.N. (1951) *Calculations of thermal processes in welding*. Moscow: Mashgiz.
5. Shchebeko, L.P. (1981) *Equipment and technology of automatic and semi-automatic welding*. Moscow: Vyssh. Shkola.
6. Gitlevich, A.D., Etingof, L.A. (1979) *Mechanization and automation of welding production*. Moscow: Mashinostrojenie.
7. Topolyanskii, P.A., Sosnin, N.A. *Multi-position backing*. USSR author's certificate **963775**, Int. Cl. B 23 K 37/04. Publ. 07.01.82.
8. Veselkov, V.D. (1984) *One-sided welding of butt joints of steel hull structures*. Leningrad: Sudostrojenie.
9. Kobets, G.A. *Backing for formation of the weld reverse side*. USSR author's certificate **770349**, Int. Cl. B 23 K 37/06. Publ. 07.09.80
10. Kolisnyk, V.N., Dolgov, Yu.P., Smirnov, N.N. *A device for formation of the weld reverse side*. USSR author's certificate **956209**, Int. Cl. B 23 K 37/06. Publ. 07.09.82.
11. Fykusima, K. *Backing for one-sided submerged-arc welding*. Pat. **45-19770** Japan, Int. Cl. B 23 K 37/06. Publ. 06.07.70.
12. Kazimirov, A.A., Nedoseka, A.Ya. (1963) Methods of lowering welding deformations in structures of aluminium-magnesium alloys. *Avtomaticheskaya Svarka*, **4**, 41 – 49.
13. Baskakov, A.P., Berg, B.V., Witt, O.K. *et al.* (1991) *Heat engineering*. Edited by A.P. Baskakov. Moscow: Energoizdat.
14. Wells, M.E., Lulens, W.E. (1986) Effect of forced gas cooling on GTA weld pools. *Welding J.*, vol. 65, **12**, 314 – 321.
15. Birman, U.I. (1985) Control of thermal processes in welding high-temperature alloys with forced cooling. *Avtomaticheskaya Svarka*, **10**, 24 – 26.
16. Gedrovich, A.I., Shevchenko, P.M., Tkachenko, A.M. *et al. A method of reduction of welding strains and stresses*. USSR author's certificate **1729723 A1**, Int. Cl. B 23 K 28/00. Publ. 30.04.92.
17. Yamaguchi, T., Fukuyama, K., Fukuyama, Y. *Method of arc welding with reverse side cooling for obtaining highly tough large-diameter welded steel pipes*. Pat. **4152568 Japan**, Int. Cl. B 23 K 031/06. Publ. 01.05.79.
18. Kalyuzhnyi, V.V. Gedrovich, A.I., Chernomorov, M.I. *et al. Copper-flux backing*. USSA author's certificate **1655745 A1**, Int. Cl. B 23 K 37/06. Publ. 15.06.91.
19. Astakhov, L.S., Zhuravlev, Yu.A., Utyushev, R.I. *et al. A method of lowering the strains and stresses in welded hull structures*. USSR author's certificate **1066765**, Int. Cl. B 23 K 28/00. Publ. 1984.
20. Astakhov, L.S., Zhuravlev, Yu.A., Dubskih, Yu.A. *et al. A device for items cooling during welding*. USSR author's certificate **1066767**, Int. Cl. B 23 K 34/04. Publ. 1984.
21. Fuzita, H., Nagai, M., Akiyama, H. *et al. A device for prevention of strains in welding of sheets*. Pat. **58-3480 Japan**, Int. Cl. B 23 37/00. Publ. 21.01.83.
22. Kasatkin, B.S. *et al. Composition of heat-absorbing paste*. USSR author's certificate **591289**, Int. Cl. B 23 K 35/36. Publ. 05.02.77.
23. Lobanov, L.M. *et al. Composition of heat-absorbing paste*. USSR author's certificate **1046052**, Int. Cl. B 23 K 35/36. Publ. 07.10.83.
24. Lobanov, L.M., Loginov, V.P., Lysak, V.V. *et al. Heat-absorbing element and a composition for its fabrication*. USSR author's certificate **1449276**, Int. Cl. B 23 K 3/36. Publ. 07.10.83.
25. Lobanov, L.M., Pavlovskii, V.I., Loginov, V.P. *et al.* (1990) Regulation of thermo-deformational cycles in welding of sheet structures with application of heat absorbers. *Avtomaticheskaya Svarka*, **9**, 30 – 42.
26. Prokhorov, N.N., Polunin, V.M. (1992) Calculation analysis of the influence of the local heat sinks on lowering of longitudinal deformations in butt welding of plates. *Svarochnoe Proizvodstvo*, **1**, 3 – 5.
27. Masubuchi, K. (1991) Research activities examine residual stresses and distortion in welded structures. *Welding J.*, **12**, 41 – 47.

SELECTION OF EQUIPMENT FOR MECHANIZED ARC WELDING, SURFACING AND CUTTING

V.A. LEBEDEV and **V.F. MOSHKIN**
The E.O. Paton Electric Welding Institute, NASU, Kyiv, Ukraine

ABSTRACT

The results of analysis, development and selection of equipment for mechanized arc welding, surfacing and cutting are considered. It is shown that the intuitive approach to selection and development of the semi-automatic machines can lead to non-rational solutions. Methods of system approach are suggested which allow performance of a highly objective analysis and selection of the equipment, lowering the probability of taking wrong decisions, also at the stage of development of new semi-automatic machines. Selection of modular design using a basic model as a principle allowing development of semi-automatic machines for various purposes with rational technical and service parameters, is substantiated.

Key words: *arc welding, surfacing, cutting, system approach, analysis, development, fabrication, production, criteria.*

Alongside a noticeable reduction of the volume of output and use of semi-automatic machines for metal-arc welding and surfacing, the number of developments of this type of equipment has markedly increased lately [1]. The new semi-automatic machines largely reproduce the design solutions of the past years, differing from each other only by the arrangement, outer design and use of advanced materials and components. Some developments of mechanized equipment are indeed based on advanced engineering solutions which expand their areas of application up to use in allied technologies [2]. This concerns the semi-automatic machines which allow performance, for instance, of gas-shielded welding with smaller loss of electrode metal, improved formation of a weld of steel [3], aluminium and its alloys [4]; strengthening and restoration surfacing with self-shielded flux- cored wires; cutting of various metals with specially selected cutting electrode wires.

It should be specially noted that the main components of the semi-automatic machines, also with the required modifications, are used to advantage in such allied technologies as surfacing and cutting. Analysis of the technical information, materials of exhibitions and consumption market leads to a conclusion that different evaluation criteria are used even for equipment of one type for any purpose whatsoever, in development of mechanized equipment, its manufacture and selection by the user. The following of the main criteria can be singled out:

minimal consumption of time and money for selection of the optimal solutions and design (for developers);

prompt reaction to the market needs, i.e. availability of reproducible design solutions for the majority or even the full range of the user inquiries with minimal production costs (for manufacturers);

minimal price, broad technological capabilities and performance with minimal cost of repair and service (for users);

technical and ecological safety (for man and environment).

It is obvious that for all the participants of the cycle of development-manufacture-use of mechanized equipment in metal-arc processes, some criteria can coincide completely or partially and others may not coincide or even contradict each other. The purpose of this work is selection and substantiation of the most general criteria of evaluation of semi-automatic machines for various purposes, which allow the developers, manufacturers and users of mechanized equipment to take the most optimal decisions.

In view of the fact that any type of equipment for mechanized arc welding, surfacing and cutting, in terms of such formal characteristics as integrity and divisibility, availability of essential stable associations and organisation, as well as integration qualities [5], is a system of a certain complexity, its analysis, can be performed using the system approaches.

It should be noted in advance that the procedure of determination of the actual quality characteristics of mechanized equipment is quite complicated. Therefore, it should be conducted in an integrated manner, mainly, at the stages of development and design of any new system, taking into account the interests of the manufacturer and the user, as well as addressing the problems of technical and ecological safety. This circumstance, certainly, does not eliminate the possibility of such analysis by individual parameters of the semi-automatic machines at the stages of manufacture or introduction into the market.

Until recently, assessment and analysis of welding equipment, also of semi-automatic machines of various purpose and different design, has mainly been conducted using different types of classifications [6], and subjective opinions allowing for the technical and technological capabilities of the machines and the ensuing complexity of the engineering solutions, as well as the equipment cost. In practice it means a purely empirical approach to constructing the equipment quality criteria.

When just such methods are used, errors are highly probable, which inevitably lead to development and design of non-optimal systems for implementation of metal-arc welding, surfacing and cutting.

A similar situation can be in place also in selection of the equipment for coping with the production problems.

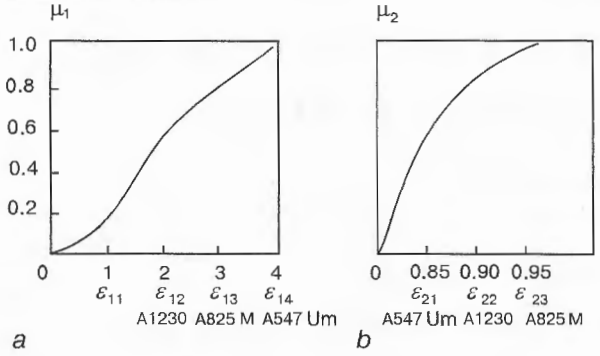

Figure 1. Confidence functions: *a* — for electrode wire diameters used in the semi-automatic machines $\mu_1(\varepsilon_1)$; *b* — for reliability indices $\mu_2(\varepsilon_2)$.

From the above-said it follows that development of sufficiently precise, unambiguous criteria for the evaluations which allow a practical comparison of equipment by the degree of its preference, is an urgent problem.

According to [7], the evaluation criteria can be of three kinds, namely: representative, indirect and non-representative. The latter, as shown by analysis, being loosely associated with the preference relations in the equipment for mechanized processes, we will use only the representative and indirect ones. They can be determined as the following ratios:

$$\text{for the representative criterion } \lim_{\varepsilon \to \delta} \mu(\varepsilon) = 1;$$
$$\text{for the indirect criterion } 0.5 < \lim \mu(\varepsilon) < 1, \quad (1)$$

where $\mu(\varepsilon)$ is the confidence function or representativeness and δ is the value characterising a concrete criterion (reliability, cost , etc.).

The confidence function $\mu(\varepsilon)$ can be regarded as a criterion only in the case, if it is of a continuously growing nature for δ. Various approaches can be used to determine the kind of $\mu(\varepsilon)$ dependence. In our case, the expert evaluation method is the simplest and sufficiently accurate, as shown by the work experience and studies of the market for semi-automatic machines for gas-shielded welding with solid electrode wires.

Let us consider as an example, selection of a semi-automatic machine for CO_2 welding with small- diameter solid electrode wires by preference from the viewpoint of a plant-manufacturer of sheet metal structures. Let us limit the set of such semi-automatic machines by the economic capabilities of the enterprise for their purchase, as well as the conditions related to the insufficient repair facilities. The simplest and relatively inexpensive designs of this type of semi-automatic machines are A547 Um, A825 M, A1230 machines. They have similar specifications and are close as to their technical capabilities. Considering conditions (1), as well as the results of the conducted expert opinion survey, which define the confidence functions $\mu(\varepsilon)$ as monotonically growing, two principal criteria of evaluation of the above semi-automatic machines can be singled-out: number of electrode wire diameters accommodated by the semi-automatic machine and reliability of operation.

Figure 1 shows the confidence functions produced by expert opinion survey:

$\mu_1(\varepsilon_1)$ — for electrode wires when one diameter is used $\varepsilon_{11} = 1$; $\varepsilon_{12} = 2$; $\varepsilon_{13} = 3$; $\varepsilon_{14} = 4$;

$\mu_2(\varepsilon_2)$ — for reliability which here is understood to be the probability of faultless operation for a year after the guarantee period is over for the reliability values $P_1 = 0.85 = \varepsilon_{21}$; $P_2 = 0.9 = \varepsilon_{22}$; $P_3 = 0.95 = \varepsilon_{23}$.

The values of the reliability characteristics are derived partially by expert opinion survey and partially from the data in [8] and for semi-automatic machines correspond to: A547 Um — 0.875; A1230 — 0.9; A825 M — 0.95.

The electrode wire diameters used in the semi-automatic machines are taken from the certificate data and have the following values: A547 Um — 4 (0.8; 1.0; 1.2; 1.4 mm); A825 M — 3 (1.0; 1.2; 1.4 mm); A1230 — 2 (1.0; 1.4 mm).

Consideration of dependencies $\mu_1(\varepsilon_1)$ and $\mu_2(\varepsilon_2)$ leads to the conclusion that all the equipment being analysed has the criteria with the function of confidence or representativeness $\mu(\varepsilon) \geq 0.5$ which, therefore, can be used for selection of the semi-automatic machine design. It is obvious that any other developments of the semi-automatic machines where electrode wire of one diameter is used, or the probability of failure-safe operation after the guarantee period is over, is below $P = 0.85$, will not be much in demand by the users. In this case it is quite easy to give preference to A825 M semi-automatic machine, as the one having the highest general values of representativeness $\mu(\varepsilon)$. In practice, however, the user can prefer some other type of the semi- automatic machine in which one of the criteria, in his opinion, the most important, can be taken as the basis to the detriment of the others.

Often enough when the tasks of development, manufacture and selection of the semi-automatic machines are addressed to solve the production problems, equipment assessment must be performed by more than two criteria. Hence, the multi-criteria problem which, if required can be solved by the methods of plotting integral criteria for each specific case by the procedures of [9]. From the above-said it follows that at any stage of decision taking on the mentioned equipment, system approaches should be used alongside the intuitive selection.

This method of evaluation of the equipment is quite simple and accessible. It is based on preferable choice proceeding from the expert data (confidence function), i.e. incorporates the subjective elements. Its disadvantage is the need to perform extensive work on generation of expert data.

A more accurate (objective) evaluation of the equipment can be provided by such a criterion as the complexity of the semi-automatic machine. It is quite important for the problems related to the mechanized systems. For the developer and the designer, the complexity is an indication of the number of implemented research-engineering solutions; for the manufacturer an indication of the tasks

of preparation for production; for the user an indication of the ability of the semi-automatic machines to effectively perform the technological processes, to be repairable, etc. It should be noted that the criterion of complexity is, as a rule, associated with the reliability of the equipment, and its cost. It follows from the above said that the complexity criterion is quite representative.

Let us consider the complexity criterion based on the system approach concepts [5] as the most objective one.

Any semi-automatic machine for implementation of mechanized metal-arc welding, surfacing and cutting in the general form can be represented hierarchically as a two-level structure where the first level are the local control systems and the determinant components of the equipment, namely arc power source, controllable motor-drive and electrode wire feed mechanism, system of shielding media feed (gas, flux). The second higher level is a system of control of the semi-automatic machine operation and regulation of the process (welding, surfacing, cutting). Such a structure of the semi- automatic machine, formalised in keeping with the procedures of [10], is shown in Figure 2. It can contain, alongside elements, blocks and individual components, a rather large number of ties of different purpose for the aims of interaction, control and information acquisition.

There is a great number of different procedures of determination of the degree of complexity of any system, allowing only for the complexity of the equipment design and relying on a certain number of the system components, as well as a number of others. None of them fully enough reflects the complexity of the currently used equipment for metal-arc welding and surfacing. Their use is possible only on the level of rather simple engineering solutions. At present an increasing number of developments in Ukraine [11] and abroad («Kemppi», «Miller», etc.) make full use of the computational means. The complexity of such an equipment can no longer be evaluated without allowing for different kinds of associations, information level of the system, its possible variability and organisation.

In our opinion, for mechanized equipment, the most objective can be the complexity index C_s described in [5] in the following form:

$$C_s = \frac{(1 + L_a)\,[I_0 + n^* \bar{y}\; Dk\,(L + 1)\ln \bar{n}\,\bar{\gamma}]}{1 + \Pi_s}, \qquad (2)$$

where L_a is the degree of the system lability allowing for the variability of both the structure and its functions; I_0 is the amount of information which should be available to the developer, designer and technologist when forming the system as a whole; n^* is the number of the system components; $\bar{y}$ is the average number of the technological operations per one component of the system (element, tie, component, etc.); D is the degree of the system differentiation allowing for the diversity of the elements and ties; k is the Boltsmann constant; L is the number of hierarchical levels; $\bar{n}\,\bar{\gamma}$ is the mean geometrical product of the number of components and ties and Π_s is degree of the system organisation ($0 > \Pi_s > 1$).

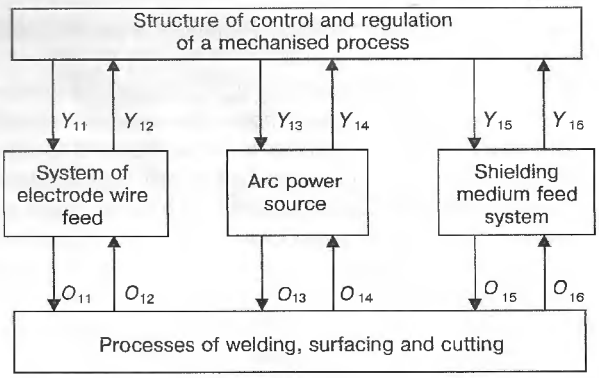

Figure 2. A formalised structure of a semi-automatic machine for welding, surfacing and cutting: Y_{11}, Y_{12}, Y_{13}, Y_{14}, Y_{15}, Y_{16} — ties of control and interaction; O_{11}, O_{12}, O_{13}, O_{14}, O_{15}, O_{16} — feedbacks and information links.

From expression (2) it follows that determination of the index of the system complexity it a quite difficult task and can only be fulfilled with a common approach used for assessment of all of its components. In this case it is only possible to derive comparative values of C_s for different systems of mechanized equipment, which will correctly reflect the actual complexity of the equipment. Such a procedure of determination of the complexity index must be performed at the stage of selection and taking the decisions in development and design of mechanized equipment.

Expression (2) can be simplified, considering that I_0 parameter incorporates k constant, and $1 + \Pi_s$ values, as shown by analysis, are close enough for the majority of the semi-automatic machine designs. In view of the above-said, expression (2) will assume a simpler form

$$C_s = (1 + L_a)\,[N + n^*\,\bar{y}\; D\,(L + 1)\ln \bar{n}\,\bar{\gamma}\,], \qquad (3)$$

where N is the parameter characterising the number of the possible combinations which provide for the formation of certain properties of the equipment components.

With the practical use of expression (3) determining the degree of complexity of the equipment, it is necessary to assume certain rules of calculation of some of its implicit components. The mechanical ties which are the same for the majority of the semi-automatic machine designs, are ignored. Only the ties which provide mechanical adjustment of the electrode wire feed rate, are an exception. From all the components of the semi-automatic machines only those are selected, which are active in provision of the machine performance and its adaptability to the technology.

The complexity indices have been calculated for a number of semi-automatic machines produced by the industry of Ukraine, which are designed for CO_2 welding, as well as for self-shielded flux-cored wire welding and surfacing, namely A547 Um with VS300 power source, A825 M with VS300B power source, A1230 with VDG303-3 power source, PDG508 with VDU506 power source, PDG516 with VDU506 power source, PDG312

with VDG303 power source, PSh107V with VS300B power source.

The simplest design is that of A547 Um semi-automatic machine. During investigations, this semi- automatic machine came to be regarded as a certain standard of simplicity and rationality of design. In this case, the complexity index of this semi-automatic machine can be taken as a criterion and used as a guideline in consideration of all the other designs. The results of calculations in the order of the increase of the complexity indices and reduction to the complexity index of A547 Um semi- automatic machine, taken as a unity, are as follows: A825 M — 1.2; A1230 — 1.7; PDG508 — 2.08; PSh107V — 2.8; PDG312 — 4.6; PDG516 — 5.5.

Analysis of the results showed that the majority of them correspond to expert opinions (of designers, technologists, operators) and some require clarification. The higher indices of complexity of A825 M and A1230 semi-automatic machines are attributable to the availability of a mechanical switch of the transmission ratio and a more complex arc power source. The complexity of PDG508 and PDG516 semi-automatic machines is determined by inclusion of VDU506 power source into their set.

Two main trends can now be singled out in design and development of mechanized equipment for arc welding and surfacing:

development of as simple as possible in design semi-automatic machines for each of the processes using new highly efficient materials, processes (modulation, pulsed modes, etc.), engineering solutions (pulsed feed of electrode wire, co-ordinated control, etc.);

development of quite sophisticated perfect systems of mechanized equipment using a greater amount of computational means (synergistic systems, adaptive control, etc.).

It is known that the system complication invariably leads to lowering of the reliability characteristics [12] and to increase of its cost, as a result of increasing of the number of elements and ties between them, the components and modules. The equipment complexity, however, is compensated for by its high technological capabilities, simplicity of setting up, and in a number of cases also by multi-purpose use (combined engineering solutions).

It is obvious that the simple designs of the semi-automatic machines in terms of the complexity criterion, invariably come into conflict with the more complex ones. This is manifested in all the stages of development, design, manufacture and operation of the semi-automatic machines. The possibility for elimination of the above contradiction should be searched in compromise variants of developments, which satisfy both the developers and manufacturers and the users. Equation (3) allowing for the most important aspects of the system approach, can in full measure serve as a practical basis for selection of such variants.

The most optimal method for development, design, manufacture and introduction of equipment for mechanized welding, surfacing and cutting of various metals, can be the modular design using a basic model which is applied with success in the Experimental Design-Technological Bureau of the E.O. Paton Electric Welding Institute when developing a wide range of semi-automatic machines for various purposes [13]. The complexity of the semi-automatic machines of modular design is minimised. Let us demonstrate that by a number of obvious statements which follow from the systemic expression of the complexity index (3). The design of the basic variant used in such development, has a quite low complexity index, and its main components are applied in all the further modifications of the semi-automatic machines. Therefore, all the subsequent required by industry models of the semi-automatic machines will have lower values of N, I_0, $\bar{\gamma}$ components, and, hence, a lower complexity index compared to the new developments performed. This is also true for equipment of any level of technical perfection.

Another argument is based on an essential lowering of the degree of differentiation D (diversity of elements and ties) for each modification of the semi-automatic machines of a modular design, compared to the semi-automatic machine being developed for solving more than one technological problem. Hence, a number of obvious advantages of the modular principle of development of a semi-automatic machine using a basic model for the manufacturer and the user, of which the main are as follows: lower cost of establishing the production, ability to quickly react to the market needs with the availability of simple diverse designs, relatively low cost, reliability, easy maintenance and repair, etc.

Use of the methods of system approach for solving the problems of mechanized equipment for welding and surfacing with a high final result, allowed extending them also to another kind of equipment, namely to automated systems for repair and strengthening surfacing. The experience of applying the system approach to development of such units is set forth in [14]. The proposed method of analysis and evaluation of welding equipment based on the system approach, by its principles and interpretation is, obviously, still far from perfect and should be regarded as one of the attempts of clarifying this issue.

CONCLUSIONS

1. Methods of system approach in analysis and design of equipment for mechanized arc welding and surfacing, provide the most rational solutions, both in development of equipment and in its assessment by the user.

2. For relatively simple designs of the semi-automatic machines, the most accessible method of their evaluation by certain representative criteria, is the preference method. In the case of the more complex designs of the semi-automatic machines, the most objective method is that of determination of the system complexity indices, allowing consideration of the engineering solutions with the aim of their rational use at the stages of development, manufacture and introduction of the equipment.

3. The methods of system approach in their various applications, can be used in development, analysis and evaluation of the kinds of welding and surfacing equip-

ment, whose diversity and serial nature of production are essentially greater than of the individual solutions and single-job production.

For mechanized and automated welding and surfacing equipment, the most rational method of development, manufacture and introduction, determined through system approach, is the method of modular design using a basic model.

REFERENCE

1. Lebedev, V.A., Moshkin, V.F., Ivanov, G.P. (1995) Equipment for arc welding in the «Welding-95» International Exhibition. (Review of exhibits and analysis of the tendencies of their production). *Avtomaticheskaya Svarka*, **11**, 58 – 59.
2. Lebedev, V.A., Moshkin, V.F., Pichak, V.G. (1995) On selection of equipment for mechanized flux-cored wire cutting. Ibid., **6**, 53 – 55.
3. Voropai, N.M., Benidze, Z.D., Buchinskii, V.N. (1980) Features of the process of CO_2 welding with a pulsed feed of electrode wire. Ibid., **2**, 23 – 26.
4. Lebedev, V.A., Pichak, V.G., Rogatkin, A.A. *et al.* (1997) Semiautomatic machines for metal-arc welding of aluminium and its alloys. Ibid., **11**, 51 – 56.
5. Nikolaev, V.I., Bruk, V.M. (1985) *Systems engineering: methods and applications*. Leningrad: Mashinostrojenie.
6. Lebedev, V.A., Moshkin, V.F., Pichak, V.G. (1997) Classification of machines for mechanized arc surfacing and cutting. *Svarochnoye Proizvodstvo*, **10**, 39 – 42.
7. Fleishman, B.S. (1982) *Fundamentals of systemology*. Moscow: Radio i Svyaz.
8. Lebedev, V.A., Moshkin, V.F., Pichak, V.G. *et al.* (1998) Reliability of the electrode wire feed mechanisms in machines for mechanized welding and surfacing. *Avtomaticheskaya Svarka*, **1**, 34 – 39.
9. Kini, R.L., Raifa, Kh. (1981) *Taking decisions with many criteria: preference and substitution*. Moscow: Radio i Svyaz.
10. Nechiporenko, V.I. (1977) *Structural analysis of systems*. Moscow: Sov. Radio.
11. Podola, N.V., Rudenko, P.M., Kobylin, A.M. (1993) Semi-automatic machine for mechanized arc welding with one button control. *Avtomaticheskaya Svarka*, **11**, 42 – 44.
12. Pronikov, A.S. (1978) *Reliability of machines*. Moscow: Mashinostrojenie.
13. Lebedev, V.A., Moshkin, V.F., Pichak, V.G. (1998) Semi-automatic machines of a unified modular design for welding, surfacing and cutting. *Svarochnoye Proizvodstvo*, **1**, 24 – 28.
14. Moshkin, V.F., Lebedev, V.A., Kovalenko, V.F. *et al.* (1998) All-purpose modular surfacing equipment. Ibid., **6**, 30 – 33.

PROSPECTS OF UTILIZATION OF A HARD COMPONENT OF WELDING AEROSOLS

A.A. ENNAN, P.A. IVANCHENKO and **G.N. SHIKHALEEVA**
Physical-Chemical Institute for Environment and Human Protection of the Ministry of Education and NASU, Odessa, Ukraine

ABSTRACT

New feasibility of utilization of a hard constituent of welding aerosol is described. Realization of a directed vapour-phase synthesis with producing highly dispersed powders of a preset composition and a developed surface of a phase contact will, probably, open up new prospects in the field of creation of materials of different functional purposes.

Key words: *welding aerosol, composite materials, hard component, dispersity, catalysts, fillers, strain-strength characteristics.*

It is known that the welding industry belongs to the ecologically hazardous industries. Expenses for environment protection and maintenance of level of the safe air contamination of the working zone can reach up to 20 % of expenses for the welding processes [1]. In this connection the reduction in non-productive expenses is a rather actual problem.

This article presents results of systematic investigations directed to a practical application of a hard component of welding aerosols (HCWA), i.e. the non-utilized toxic waste of welding industry.

When a series of successive experiments was planned we were coming from known general theoretical concepts, namely: the welding processes are proceeding, in principle, in open-type «reactors», where components of coatings and fluxes, and also metals, which form the finest aerodispersed particles in oxidation and condensation beyond the welding arc, are intensively evaporated under the action of high temperatures and infrared radiation. In addition, we used data, summarized in manuscript [2], about the dispersed and chemical composition, morphology of HCWA, whose producing was stimulated mainly in the interests of hygienists, designers of gas purification equipment and means of individual protection of respiratory organs of welders.

Physical-chemical properties of HCWA

For investigations the HCWA samples were used, which were obtained by burning of electrodes ANO-4 (4 mm diameter, burning rate is 0.3 of electrode per minute, I = = 200 A, U = 28 – 30 V, power source is rectifier VDU-506 with a rigid characteristic) on 10 mm thick substrate from St.3 grade steel.

Element composition of HCWA was determined by the method of X-ray photoelectron spectroscopy (instrument «Krab-3UM»), wt. %: 37.0 Fe, 5.5 Mn, 2.5 Si, 8.5 K, 3.6 Na, 0.9 Ti, 0.5 Mg, traces of aluminium and calcium, the rest - oxygen and microimpurities.

Judging from the results of analysis of a dispersed composition of particles of several samples of HCWA [3], obtained with the help of a laser analyser «Analisette-22» of «Fritch» company and electron microscopy (EM UEMI-100K, ×29,000), they have a spherical shape and their diameter does not exceed 0.78 μm, the maximum size of formed agglomerates is not more than 1.5 μm, the specific geometric surface is 2.1 – 2.5 m^2 / g. The specific surface of HCWA determined by the BET method using instrument «Quantisorb» is about 22 m^2 / g, i.e. exceeds the specific geometric surface approximately by 10 times. The latter testifies a slightly expressed porosity of HCWA particles.

The thermographic examination (derivatograph of MOM company) and results of volumetric measurements of ethane yield during the HCWA sample treatment with triethylaluminium showed that all the volatile elements (2 – 3 wt. %) are removed from HCWA within the 100 – 200 °C temperature interval, content of water and – OH groups at the surface of particles being decreased from 0.21 to 0.002 mmole / g. The further heating (to 970 °C) leads to the increase in mass and subsequent changing of HCWA colour (brown → red-brown → black) due to increase in depth of metal oxidation. This is proved by exoeffects in a differential curve at 360 and 785 °C, and also by reflexes in the diffractograms caused by the presence of iron oxides with a structure of the corundum type (hematite α-Fe_2O_3) and spinel ($MnFe_2O_4$, $FeFe_2O_4$). The application of method of a paramagnetic resonance could establish the clearly expressed ferro- and paramagnetic properties of HCWA and products of its thermooxidizing treatment.

Catalytic properties of HCWA

The basic component of a natural gas is methane which is used instead of an oil raw material to produce valuable petrochemical products, and, first of all, ethylene (up to 40 % of total output of petrochemical products). Reaction of oxidative condensation of methane (OCM) which proceeds according to data of works [4, 5] only in the presence of catalysts, i.e. complex systems containing oxides of transition metals (titanium, tungsten, chromium, manganese, iron, etc.) and also silicon, aluminium, calcium, sodium, potassium, H_2O, – OH group, is one of the promising production reactions. As was above-mentioned, HCWA contains all necessary components for OCM realization.

Experiments in 16 mm diameter quartz reactor with a fixed layer of HCWA (p = 101.3 kPa, mole ratio of CH_4:

Table 1. Effect of temperature on composition of products and selectivity of the OCM reaction

Temperature, °C	Composition of OCM reaction products, %				Selectivity of OCM reaction, %			
	C_2H_4	C_2H_6	CO	CO_2	C_2H_4	C_2H_6	CO	CO_2
700	3.2	1.76	0	23.2	12.4	6.80	0	80.8
800	3.4	0.55	7.8	18.7	10.7	1.75	24.6	58.6
900	4.3	0.38	16.6	18.0	10.0	0.75	46.4	42.8

$O_2 = 2$, $T = 700 - 900$ °C, $\tau_c = 1.5$ s) showed that ethylene, ethane, oxide and dioxide of carbon, hydrogen, water were the products of OCM reaction under these conditions [6]. The Table 1 shows that with an increase in temperature up to 900 °C the ethylene yield is respectively increased as a result of dehydrogenation of ethane. However, maximum of OCM reaction selectivity for the yield of hydrocarbons with two molecules of carbon was observed at 700 °C and amounts to 19.2 % at the 20.3 % methane conversion. At 900 °C the methane conversion increases up to 41.8 %, but, unfortunately, due to deeper oxidation of methane. In our opinion, implementation of catalysts on the base of HCWA will require the more thorough study of the OCM mechanism and selection of optimum composition of the catalysts to ensure selective transformation of $CH_4 \rightarrow C_2H_4$ and high yield of the reaction.

HCWA is a filler of polymeric composites

Increase in cost of an oil raw material and also in the requirements to the polymeric materials used under the extreme conditions and in new branches of engineering [7] makes the production of filled polymers actual.

Highly dispersed and fibrous materials, whose high cost is attributed mainly to the power consumption at the stages of dispersion and drying, are used as fillers of polymeric composite materials (CM). It is evident that the cost of composite materials can be significantly decreased by eliminating both or one of these stages.

Due to a peculiar combination of physical-chemical characteristics (size, shape, dispersed composition of particles and negligible content of moisture), HCWA can serve as the ready filler for mixture-type CM, while titanium oxides contained in it are, in addition, the catalysts of the ethylene polymerization [8, 9].

To produce the mixture-type CM the thermoplastic high-molecular compounds, such as: polyethylene (PE) of a low pressure (GOST 16338–77), superhigh molecular PE (SHM-215) (TS 6-05-1896–80) and PE of German company «Hostalen Gur» (HG) were used.

The process was realized in two stages: mixing of polymer and HCWA; hot pressing (PEHG and PESHM-215), die casting (PE of a low pressure).

Table 2 gives data about the effect of a degree of filling the PEHG on the strain-strength properties of the mixture-type CM. As it follows from this Table the rupture strength σ_r of CM is somewhat increased with an increase in the HCWA content of up to 20 wt. % and decreased abruptly at the degree of CM filling of more than

Table 2. Variation of strain-strength characteristics of mixture-type CM depending on the degree of filling of PEHG with HCWA

HCWA content		σ_y, MPa	ε_y, %	σ_r, MPa	ε_r, %
wt. %	vol. %				
0	0	25.7	15	38.1	350
0.5	0.14	24.7	15	52.9	360
2.0	0.58	23.0	12	43.0	350
10.0	3.10	23.3	12	39.8	340
15.0	4.80	23.7	11	40.3	325
20.0	6.70	24.2	12	37.3	285
25.0	8.70	25.0	11	34.2	270
30.0	11.0	24.8	10	33.5	240
35.0	13.0	25.1	10	26.8	70
50.0	20.0	19.0	5	21.0	10

Note. Here, σ_y is the load which corresponds to a conditional yield strength; ε_y is the elongation at yield strength.

35 wt. %. Elongation at rupture (ε_r) is decreased monotonically from 350 – 360 to 10 % (50 wt. % HCWA). In this case the material becomes brittle.

Polypropylene, emulsion polystyrene and polyvinylchloride can be used as thermoplastics alongside with PE of different grades, thus saving the polymer and reducing the cost of the composite.

The idea of producing synthetic CM using HCWA both as a filler and a catalyst is correlated with data about the feasibility of realization of polymerization processes at the surface of solid bodies, i.e. materials of a natural and synthetic origin, which contain active centres [10, 11]. This method of CM synthesis, called a polymerization filling, is theoretically grounded in [12 – 14].

The HCWA surface was activated by complex metalloorganic catalysts [$TiCl_4$ + Al(iso-$C_4H_9)_3$] or [$VOCl_3$ + + Al(iso-$C_4H_9)_3$] in inert medium with a subsequent polymerization of ethylene at the activated surface of HCWA in the medium of a dearomatized benzine in a suspension condition.

It was established [3] that PE–HCWA (synthetic CM containing up to 40 wt. % HCWA) can be produced using a high-pressure installation ($T = 60 - 70$ °C, $p = 0.3 - 1.0$ MPa, HCWA concentrations 50 g / l, $\tau_c = 30$ min). Other conditions being equal the rate of polymerization of ethylene in the case of using the [$VOCl_3$ + Al (iso-$C_4H_9)_3$] system is by an order higher than when using [$TiCl_4$ + Al (iso-$C_4H_9)_3$].

Strain-strength characteristics of synthetic and mixture-type composites PESHM–HCWA, containing up to 30 wt. % HCWA, are almost similar. With the increase of the filling degree the synthetic CM possess higher (by 10 – 20 %) characteristics of strain-strength properties due to a decrease in aggregation and a uniform distribution of HCWA particles in the polyethylene matrix.

As to the combination of properties, the mixture-type and synthetic composites PE–HCWA containing 20 – 40 wt. % HCWA can be used as structural materials and can find application in automobile, electrical engineering, machine-building, construction and other industries and

Table 3. Properties of polymeric composites on the base of epoxy resins filled with HCWA

Composition	Ratio of components, wt. %*				Duration solidification, h	Rupture stress at compression, MPa	Shear stress, MPa	Heat resistance, °C
	I	*II*	*III*	*IV*				
Known [17]	100	–	6	50**	6 – 7	60	5.0	120
Suggested	50	50	6	40	6	75	7.0	270
	50	50	5	45	7	80	7.5	270
	48	52	4	38	8	69	5.5	120

*Here, *I* — epoxidian resin ED-20; *II* — epoxysilicon organic resin; *III* — simplified of polyethylenepoliamine; *IV* — filler HCWA.
**Filler is the waste of potassium pomegranate production.

for the manufacture of containers, pipes (gas distribution, sewerage, irrigation), pickers for looms and other products of household and special application.

Synthetic composites PE–HCWA containing 60 – 95 wt. % HCWA are the concentrates of a filler for producing a secondary composite which is processed by extrusion and die casting. Producing of cellular ceramics, membranes and filters by burning of an organic phase (polymer) from them in an oxygen flame is another promising application of PE–HCWA concentrates.

In accordance with data of [15 – 16] the HCWA can be used as a filler of epoxidian and epoxysilicon organic resins (degree of filling is 40 – 45 wt. %).

As is seen from Table 3, the epoxidian and epoxysilicon organic resins filled with HCWA (up to 50 wt. %) can be recommended as heat-resistant coatings, putties and pastes for repair of metallic surfaces and parts, including those used under the conditions of an increased humidity.

The pressed polymeric plates are imparted the decorative properties: at a low degrees of filling (0.5 – 2.0 wt. %) the HCWA causes colouring of a polymer and, thus, it can be used as a pigment for thermoplastic and thermosetting plastic materials.

The feasibility of producing CM with a high degree of filling on the base of oligomers (polyethylene wax, atactic polypropylene, drying oils «Oksol», oligoether acrylates, etc.) was grounded [17]. For example, on the base of drying oil «Oksol» the aerobically dried paints of brown, red-brown and black colours for protection of wooden, metallic and reinforced-concrete structures were produced.

Sorption properties of HCWA

As has already been noted, there are functional groups at the surface of HCWA particles. This fact served a basis for the development of a unique technology of HCWA modifying with the demethyldichlorsilane in an ultrasonic field [18] with producing a highly dispersed hydrophobic material «Oilfil». The estimation of its effectiveness during cleaning the water area surface from the film oil impurities showed that the complete removal of the oil film is attained at a 2.5 mass ratio of sorbent to the oil. When the sorbent is used the spraying process becomes highly efficient, the sorbent is distributed instantaneously (in seconds) along the surface of the oil film, being accompanied by its quick disintegration and formation of afloat aglomerates, which, due to paramagnetic properties of sorbent «Oilfil», are easily removed from the water surface using a magnetic device [19].

As is shown in [20], HCWA is an effective chemisorbent of fluorine-containing gaseous compounds (150 mg F^- / g of dust). Therefore, it should also sorb the rest acid gases, i.e. in interaction of metal oxides with acid gases in the presence of water vapours, the acid-basic reactions are proceeding with a formation of appropriate salts.

In this connection, it can be stated apriory that the filtering elements, used for HCWA trapping (for example, in FVI of the «Mriya» type), play simultaneously the role of gas absorbing elements of acid gases. However, it should be noted that earlier this problem was not discussed and, thus, it will require a special study.

The results given in this article are the first attempt to demonstrate on different examples the feasibility of utilization of HCWA to improve the economical characteristics and ecology of the welding processes.

In our opinion, the realization of a purposeful vapour-phase synthesis for producing highly dispersed powders of a preset composition and a highly developed surface of a phase contact is a problem of a higher level, whose solution will open up the new, hardly now predictable, prospects, first of all, in the field of the development of new materials of different functional purposes.

REFERENCES

1. Paton, B.E., Mazur, A.A., Metlitsky, V.A. *et al.* (1995) Ecological and economic aspects of fusion welding. *Avtomaticheskaya Svarka*, **5**, 40 – 44.
2. Voitkevich, V. (1995) *Welding fumes: formation, properties and biological effects*. Cambridge: Abington.
3. Matkovsky, P.E., Raspopov, L.N., Ennan, A.A. *et al.* (1997) Electric welding dust is a filler of thermoplastics. *Mashinostroitel*, **2**, 2 – 7.
4. Minachev, Kh.M., Usachev, N.Ya., Ujdut, V.N. *et al.* (1985) Oxidizing condensation of methane. *Uspekhi Khimii*, **3**, 385 – 404.
5. Krylov, O.V. (1992) Ways of improving efficiency of catalysts of oxidizing condensation of methane. Ibid., **5**, 1550 – 1563.
6. Vlasova, N.N., Gavrishova, T.N., Bozhok, V.P. *et al.* (1994) Peculiarities of oxidizing condensation of methane into ethylene on oxide catalysts. *Neftekhimia*, **5**, 473 – 478.
7. (1981) *Fillers for polymeric composite materials*. Handbook. Edited by P.G. Babaevsky. Moscow: Khimiya.
8. Chirkov, N.M., Matkovsky, P.E. Djyachkovsky, F.S. (1976) *Polymerization on complex metal-organic catalysts*. Moscow-Leningrad: Khimiya.
9. Chirkov, N.M., Matkovsky, P.E. (1974) *Sopolymerization on complex catalysts*. Moscow: Nauka.
10. Bryk, M.T. (1981) *Polymerization on hard surface of inorganic substances*.Kiev: Naukova Dumka.
11. Bruk, M.A., Pavlov, S.A. (1990) *Polymerization at the solid body surface*. Moscow: Khimiya.

12. Djyachkovsky, F.S., **Novokshonova, L.A.** (1984) Synthesis and properties of polymerization-filled polyolefines. *Uspekhi Khimii*, **2**, 200 – 222.
13. Konovalenko, V.V., **Ivanchev, S.S., Khoiblain, G.** *et al.* (1987) *Reactions in polymeric systems*. Leningrad: Khimiya.
14. Enikolopov, N.S., **Volfson, S.A.** (1978) Producing and properties of filled thermoplastics. *Plastmassy*, **1**, 39 – 40.
15. Ennan, A.A., **Ivanchenko, P.O., Marinyanko, L.A.** *et al. Polymeric composition*. Pat. **17837 A** Ukraine, Int. Cl. C 08L63/02. Publ. 03.06.97.
16. Ennan, A.A., **Ivanchenko, P.O., Marinyako, L.A.** *Heat-resistant coating*. Pat. **18075 A** Ukraine, Int. Cl. C 08L63/02. Publ. 17.06.97.
17. Dvali, T.M., Otarashvili, A.G., Bakhtadze, E.I. *et al. Composition for coating*. USSR author's certificate **857197**, Int. Cl. C 09 D 1/58. Publ. 23.08.81.
18. Ennan, A.A., Chistov, O.S., Asaulova, T.O. *et al. Method of sorbent production*. Pat. **10186 A** Ukraine, Int. Cl. B 01120/16. Publ. 25.12.96.
19. Ennan, A.A., Shikhaleeva, G.N., Chistov, A.S. (1997) Sorbent for removing oil film from water area surface. In: *Challenging trends in development of ecology, economy and power engineering*. Collection of articles, 106 – 110. Odessa: AOZT IRENTT.
20. Solodov, V.M., Bairamukov, A.S., Butvin, A.N. *et al. Adsorbent of fluorine from gas*. USSR author's certificate **1324677**, Int. Cl. B 01D53/02. Publ. 23.07.87.